AD-A148 679 RF FIBER OPTIC LINK(U) HARRIS CORP MELBOURNE FL 1/2
J J PAN JUN 84 RF-001/0161A RADC-TR-84-118
F30602-81-C-0259

UNCLASSIFIED F/G 17/2 NL

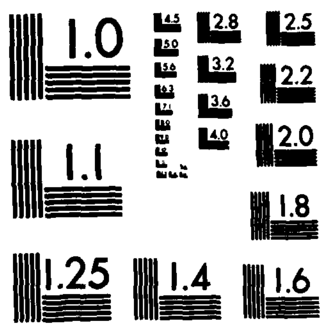

MICROCOPY RESOLUTION TEST CHART
NATIONAL BUREAU OF STANDARDS-1963-A

AD-A148 679

RADC-TR-84-118
Final Technical Report
June 1984

RF FIBER OPTIC LINK

Harris Corporation

J. J. Pan

APPROVED FOR PUBLIC RELEASE; DISTRIBUTION UNLIMITED

This effort was funded totally by the Laboratory Directors' Fund

ROME AIR DEVELOPMENT CENTER
Air Force Systems Command
Griffiss Air Force Base, NY 13441

This report has been reviewed by the RADC Public Affairs Office (PA) and is releasable to the National Technical Information Service (NTIS). At NTIS it will be releasable to the general public, including foreign nations.

RADC-TR-84-118 has been reviewed and is approved for publication.

APPROVED: Paul Sierak

PAUL SIERAK
Project Engineer

APPROVED: Bruno Beek

BRUNO BEEK, Technical Director
Communications Division

FOR THE COMMANDER: Donald A. Brantingham

DONALD A. BRANTINGHAM
Plans Office

If your address has changed or if you wish to be removed from the RADC mailing list, or if the addressee is no longer employed by your organization, please notify RADC (DCLW) Griffiss AFB NY 13441. This will assist us in maintaining a current mailing list.

Do not return copies of this report unless contractual obligations or notices on a specific document requires that it be returned.

UNCLASSIFIED
SECURITY CLASSIFICATION OF THIS PAGE

REPORT DOCUMENTATION PAGE

1a. REPORT SECURITY CLASSIFICATION
UNCLASSIFIED

1b. RESTRICTIVE MARKINGS
N/A

2a. SECURITY CLASSIFICATION AUTHORITY
N/A

2b. DECLASSIFICATION/DOWNGRADING SCHEDULE
N/A

3. DISTRIBUTION/AVAILABILITY OF REPORT
Approved for public release; distribution unlimited.

4. PERFORMING ORGANIZATION REPORT NUMBER(S)
RF-001/0161A

5. MONITORING ORGANIZATION REPORT NUMBER(S)
RADC-TR-84-118

6a. NAME OF PERFORMING ORGANIZATION
Harris Corporation

6b. OFFICE SYMBOL *(If applicable)*

7a. NAME OF MONITORING ORGANIZATION
Rome Air Development Center (DCLW)

6c. ADDRESS *(City, State and ZIP Code)*
P. O. Box 37
Melbourne FL 32901

7b. ADDRESS *(City, State and ZIP Code)*
Griffiss AFB NY 13441

8a. NAME OF FUNDING/SPONSORING ORGANIZATION
Rome Air Development Center

8b. OFFICE SYMBOL *(If applicable)*
DCLW

9. PROCUREMENT INSTRUMENT IDENTIFICATION NUMBER
F30602-81-C-0259

8c. ADDRESS *(City, State and ZIP Code)*
Griffiss AFB NY 13441

10. SOURCE OF FUNDING NOS.

PROGRAM ELEMENT NO.	PROJECT NO.	TASK NO.	WORK UNIT NO.
61101F	LDFP	21	C1

11. TITLE *(Include Security Classification)*
RF FIBER OPTIC LINK

12. PERSONAL AUTHOR(S)
J. J. Pan

13a. TYPE OF REPORT
Final

13b. TIME COVERED
FROM Oct81 TO May83

14. DATE OF REPORT *(Yr., Mo., Day)*
June 1984

15. PAGE COUNT
186

16. SUPPLEMENTARY NOTATION
This effort was funded totally by the Laboratory Director's Fund

17. COSATI CODES

FIELD	GROUP	SUB. GR.
17	02	

18. SUBJECT TERMS *(Continue on reverse if necessary and identify by block number)*
Fiber Optic Communication Link
Narrowband Analog Modulation
4.4-5.0 GHz Passband
Single Mode Fiber
Laser
APD Short Wavelength

19. ABSTRACT *(Continue on reverse if necessary and identify by block number)*

A fiber optic link which sets the state of the art (July 1982) in direct optical source modulation in passing a RF carrier and its associated modulation was developed under this Laboratory Director's funded program to Harris Corporation. The 1 kilometer long link has a 600 MHz passband and operates between 4.4 to 5.0 GHz. The gain flatness across the band was measured at ± 1.5 db at a modulation depth of 65%. The input/output VSWR is 1.5 to 1 db. The link employs a 3 state amplifier in the APD receiver and has provided a S/N of 48 db measured over a 300 KHz bandwidth. The S/N can be further improved by additional amplifier stages. Optical componentry within the link includes an injection laser diode operating at a wavelength of 840 nm and a single mode fiber with bandwidth greater than 7 GHz and a core size of 6 micron. The fiber is terminated in a demountable single mode fiber connector with an insertion loss of 1 db. The link in setting the state of the art represents a significant technical breakthrough in RF carrier transmission over fiber optics and is (July 82) the only link of its kind with these system characteristics. Link operation to 6 GHz was

20. DISTRIBUTION/AVAILABILITY OF ABSTRACT
UNCLASSIFIED/UNLIMITED ☐ SAME AS RPT. ☒ DTIC USERS ☐

21. ABSTRACT SECURITY CLASSIFICATION
UNCLASSIFIED

22a. NAME OF RESPONSIBLE INDIVIDUAL
Paul Sierak

22b. TELEPHONE NUMBER *(Include Area Code)*
(315) 330-4092

22c. OFFICE SYMBOL
RADC/DCLW

DD FORM 1473, 83 APR   EDITION OF 1 JAN 73 IS OBSOLETE.

UNCLASSIFIED
SECURITY CLASSIFICATION OF THIS PAGE

Item #19 (Continued)

shown but was amplifier limited. Direct modulation of the long cavity laser used in this link appears viable to 8 GHz based upon data within this report.

Evaluation

This report describes work prformed by Harris Corporation on developement of a feasibility model of a state of the art direct modulation fiber optic communications link which passes modulated carrier signals whose center frequency lies in the 4.4 to 5.0 GHz passband. The first version of the link set the state of the art performance in 1982. The second version of the link had performance which was reduced from that of the first version. The report was delivered 1 year late by the contractor to RADC. Despite these difficulties, material on version one of the feasibility model indicates that fiber optic links can be operated in the microwave arena with useful link characteristics. These link characteristics open new areas of application for fiber optics technology for the military system designer.

Future work will involve evaluation of long wavelength optical sources, comparison of short cavity length laser operation with long cavity length laser operation and systems level exploration of performance at frequencies to 10 GHz. Based upon this work, systems designers will be able to confidently design for the new options made available by this synthesis of fiber optics and microwave technology.

Paul Sierak

PAUL SIERAK
RADC Project Engineer

TABLE OF CONTENTS

PREVIOUS PAGE IS BLANK

TABLE OF CONTENTS (Continued)

TABLE OF CONTENTS (Continued)

LIST OF ILLUSTRATIONS

LIST OF ILLUSTRATIONS (Continued)

LIST OF TABLES

1.0 INTRODUCTION

1.1 Objective

The major objective of RF Fiber Optic Link Program is to investigate the performance attainable by a feasibility model of a simplex, one kilometer long, analog fiber optic communications link having a passband of 4.4 to 5.0 GHz. A feasibility model of the 4.4 to 5.0 GHz link was fabricated to practically determine the attainable performance.

The feasibility model of RF Fiber Optic Link had the following design goals: [1]

Parameter	Design Goals
a. Transmission Mode	Simplex
b. Data Source	Preselector output of AN/TRC-97A
c. Data Sink	TWT Input Part of AN/TRC-97A
d. Passband	4.4 - 5.0 GHz
e. Link Length	One kilometer
f. Signal Degradation	No degradation of signal between preselector output port and TWT input port.

Additional performance requirement:

Instantaneous Bandwidth:	1 - 300 kHz
Radio Modulation:	FM/FDM
Radio Information Channel:	24 Channels plus orderwire
Input Signal Level:	0 dBm

1. SOW Paragraph No. 4.1.

Input Impedance:	50 Ohms
Input VSWR:	2.0:1
Output Signal Level:	0 dBm
Output Impedance:	50 Ohms
Output VSWR:	2.0:1
Operational Wavelength:	0.84 μm
Fiber Optic Transmitter:	ILD Transmitter
Optical Fiber Type:	Single Mod , 125 μm cladding diameter, 6 μm core diameter, glass-on-glass fiber
Fiber Optic Receiver:	APD or MESFET receiver
Signal-to-Noise Ratio (S/N):	45 dB
Intermodulation Product (3rd order):	-45 dBc
Gain Flatness:	$\pm$1.5 dB

1.2 Approach

The program consisted of four phases: a) Feasibility Study, b) Device Analysis, c) Computer-Aided Design (CAD) and Optimization, and d) System Test. Figure 1.2 is a flow chart indicating the relationship of the tasks to each phase and the chronological position of each within the program. The tasks performed in each phase are illustrated as the following:

a. Feasibility Study

- Investigate Injection Laser Diodes (ILD's), Avalanche Photodiodes (APD's), and MESFET's.
- Use of wideband F/O cables
- Applicable conceptual impedance measurement, matching techniques, and modeling

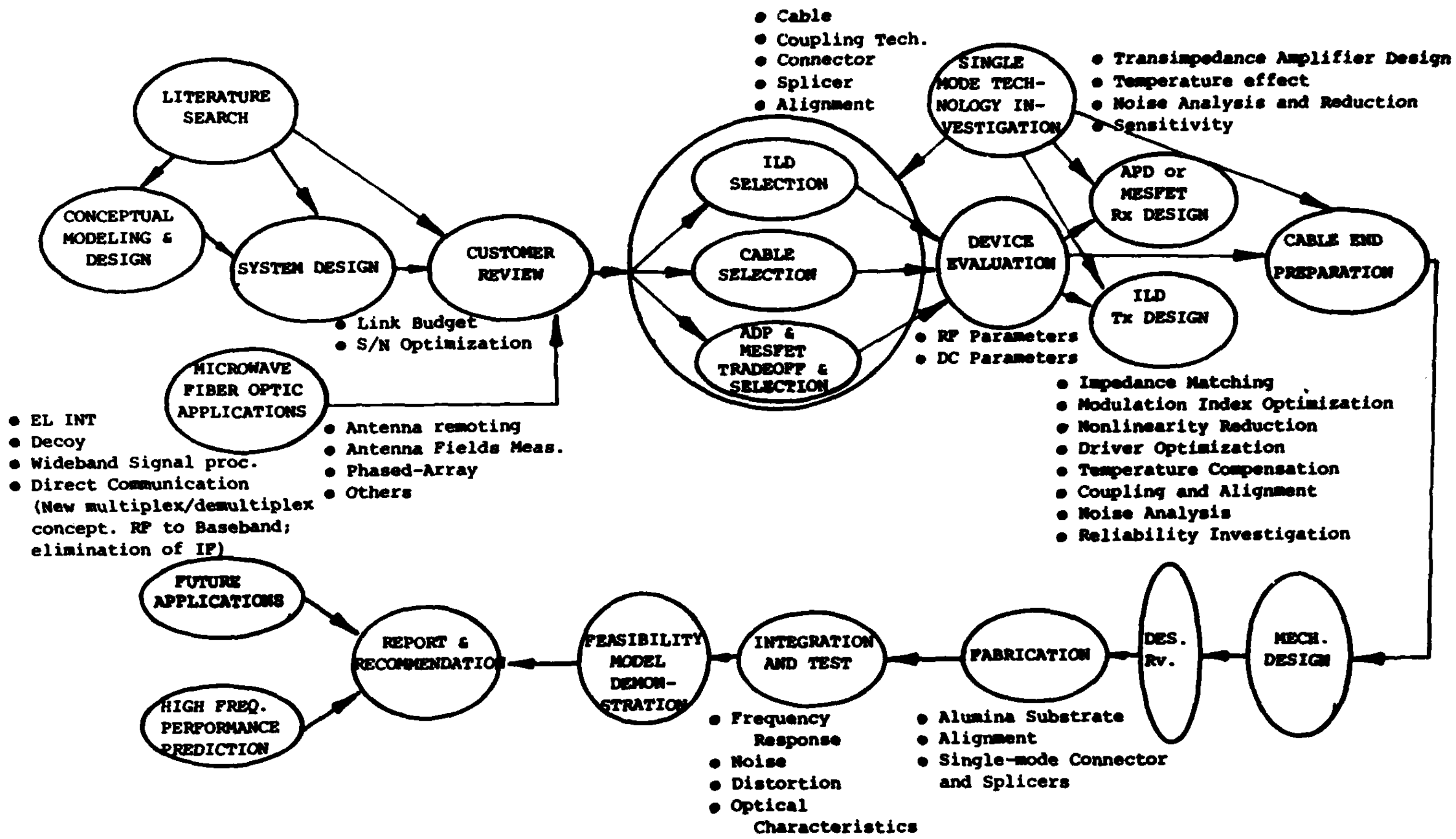

Figure 1.2. The Approach Methodology of RF Fiber Optic Link

- System design
- Customer Review (Key to Feasibility Model Start)

b. Device Analysis

- ILD selection
- Cable selection
- MESFET and APD tradeoffs/selection
- Device evaluation

  Characterize for temperature effects, bias, noise, nonlinearity, frequency response, time delay, etc.

- Single mode technology investigation

c. CAD and System Optimization

- Use of distributive microwave integrated circuit techniques for the Transmitter/Receiver design
- Temperature effects and compensation networks
- Reliability investigation
- Mechanical design
- Utilization of proper test fixtures and impedance matching networks
- Consider the bandwidth, noise figures, gains, gain flatness, group delay, and input/output VSWR's
- Use of automatic network analyzers to perform as many of the above functions as possible
- Alignment problems concerning optical fiber connectors

d. System Test (The Feasibility Model)

- Evaluate system criteria such as signal-to-noise ratio, frequency response, bandwidth, coupled optical power, and all other efforts required to prove the feasibility of the design concepts of the communications link.

- Continual check with component manufacturers as to future development considerations
- Relate upgrading to higher frequency bands
- Review final data, analyze, and highlight risk areas
- Write the final report

1.3 Results

The major accomplishments of the program were:

a. Investigated the applications of RF Fiber Optic Link for radar, communications, electronic warefare, etc.

b. Surveyed the state-of-the-art and commercially available microwave fiber optic devices and components for RF Fiber Optic Systems in microwave frequencies.

c. Designed, fabricated, and evaluated a simplex, one kilometer, wideband fiber optic link at 4.4 - 5.0 GHz. The link, as shown in Figure 1.3, is for AN/TRC-97A tropo-radio decoy application.

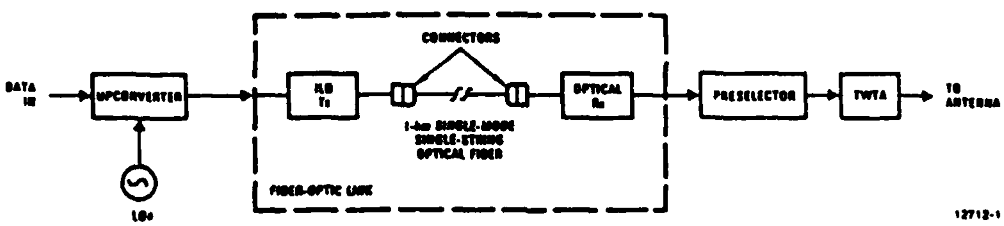

Figure 1.3. Fiber Optic 4.4 - 5.0 GHz Tropo-Radio Decoy Application

1.4 Survey of State-Of-The-Art Wideband RF Fiber-Optic Link

With the rapid growth of solid state optoelectronics and optical fiber technologies, fiber optic communications have progressed into gigabit (Gb/s) digital, and microwave analog systems. Mutually advantageous enhancements in optical fiber and GaAs technologies make the evolution of microwave fiber optic communications more promising.

During this program, state-of-the-art microwave and wideband fiber optic links and components have been surveyed. Table 1.4 summarizes the survey results. Most of these links are digital and use an NRZ format. The 1.1 km, 2 to 6 GHz link was reported by RCA, and performed for the U.S. Air Force Avionic's Laboratory. Since the link has resonant problems near 3.5 GHz, the 4.4 to 5.0 GHz fiber optic link described in this report is believed to be the first useful link operating above 4 GHz with a sufficient signal-to-noise ratio (larger than 48 dB with 300 kHz instantaneous bandwidth).

2.0 FIBER OPTIC LINK APPLICATION

Microwave fiber optics have many attractive immediate applications and, as illustrated in Figure 2.0-1, most of these have been practically implemented. The use of optical fiber to replace the conventional metallic waveguide and coaxial cable is based on the following fiber optic advantages:

- Immunity to EMP and EMI

- Extremely wide operational bandwidith or time bandwidth products (for delay line related applications)

Table 1.4. State-Of-The-Art Microwave and Wideband Fiber Optic Link or Component

SYSTEM/COMPONENT	FREQUENCY	REFERENCE
1. 1.1 km Link Using Single Mode Fiber	2-6 GHz	Cleo '82, April 13-16, 1982 Paper ThFF3
2. ILD and PIN Link	8 Gb/s	Elect. Lett. 19 June 1980, pp. 497-498
3. 0.5 km Single Mode TJS ILD and APD System	5 Gb/s	Applied Optics, November 1981
4. 44.3 km Link Single Mode Fiber 1.3 m ILD, Ge APD	2 Gb/s	Electronic Lett. 25 June 1981 pp. 497-498
5. 5.5 km Link, ILD, APD	2.24 Gb/s	IOOC '81 Post Deadline paper Number TuL5
6. TJS ILD	4.5 GHz	IOOC '81 Paper TuB4
7. GaAs Photodetector 25 percent QE, 10 V	10 GHz (3 dB)	Cleo '82 April 13-16, 1982 Paper ThE2
8. Single Mode Fiber	100 GHz km	IEEE J. QE, p215, 1980

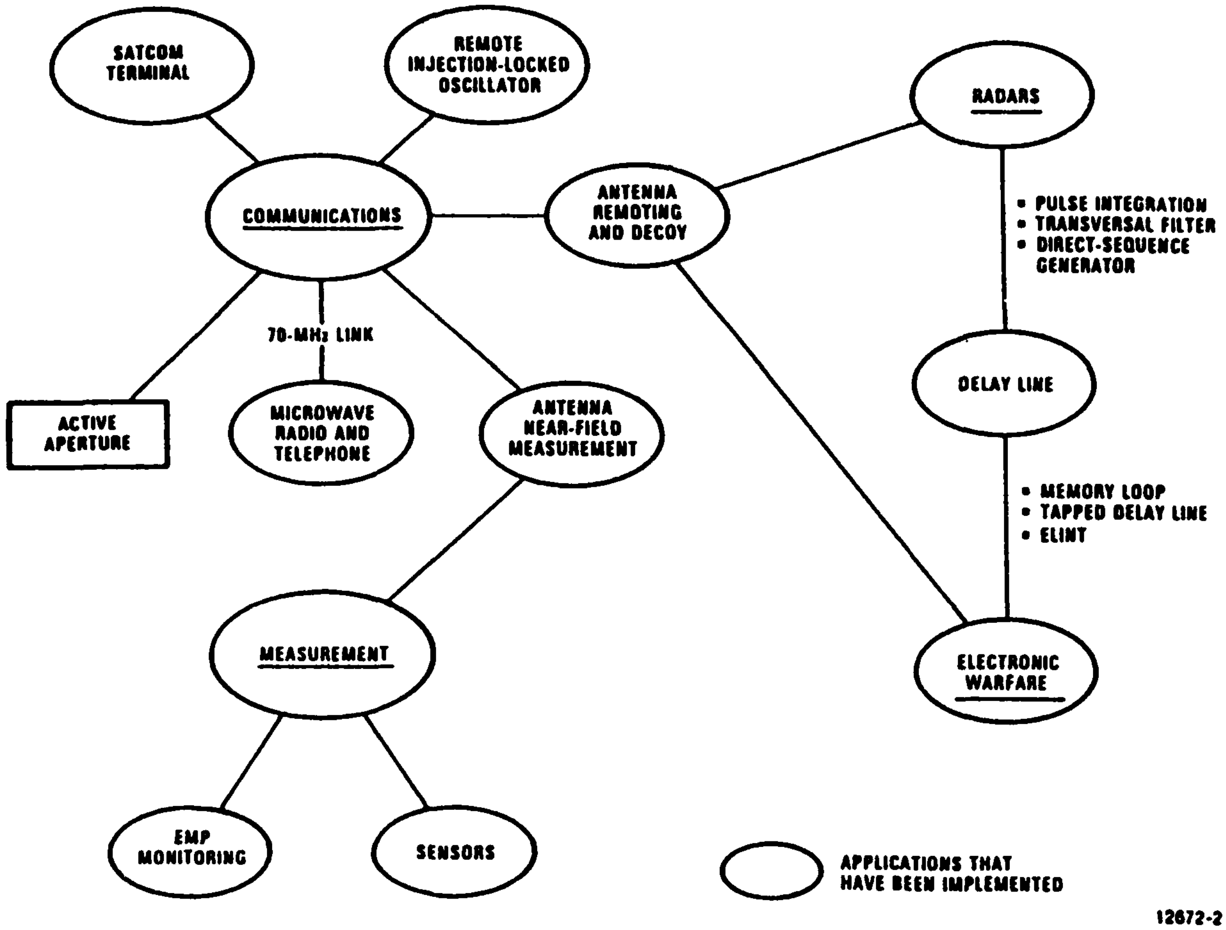

Figure 2.0-1. Microwave Fiber Optic Applications

- No pressurization required
  - In many cases, waveguide or coaxial cable requires pressurization to prevent moisture and dust. The pump and piping add system complexity, increase power consumption, and degrade the system reliability.
- Low temperature effect
- Low weight/size

For microwave radar systems and communications terminals applications, as shown in Figure 2.0-2, fiber optic links can interconnect the Low Noise Amplifier (LNA) to the downconverter and upconverter to the High Power Amplifier (HPA). These terminal fiber optic links also can be applied to radar (or microwave radio) remoting and decoy. The decoy and remoting applications are extremely attractive for minimization of equipment damage and casualties during radiation seeking missile attack.

High resolution radars must be able to process exotic signals with very narrow pulse widths and extremely large Time Bandwidth (BT) products (larger than 10^6). A large BT processing system means good frequency measurement resolution, high sensitivity, and low distortion of collected information. The conventional electronic approach has relatively narrow bandwidth and limited time delay which distort's the spectral analysis and pulse parameter measurement. SAW (Surface Acoustic Wave) components, CCD's (Charge Coupling Devices), Bragg cells, and GaAs giga-bit logic have performance disadvantages and fabrication complexities. The wideband optical fiber not only can be utilized to construct a delay line and a tapped delay line, which performs a matched filtering function for RF Radar, but also for optical radar processing.

2.1 The Time Delay of Optical Fiber

The optical fiber consists of a core having a refractive index n_1, and surrounded by a cladding having an index n_2. Since the light propagates in the core, then the group velocity should be expressd as

$$V/c = \frac{1}{n_1} \tag{2.1}$$

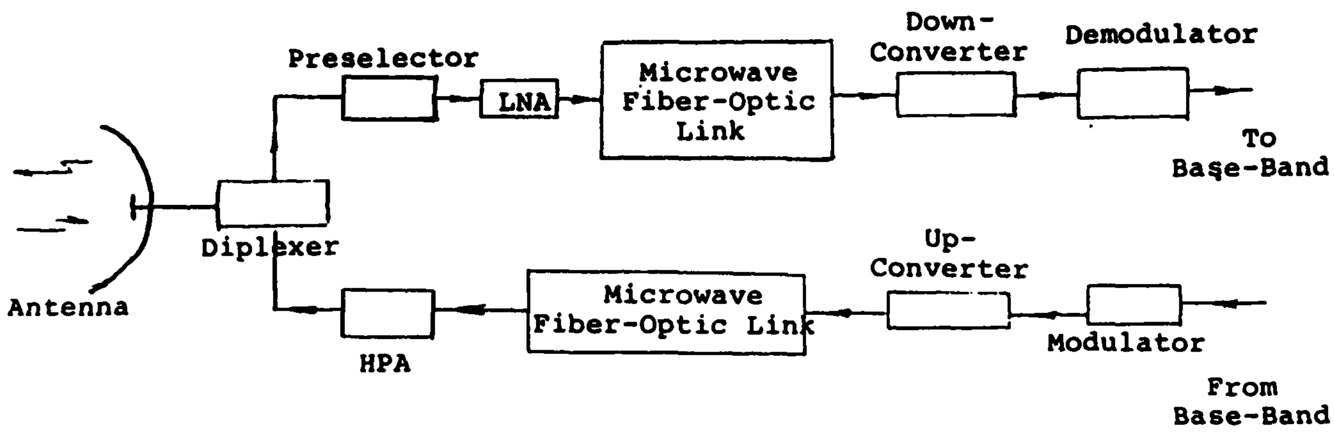

LNA: Low Noise Amplifier

HPA: High Power Amplifier

Figure 2.0-2. Microwave Fiber Optic Application for Radar and Communication Systems

where n_1 is frequency dependent and varies with optical wavelength and is velocity of light. If the core refractive index is about 1.5, then the propagation delay is approximately 5 μs/km. Because n_1 is changing with frequency and material dispersion, the group delay of a single-mode fiber varies with wavelength according to Equation (2.1).

$$S = \frac{-L}{\lambda C} \quad \frac{\lambda^2 d^2 n}{d\lambda^2} + 4nV \frac{d^2 (Vb)}{dV^2} \tag{2.2}$$

where b is the waveguide parameter. For example, a 10 km single mode silica fiber has 2 GHz bandwidth and 100 μs time delay at 0.85 μm wavelength, and 12 GHz bandwidth and 100 μs time delay at 1.06 μm.

Both single mode and multimode fibers have recently achieved less than 1 dB/km insertion loss at wavelengths of 1.06 μm and 0.9 μm, respectively. The OH radical concentration has been reduced to less than 50 ppb and the minimum transmission loss of the multimode fiber was 0.2 dBm/km at 1.3 and 1.55 μm wavelength. The 3 dBm bandwidth of single mode fiber currently exceeds 10 GHz/km. Graded index multimode fiber has 3 GHz/km bandwidth while step index fiber has approximately 400 MHz/km. In the near future improvements in the material dispersion of glass may allow single mode bandwidths well above 100 GHz at 1 km length.

The dispersive characteristics of the single mode fiber may offer the possibility of realizing pulse compression filters for linear frequency modulated (chirp) signals for optical radar.

2.2 Microwave Fiber Optic Signal Processing: Examples

When the electronic information is converted to optical information and coupled into one end of the fiber and converted back to an electronic signal at the other end, the optic fiber can serve as a delay line. Since it possesses long delay and low-loss over a wide bandwidth, the fiber delay line can have the following radar and EW applications:

- Pulse-to-Pulse integration to supress clutter.

- Wideband Tapped Delay Line, transversal filter, and matched filter.
- Electrooptic generation of pseudorandom binary sequences.
- Electrooptic analog-to-digital converter.
- Recursive electrooptical integration of high resolution radar return.

2.2.1 Signal Processing: Pulse-to-Pulse Integration for Radar and ELINT Signal Processing

Radar detection of targets in clutter can be improved by reducing range-cell size (increasing the range resolution) so that the total amount of clutter within one range cell is much smaller than the target cross section. Thus, when targets to be detected are small, such as tactical missiles, small boats, etc., the signal bandwidth must be large (>500 MHz). Additional clutter suppression can be achieved by pulse-to-pulse integration of the radar returns. If the itegration is coherent (i.e., phase information is preserved), the gain in signal-to-clutter ratio is proportional to the number (N) of pulses integrated. For noncoherent integration, the gain is approximately proportional to N. Pulse-to-pulse integration of wideband radar returns has generally not been feasible because there has been no technique for storing wideband (>500 MHz) signals for long (approximately 200 μs) interpulse periods. SAW's Bragg cells folded meander lines, and YIG crystal delay lines cannot fulfill the system time-bandwidth requirements for the high performance wideband radars. However, fiber optic delay line can be used to store wideband signals, and to integrate high resolution radar returns on a pulse-to-pulse basis.

The fiber optic pulse-to-pulse integration is illustrated in Figure 2.2.1-1. The total delay through the ILD driver, optical fiber and detector/amplifier combination is matched to the interpulse period so that radar signals (or echoes) from the same range cell appear at the amplifier outputs at the same time and are integrated. A simpler circuit for performing pulse-to-pulse integration may be fabricated in the fashion shown in Figure 2.2.1-2.

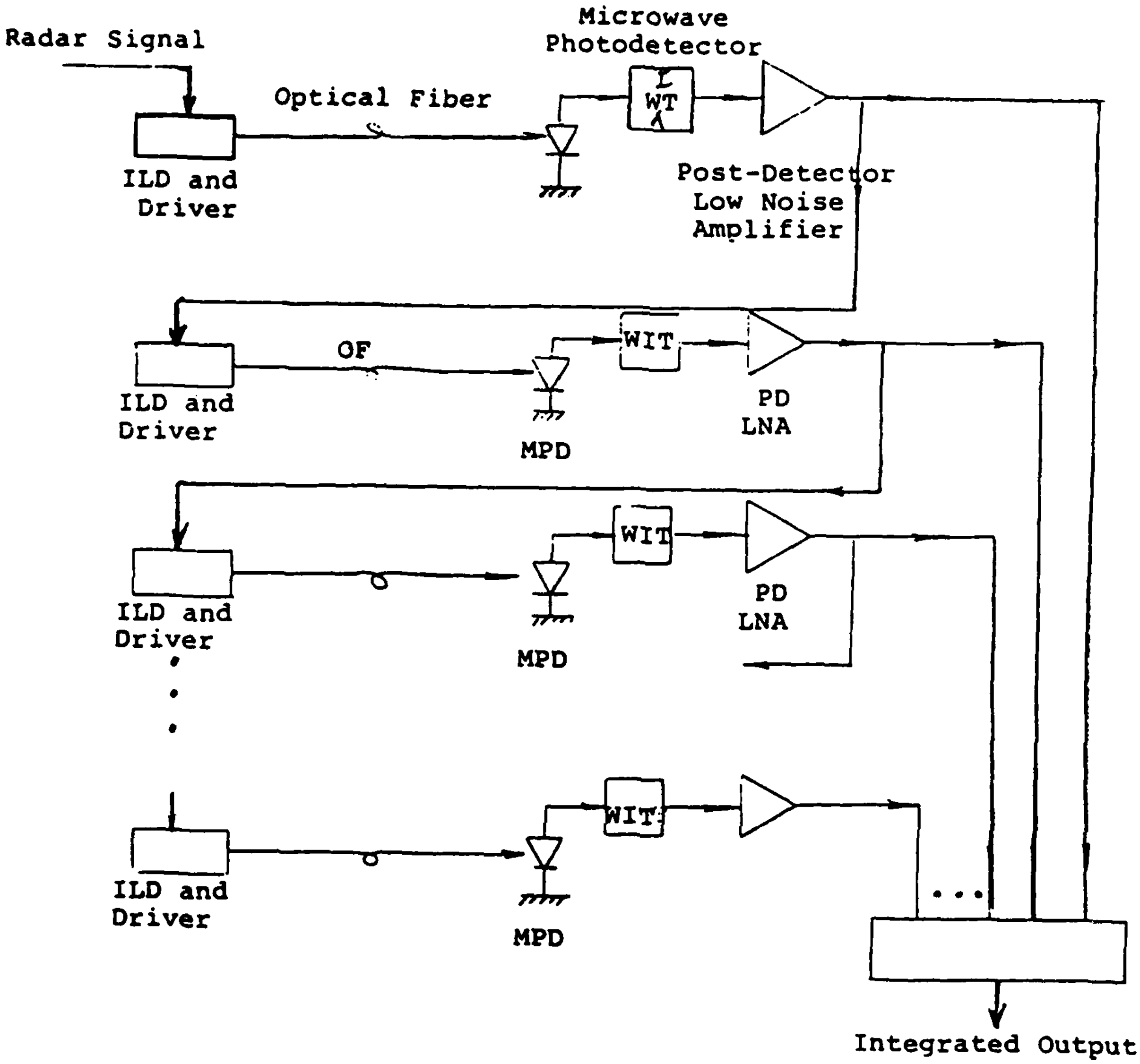

ILD:	Injection Laser Diode
OF:	Optical Fiber
MPD:	Microwave Photodetector
WIT:	Wideband Impedance Transformer
P.D. LNA:	Post Detector Low Noise Amplifier

Figure 2.2.1-1. Block Diagram of Pulse-to-Pulse Integration of High Resolution Radar (or ELINT Collection System) Using Fiber Optic Delay Lines

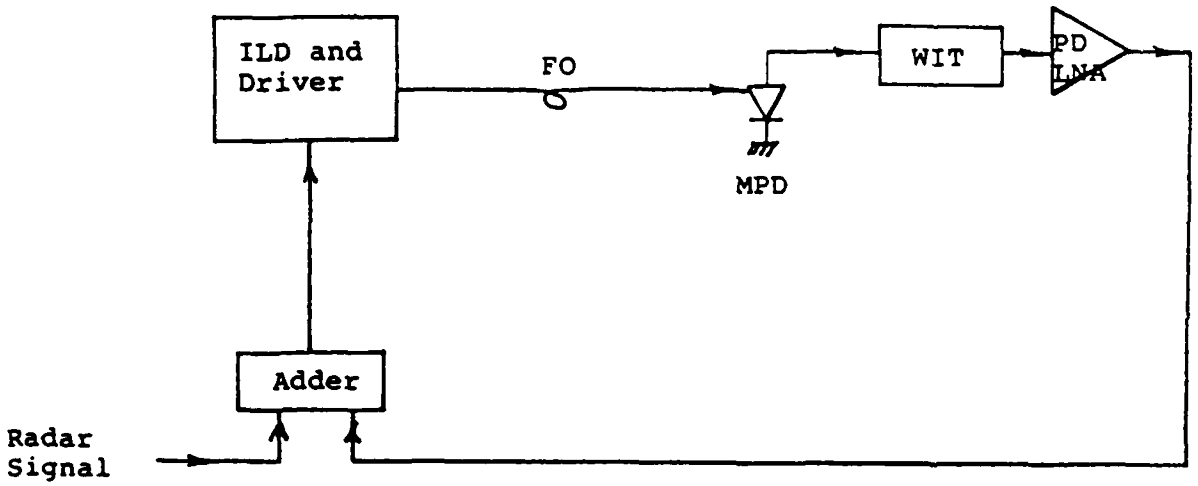

Figure 2.2.1-2. Recursive Integration of High Resolution Radar Using Fiber Optic Delay Lines. (Abbreviations are as shown in Figure 2.2.1-1.)

2.2.2 Wideband Tapped Delay Lines, Transversal Filter and Matched Filter

Many radar, adaptive phased array antenna, spread spectrum, ELINT, and noise reduction applications require filtering and correlation functions in signal processing. These filters and correlators often take the form of tapped delay lines with specified weights at each tap. Figure 2.2.2-1 depicts the block diagram of a typical tapped delay line using an injection laser diode, wideband single mode optical fibers, fiber optic variable attenuator, weighting networks, and a summer. For radar application, the detection of a target by high resolution radar can be enhanced by spatial matched filtering when the radial dimension of the target is large compared with the range resolution. If a tapped delay line is implemented so that the dalay between taps corresponds to the distance between scatters and the attenuation (weight) at each tap corresponds to the scatter cross section, then this "matched" filter will increase the SNR and enhance detection. For rada having a range resolution of one foot, the required tap spacing accuracy easily can be met using several fibers cut to te appropriate lenghts, or a single fiber tapped by reduction of cladding diameter by etching. Similar applications can be applied to the adaptive phase array antenna signal processing. Figure 2.2.2-2 illustrates an application of the transversal filter in the multifunction phased array antenna.

2.2.3 Key Fiber Optic Components for Microwave Signal Processing

The key components for fiber optic signal processing consists of an optical source, detector, fiber, directional coupler, switch, variable attenuator, modulator, etc. The single individual fiber is preferred rather than the fiber bundle for simplicity and low cost.

The fiber attenuation can be varied by adjusting the axial spacing between two fiber ends. A mechanically operated single fiber switch has been fabricated and demonstrated with 0.5 to 2.0 dB insertion loss. Variable attenuators offer the flexibility of amplitude adjustment. Since fiber diameter is small, the size of the bundle is not prohibitive; also, the tap spacing can be located very accurately. With the tapped delay line performing as a "matched filter", it not only improves S/N of ELINT recognition and identification processes, but also has the capability to increase range resolution of high resolution radar.

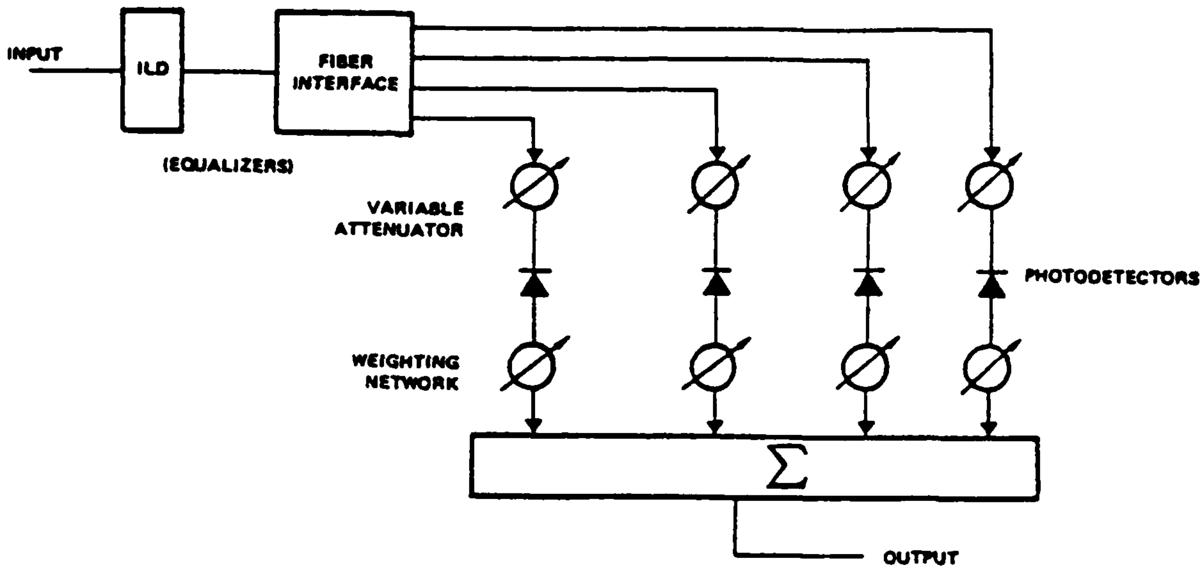

Figure 2.2.2-1. Fiber Optic Wideband Tapped Delay Line for Microwave Signal Processing

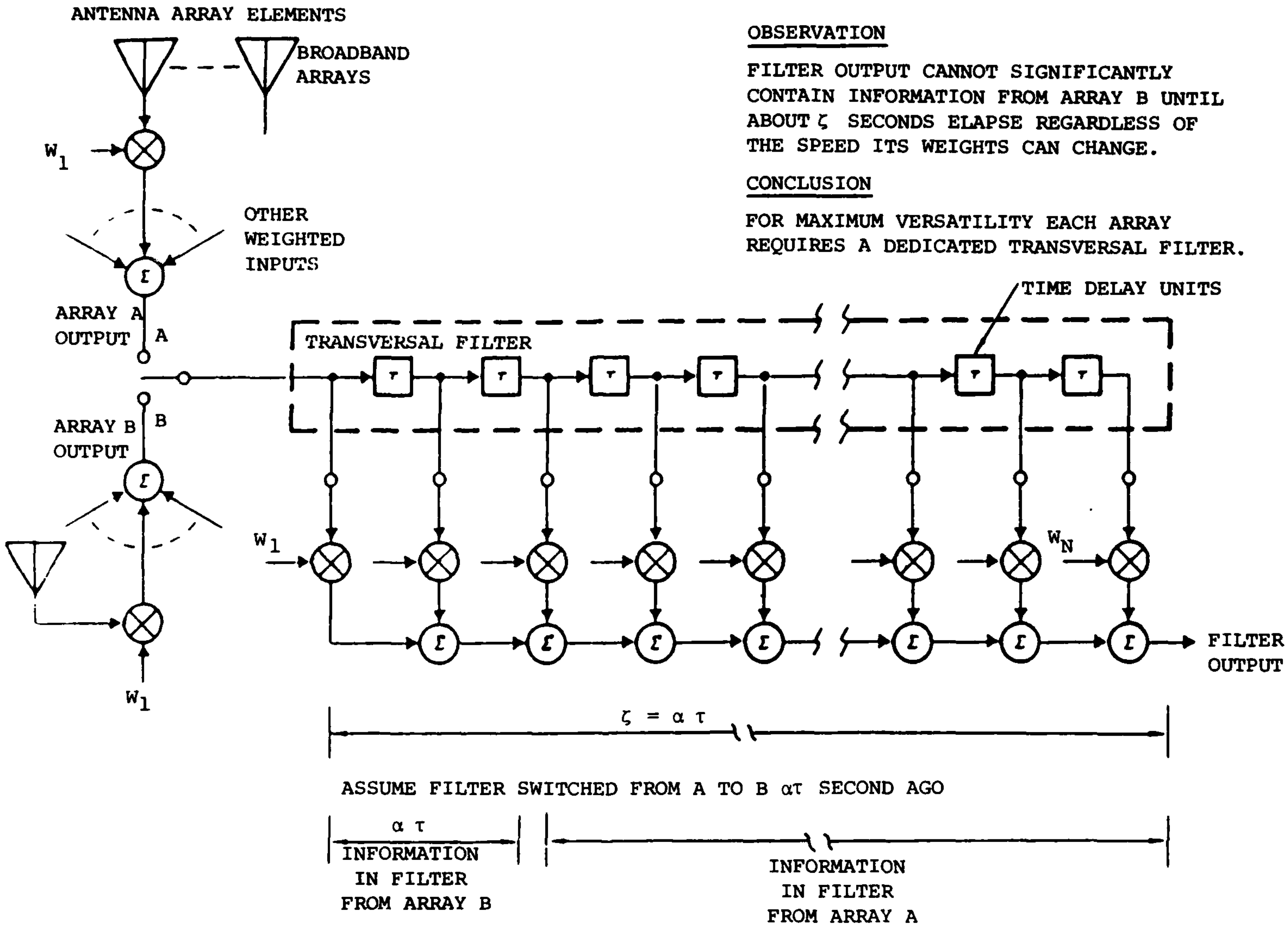

Figure 2.2.2-2. Fiber Optic Delay Lines Can Operate as the Transversal Filter for High Performance Phased Array Antenna

2.3 ELINT Applications

ELINT collection systems have focused on monitoring and recording sorting parameters such as frequency, pulse width, and pulse repetition interval to derive intelligence information. In sparse radar environments, this task could be performed fairly simply. As emitters became more numerous, sorting parameters had to be expanded in order to differentiate between radars belonging to the same general class. Also, new sophisticated emitters which may have one or more of the following characteristics have become available:

- Intentional frequency modulation on a pulse
- Submicrosecond or nanosecond pulse width
- Frequency agility

The system designer not only had to design an ELINT receiver using advanced technology which could process wideband signals without adding receiver distortion, but also needs good receiver sensitivity and frequency resolution. Moreover, as IF bandwidth increases, signal traffic increased and deinterleaving and pulse overlap becomes more of a problem.

As described previously, the optical fiber provides a very large time-bandwidth product and a very wide bandwidth. It is attractive to use optical fiber to construct for advance ELINT receiver the following:

- Delay Line/Variable Delay Line
- Matching Filter
- Transversal Filter/Tapped Delay Line

In addition to the bandwidth advantage, these fiber optic components also have the following attractiveness:

- Excellent reproducibility
- Low weight
- Small size

- Large dynamic range
- Wide design flexibility

2.4 Communication/Radar RF Applications

Using the ILD transmitter and an APD (or MESFET) receiver, the fiber optic link is capable of transmitting more than 20 channels of high quality video signals. Both CATV and C-band TVRO (TV Receive Only) have been demonstrated using fiber cable. Conceivably, the FO link will even become more attractive for K-band (12 GHz) TVRO, high definition TV channels, as well as the SBS (Satellite Business Systems) operation, in the near future.[1] Jamming resistance microwave and millimeter wave communications and target acquisition systems can directly transmit information at the RF frequencies through fiber to minimize transmission losses and improve S/N and dynamic range.[1] Wideband fiber optic hydrophones and sensor arrays also offer potential improvements in sensitivity, noise rejection, EMI/EMP resistance, versatility, ruggedness, and reliability over conventional sensors.[1]

Many sophisticated microwave radio, radar, and satellite communications (SATCOM) terminals are designed toward higher frequency, lower cost, high reliability, remote operation, and lower maintenance. Particularly, the millimeter wave and military microwave systems require a wide bandwidth, either to accommodate high data rate, or to use wideband frequency hopping and/or PN spread for jamming resistance.[1] Conventionally, the radar/radio/SATCOM terminals have been designed with the Low Noise Amplifier (LNA) output signal routed by coaxial cable or waveguide, from the back of the antenna to the downconverter located some distance away from the antenna. The extra length of waveguide or coaxial cable causes interface losses, degraded VSWR, and group delay distortion, which decrease the performance of phase modulated or frequency modulated systems. These problems can be eliminated when the coaxial cables are replaced by a fiber optic link. The use

1. J. J. Pan, "Microwave Fiber Optic Communications Systems:, 1981 National Telecommunications Conference, Nov. 29 to Dec. 2, 1981, New Orleans, LA.

2. J. J. Pan, "1 GHz 1 km Fiber Optic Link for Satellite Communication Integrated Terminals", 1981 International Conference on Communications, June 14-17, 1981, Denver, Colorado.

of fiber optics as the transmission line media is very attractive in the microwave systems applications for the following reasons:[1]

- Does not generate, not is it susceptible to EMI.
- Complete electrical ground isolation is achieved. It eliminates ground loops that plague systems with long-distance remote antennas and provides high-voltage (lightning) isolation.
- Provides some transmission security without steel conduit, therefore, reducing installation cost.
- Eliminates crosstalk
- Eliminates short circuit loading, ringing, and spark/fire hazards.
- Extremely flat bandwidth over the desired signal range.
- Provides ready break detection of cut fibers.
- Being a no-loss, no-gain link, a low dynamic range, and therefore, less expensive downconverter and demodulator, are utilized in the overall system design.
- Gain in the Low Noise Amplifier (LNA)/downconverter combination is reduced, therefore, reducing potential compression and isolation problems with high-gain front ends.

2.5 Many Other Optical Fiber Optic Applications

Compared to metallic waveguides and coaxial cables, optical fibers have small size, low loss, wide bandwidth with extremely flat frequency response and, being unsusceptible to EMI, prove to be far superior to the conventional approaches

1. J. J. Pan and D. E. Halley, "Fiber-Optic Links for Microwave and Satellite Communication Terminals", 1976 National Telecommunication Conference, Dallas, Texas, Nov. 1976.

to radar/radio remoting, decoy, and microwave signal processing. Some additional attractive applications include:

- Gyroscope, or Rotation Sensor
  - Wideband rotation sensing provides high measurement resolution and accuracy
- EMP Monitoring
  - The dielectric glass fiber offers a minimal perturbation to electromagnetic fields and thus has excellent monitoring accuracy.
- Antenna Near-Field Measurement
  - Nearly o EM field distortion.
- Remote injection-locked oscillator, or local oscillator distribution
  - Low Cost
  - No noise pick-up and is not susceptible to EMI

3.0 SYSTEM DESIGN

3.1 System Design Criterion

The design of a microwave fiber optic system must consider the following design criteria:

- Noise
  - System signal-to-noise ratio (S/N)
  - Laser diode noises
  - Transmission media noises
  - Post-detector amplifier noises

- Frequency response and flatness
  - Frequency responses of laser diode, laser driver, photodetector, and post-detector amplifier.
  - Optical cable bandwidth
  - AM-to-PM conversion caused by gain flatness
- Nonlinearity Distortion
  - Harmonic and IMP (Intermodulation Product) distortions caused from laser diode and amplifiers.
- Delay Distortion
  - Nonlinear delay distortion in laser diode, photodetector, and amplifier.
- Impedance Matching
  - *Impedance matching affects the system input/output VWSR*, system noise, and modulation/detection efficiency.

3.1.1 System Noise/Nonlinearity

All of the microwave FO systems, including analog, digital, and delay line applicabions, must have sufficient system S/N over the desired bandwidth to ensure proper performance. In the absence of laser diode noise, the S/N is defined as:

$$S/N = \frac{\text{Input Signal Power (Peak)}}{\text{Equivalent Input Noise Power (rms)}} \tag{3.1}$$

$$= \frac{(m\ r\ G\ P)^2}{2q\ B_n\ [rG^{2+\alpha}\ P_B + r\ G^{2+\alpha}\ P + I_s\ G^{2+\alpha}\ I_b]\ I_a^2}$$

where m = modulation index, r = unity gain responsivity of the photodetector, G = mean avalanche gain of the APD or mean amplification gain of the MESFET photodetector, P = average optical power incident on the photodetector, q = charge on an electron, B_n = information bandwidth, α = excess noise factor of the photodetector, I_b = bulk or multiplied leakage current component of the photodetector dark current, I_S = surface or nonmultiplied leakage current component of the photodetector dark current, and I^2 = mean-square amplifier noise current referred to the amplifier input. For microwave and high data rate systems, m, r, G, and P are all functions of the frequency. The performance of wideband analog fiber optic systems is also sensitive to nonlinear distortion, delay distortion, system frequency response and flatness, and impedance matching. Each component, as depicted in Table 3.1.1, affects the various system performances. Component nonlinearities cause harmonic and intermodulation product distortion, and the response flatness causes the AM-to-PM conversion. The input/output VSWR's, noise, and modulation and detection efficiencies are determined by the FO transmitter/receiver design and impedance matching.

Table 3.1.1. Microwave System Parameters Affected by Individual FO Components

PARAMETERS / COMPONENTS	NOISE	NONLINEARITY DISTORTION	FREQUENCY RESPONSE FLATNESS	INPUT/OUTPUT VSWR
Optical Source Driver	*	**	**	**
Optical Source	*	***	*	-
Fiber Cable/Connector/ Splice	*	-	*	-
Optical Detector	***	*	*	-
Postdetector Amplifier	**	**	**	**
Bias Circuits	*	*	*	*

- = No Effect
* = Minor Effect
** = Influential Effect
*** = Dominant Effect

Nonlinearity distortions and noise are severe problems for broadband, microwave analog, and Gb/s digital systems. Causes and solutions are described separately in the following two paragraphs.

3.1.1.1 Optical Transmission Channel Noise

There are four basic noise sources associated with the fiber optic transmission channel for microwave modulation.[1]

1. Laser Noise - Total intensity fluctuation emitted by the laser diode. this noise is caused by a reflection of optical power back into the laser resonator from laser/fiber interfaces. The phase, amplitude, and frequency of the reflections all contribute, either constructively or destructively, to laser emission.

2. Partition Noise - Individual wavelength intensity variations with constant total spectral intensity.[2] As a multimode laser is modulated, the intensity of each wavelength can fluctuate, redistributing its energy to other modes. Prerequisites for partition noise are:

   a. multimode (longitudinal) emissions from the laser,

   b. individual mode amplitude fluctuations, and

   c. wavelength dependent losses within the transmission channel.

   These modal intensity perturbations are influenced by laser thermal conditions, signal reflections into the laser diode resonator, aging, operating point, and other ILD related conditions.

1. E. J. Miskovic, "Optical Transmission Channel Noise Phenomena for High Bit Rate Fiber Optic Systems", Electro-Optics/Laser '79 Conference, Anaheim, California, October 1979.

2. Y. Okano, et al., "Laser Mode Partition Noise Evaluation for Optical Fiber Transmission", IEEE Trans. on Communications, February 1980, pp. 238-243.

3. Modal Noise - Undesired modulation of guided light intensity arising from multipath effects in a multimode fiber. The speckle pattern of the multi-mode fiber randomly fluctuates with time at the spatial filter (output) plane, under three conditions:[1,2,3] 1) a source spectrum sufficiently narrow (i.e., a coherence time sufficiently long) to permit light guided in different modes to interface at the fiber output plane; 2) some form of spatial filtering at the output plane, such as would occur with a misaligned connector, splice, coupler, or splitter which limits the power passing beyond that plane; and 3) either a source wavelength shift or movement of the fiber or both.

4. Delay Noise[4] - Jitter in the time of arrival of optical pulses transmitted through long optical fibers. This delay noise may significantly deteriorate the bit error rate of high date rate systems.

Both electronic compensation[5] and optical feedback[6] methods have been applied to minimize the noises in the ILD. Unfortunately, none of them is practical for high frequency, long distance operation. Some system design considerations for efficiently reducing the ILD noises are given in Table 3.1.1.1.

1. E. G. Rawson, et al., "Frequency Dependent of Modal Noise in Multimode Optical Fiber", J. Opt. Soc. Am, August 1980, pp. 968-976.

2. K. I. Kitayama, et al., "Mode Conversion at Splices in Multimode Graded-Index Fibers", IEEE J. of Quant. Elect., September 1980, pp. 971-978.

3. J. W. Goodman and E. G. Rawson, "Statistics of Modal Noise in Fibers: A Case of Constrained Speckle", Opt. Lett., July 1981, pp. 324-326.

4. E. J. Miskovic, "Optical Transmission Channel Noise Phenomena for High Bit Rate Fiber-Optic Systems", Electro-Optics/Laser '79 Conference, Anaheim, California, October 1979

5. A. Dandridge and A. B. Tveten, "Noise Reduction in Fiber Optic Interferometer Systems", Appl. Opt., 15 July 1981, pp. 2337-2339.

6. C. Baack, et al., "Modal Noise and Optical Feedback in High-Speed Optical Systems at 0.85 um", Elect. Lett., 17 July 1980, pp. 592-593.

Table 3.1.1.1. Laser Diode Noise Reduction Approaches

NOISE TYPE	NOISE REDUCTION APPROACHES
Laser Noise	• Use of an optical isolator • Reduction of the coupling efficiency between ILD and optical fiber
Partition Noise	• Use of a single mode ILD
Modal Noise	• Use of a single mode fiber (the best approach) • Reduction of the total number of connectors, splices, couplers, and splitters • Improve the connector and splice alignment • Use of the multimode fiber with a large number of modes • Optimization of the coupling between fiber and photodetector • Use of an ILD with broad spectral width
Delay Noise	• Thermal stablization of ILD • Use of a broadband optical fiber

Conclusively, the best approach in microwave fiber optic design is to use a temperature stabilized single mode ILD, a single mode fiber cable, and an optical isolator.

3.1.1.2 Nonlinearity Minimization

The nonlinearity of fiber optic systems arises from the ILD, the ILD driver, and the postdetector amplifier. Proper transistor selection and circuit design can significantly improve the linearity of an ILD driver and postdetector amplifier. The inherent nonlinear junction capacitance, power versus current relationship, and thermal gradient of the ILD create undesired harmonics and IMP's.

Linearization approaches such as:

- Feedback control
- Feedforward[1]
- Quasi-feedforward[2]
- Balanced compensation[3]
- Circuit predistortion[4]

have been explored by many authors. Unfortunately, any one of these techniques will involve a precision fabrication process or expensive characterization procedures and components. This report introduces an inexpensive "antiseries" push-pull technique[5] to reduce ICD nonlinearity. As depicted in Figure 3.1.1.2, a compensation diode of opposite polarity is inserted in RF series wth the ILD. The direct currents through the diodes are in parallel and are independently adjustable. Without nonlinear compensation, the second- and third-order IMP's of a two-tone test are 24 dB below the carrier. With the compensation network, IMP's better than 60 dB below the carriers were obtained.

3.2 Design Analysis and Approach

The approach and procedure of microwave fiber optic hardware design, fabrication, and evaluation is illustrated in Figure 3.2. The major tasks of design including devices (electrical devices, optical devices and optical fiber)

1. J. J. Pan, "Temperature Effects on Military Fiber Optic Systems", Electronics Expo '78, Anaheim, California, 14-16 November 1978.

2. J. Straus and O. I. Szentesi, "Lineratization of Optical Transmitters by a Quasi Feed Forward Compensation Technique", Elect. Lett., 17 March, 1977, pp. 158-159.

3. J. Straus, et al., "Phase-Shift Modulation Technique for Linearization of Analogue Optical Transmitters", Elect. Lett., 3 March 1977, pp. 149-150.

4. K. Asatani and T. Kimura, "Linearization of LED Nonlinearity by Predistortions", IEEE Trans. on Elect. Devices, February 1978, pp. 207-212.

5. U.S. Patent 4,032,802.

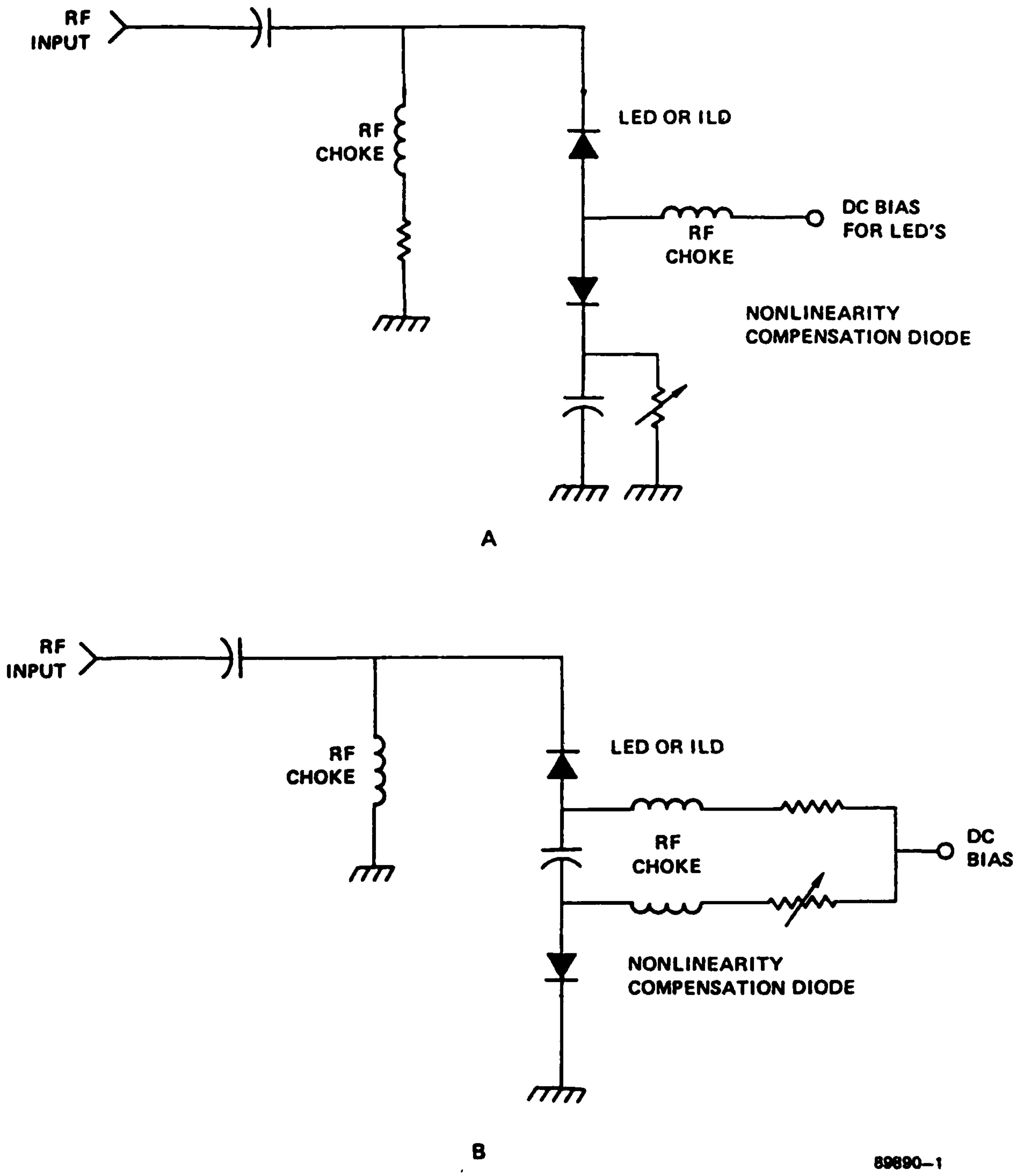

Figure 3.1.1.2. Schematic Diagram of "Antiseries" Compensation to Reduce ILD and LED Nonlinearity

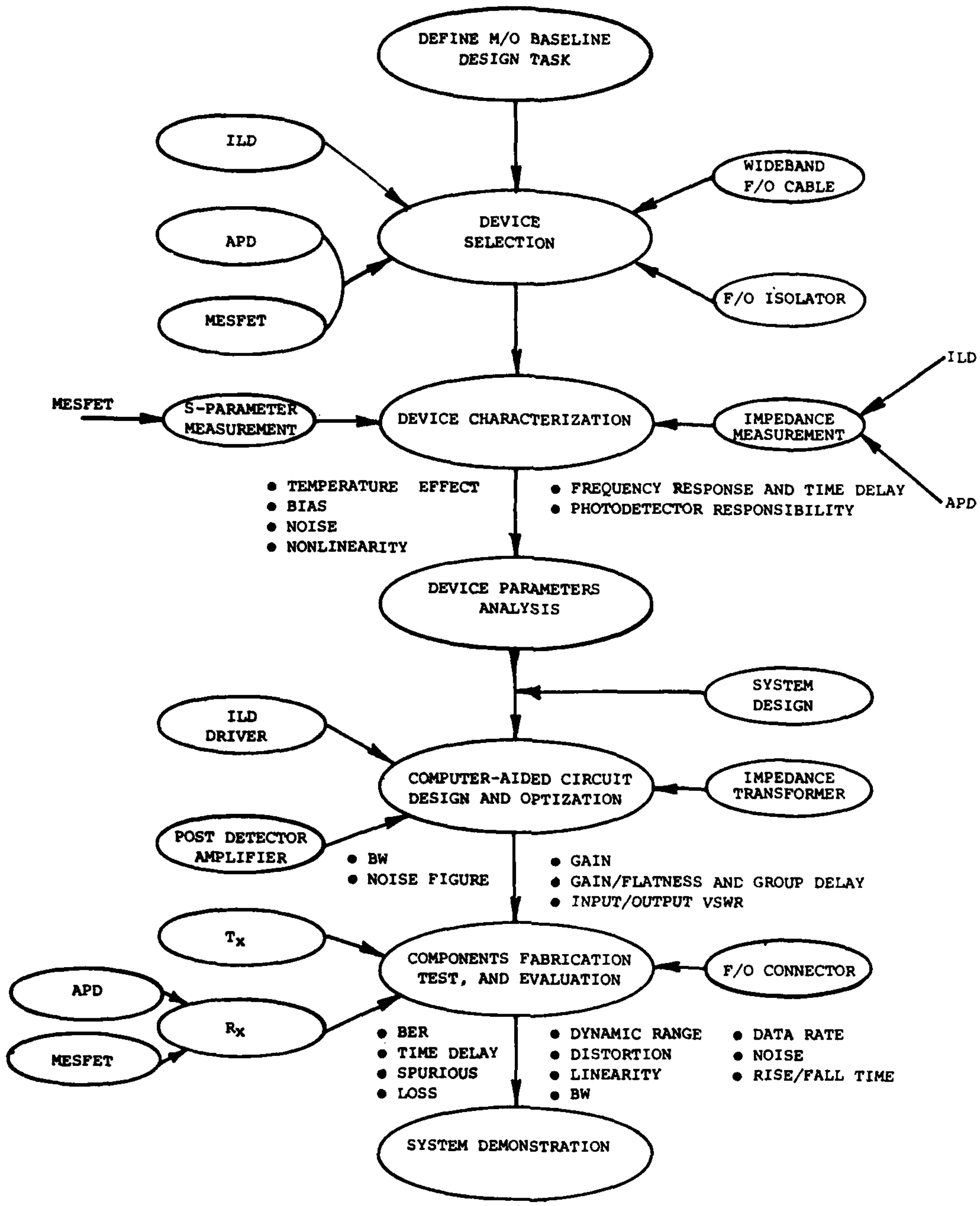

Figure 3.2. Procedure of Microwave Fiber Optic Hardware Design, Fabrication, and Evaluation

selections, devices characterization and computer-aided circuit design and optimization. The detail description of each of those tasks will be presented in Sections 4 through 7.

3.2.1 Long Wavelength versus Short Wavelength Operation

The reduction of optical loss in silica fibers has stimulated in the development of long wavelength in GaAsP/InP lasers, in addition to short wavelength GaAlAs/GaAs lasers. Two wavelength regions, 0.8 - 0.9 and 1.1 - 1.6 μm, are attractive for microwave fiber optics and can be used with fiber losses of approximately 1 - 2 dB/Km and 0.2 - 0.5 dB/Km, respectively. The long wavelength (1.1 - 1.6 μm) range is growing in popularity for telecommunication applications, because of the minimum attenuation, nearly zero material dispersion, and high radiation resistance. Low material dispersion means the fiber will have little pulse spreading and wide operational bandwidth. However, during the beginning of this contract, the performance of long wavelength laser diode was very uncertain. Particularly, there was not sufficient data on long wavelength laser diode lifetime and frequency response to predict whether it could be operated in the 5 GHz range. Also, no InGaAsP/InP long wavelength photodetectors were commercially available at that time. Ge avalanche photodetectors were available, but have the disadvantage of high dark current which degrades the total system S/N. Therefore, the short wavelength at 0.84 μm region was selected for 4.4 - 5.0 GHz fiber optics study.

3.2.2 Strongly Guided Laser Diode, Weakly Guided Laser Diode and LED

Both LED's laser diodes have been used in fiber optic telecommunication. LED's have operated up to 800 MHz, but are definitely not feasible for microwave application.

Recent work of laser diodes have centered on sophisticated structures for truly single frequency operation, which will permit the long distance transmission of high frequency and high data rate signals without fiber dispersion penalties. The structures in which single transverse mode operation have been demonstrated include a variety of waveguiding geometrics (strip-buried, plano-convex-buried, planar-buried, buried-crescent, and ridge waveguide) design. These waveguide

geometric structures may offer advantages in fabrication and performance. The buried hetrostructure and the buried crescent lasers have strong index guiding for field confinement and have low threshold current (I_{th}: 10 - 20 mA). At the beginning of this program, the strongly guided laser diode was not commercially available. The available laser diodes were in stripe, channel substrate or ridge configuraion. These three types have weak index guiding which yields a large number of modes and, hence, the potential for higher output; more importantly, they are also easy to fabricate.

The multimode laser is feasible for microwave fiber optics, over short distances, because reflection noise is reduced when the spectral width of the carrier wave is broad.[1] Of course, single mode lasers are desirable for microwave or ultra-high-speed systems employing conventional single mode fibers. Recently, high power (>50 mW) and low threshold ($\leq$20 mA) have been demonstrated in a double channel, planar, buried heterostructure laser having an effective current confinement scheme which allows continuous operation to 130^{o} C[2] and definitely would be beneficial to microwave fiber optics development.

3.2.3 Single Mode Fiber versus Multimode Fiber

With extremely close control of the deposition process, the MCVD (Modified Chemical Vapor Diposition) and OVD (Outside Vapor Disposition) process can fabricate multimode fiber with several GHz/km bandwidth (9.7 GHz/km at 1.3 μm[1]). However, commercially available multimode fibers have bandwidth specification lower than 1.2 GHz/km and are definitely not feasible for 4.4 to 5.0 GHz application.

1. R. E. Epworth, "The Phenomenon of Modal Noise in Analogue and Digital Optical Fiber Systems", in Proc. 45h Europ. Conf. Opt. Commun., Genoa, Italy, Sept. 1978, Paper X.1: also K. Peterman and G. Arnold, "Noise and Distortion Characteristics of Semi-Conductor Lasers in Optical Fiber Communication Systems", IEEE J. Quantum Electron., vol. QE-18, pp. 543-555, Apr. 1982.

2. I. Mito, M. Kitamura, Ke Kobayashi, and Ko Kobayashi, "Double-Channel Planar Buried Heterostructure Laser Diode With Effective Current Confinement", Electron, Lett. vol. 18, pp. 953-954, October 1982.

Single mode fibers have shown slightly less transmission loss than multimode fibers because the lower dopant concentration in the core favors lower rayleigh scattering loss. The ultimate bandwidth of a single mode fiber is extremely large because of the absence of intermodal dispersion, especially if it is excited by a single mode (single frequency) laser at the chromatic dispersion minimum.[2] Therefore, the single mode optical fiber was selected for the RF Fiber Optic Link Study at 4.4 - 5.0 GHz modulation frequency.

3.2.4 APD/PIN PD/MESFET

Avalance Photodectors (APD), PIN Photodetectors (PIN PD), and Metal-Semiconductor Field-Effect Transitors (MESFET) are all feasible in microwave fiber optic communication systems to convert optical signals into electrical currents for further amplification and processing. The APD has an internal multiplication gain and enhances receiver sensitivity by amplifying signal photo current to a level substantially above that of the noise at the input stage of the post detector amplifier. Indeed, the silicon APD has excellent performance characteristics: high quantum efficiency close to 100 percent, 20 dB multiplication gain and Noise Equivalent Power (NEP) of 1×10^{-12} w/$\sqrt{Hz}$. However, it requires high bias voltage (160 - 370 volts). The PIN photodiode does not offer internal gain and is difficult to impedance match over wide bandwidths.

1. M. Horiguchi, M. Nakahara, N. Inagaki, K. Kokura, and K. Yoshida, "Transmission Characteristics of Ultra-Wide Bandwidth VAD Fibers", in Proc. 8th Euro. Conf. Opt. Commun., Cannes, France, Sept. 1982, paper A111-4.

2. D. Marcuse and C. L. Lin, "Low Dispersion Single-Mode Fiber Transmission - The Question of Practical Versus Theoretical Maximum Transmission Bandwidth, "IEEE J. of Quantum Elect., June 1981, pp. 869-878.

It is inexpensive for the system of short distance where receiver performance is not critical. The GaAs MESFET, with a gate length of less than 1.0 μm, has demonstrated a noise figure of 0.7 - 2.0 dB at frequencies of 2 - 6 GHz and 1.0 - 3.0 dB at 12 GHz. For optical detection, the MESFET has proven to be equal or superior to the APD at frequencies below 6 GHz.[1-9]

The MESFET offers the following attractive advantages over the APD and PIN ID:

- Low noise
- Nearly resistive output impedance, thereby providing wideband operation capability
- A frequency response well above X-band
- Low bias voltage required (4 - 6 volts)

1. J. J. Pan, "Advance Photodetectors for Fiber Optic Communications Systems", NEPCON '79, Anaheim, California, Feb. 1979.

2. J. J. Pan, "GaAs MESFET for High-Speed Optical Detection", 22nd SPIE International Symposium, San Diego, August 1978.

3. J. C. Gammel and J. M. Ballantyne, "The OPFET: A New High-Speed Optical Detector", IEEE International Electronic Device Meeting, Washington, DC, December, 1978.

4. J. M. Osterwalder and B. J. Rickets, "GaAs MESFET Demodulates Gb/s Signal Rates from GaAs Injection Laser", IEEE Proc., June 1979, pp. 966-967.

5. E. I. MacDonald, "High Gain Optical Detection with GaAs FETs", Appl. Optics, No. 4, Volume 20, 1981, pp. 591-594.

6. W. D. Edwards, "Two and Three Terminal GaAs FET Optical Detectors", IEEE Elect. Device Lett., August 1980, pp. 149-150.

7. E. H. Hara and R. I. MacDonald, "A Broadband Optoelectronic Microwave Switch", IEEE Trans. on MTT, June 1980, pp. 667-669.

8. T. J. Diesel, et al., "The Effect of Substrate Chromium Doping on Backgating and Light Sensitivity of GaAs MESFETs, 1980 GaAs ICS Conference, Las Vegas, Nevada.

9. J. Graffeuil, P. Rossel, and H. Martinot, "Light-Induced Effects on GaAs FETs", IEE Elect. Lett., 5 July 1979, pp. 439-441.

- Provide amplification gain
- Good temperature stability
- Low cost

The detailed MESFET photodetector performance was not investigated due to insufficient funding.

3.3 Devices/Optic Fiber Selection and Systems Implementation

To design, fabricate and implement the feasible model of the 4.4 - 5.0 GHz microwave fiber-optic system, the following devices and fiber were selected:

- Operation wavelength: 0.84 μm
- Optical Source: GaAlAs laser diode
- Optical Fiber: Glass-on-glass, single-mode
- Optical Fiber Connector: Single-mode connector with ceramic precision ferrule.
- Photodetector: Si APD
- Impedance Matching of ILD: Active matching
- ILD Driver and Post Detector Amplifier: MESFET Amplifier

To achieve an optimized system performance, the active devices must, at least, be characterized according to the following parameters:

- ILD
  - RF impedance
  - Kinks
  - Threshold characteristics and optical power versus temperature
  - Capacitance and nonlinearity
- ADP
  - Active RF impedance

- Noise and responsivity
- Dark current

- MESFET
  - Noise figure
  - S-parameter
  - Responsivity

The ILD must be free from kinks, otherwise, severe nonlinear distortion and poor reliability will result. The impedance of the ILD, APD, and MESFET can be measured, using a computer controlled automatic network analyzer, such as the HP 8409B, over a wide frequency range at various bias conditions. The parasitic reactance of test fixtures will be automatically calibrated "out" by the computer. Since ILD impedance is much lower than the 50 ohm measurement system, there must be special caution to ensure a good impedance transition and to minimize measurement error. ILD threshold current and APD multiplication gain change with the temperature and have to be measured as functions of the temperature during the characterization evaluation. The ILD nonlinearity versus input RF driving power is computed from the amplitudes of the harmonics. The photocurrent in a GaAs MESFET collected by the drain is a function of illuminating position, gate voltage, drain voltage, light intensity, and wavelength. Responsivity, quantum efficiency, and spectral response vary with bias condition. The S-parameters of a MESFET also change with light intensity and bias conditions and, therefore, should be measured.

4.0 LASIER DIODE AND LASER DIODE TRANSMITTER

4.1 <u>The State-of-the-Art Laser Diode and Trend</u>

In 1970, Hayashi, et al,[1] first reported the CW injection laser diode operated at room temperature. The laser diode was made with AlGaAs

1. I. Hayashi, M. B. Panish, P. W. Foy, and S. Sumski, "Junction Lasers Which Operate Continuously at Room Temperature", App. Phys. Lett., August 1970, pp. 109-111.

double-heterostructure material epitaxially grown and latticed matched to GaAs crystalline substrate. These early devices had lifetimes of a few minutes to a few hours. Several years of intensive work directed at improving device reliability produced practical lasers, which have projected MTBF (Mean-Time-Before-Failure) of 1,000,000 hours for continuous operation at room temperature, based on temperature-accelerated-aging tests on a large number of units.[2] High reliability was obtained by paying scrupulous attention to all aspects of:

- Crystal growth
- Device processing
- Coating of mirror facets
- Proper heat sinking

Long lived AlGaAs/GaAs stripe geometry laser diodes are well suited for application in first generation fiber systems because they emit several milliwatts of power with a narrow spectral width in the wavelength region near 0.85 μm, and can be directly modulated by varying their drive currents at frequencies exceeding 1 GHz. However, laser diode research is improving the material processing and diode structure to achieve the following aspects:

- Reliable long wavelength laser diode
- Low threshold current
- True single-mode operation
- Operation without thermoelectric cooling; longlife
- High frequency response
- High linearity and kink free

2. R. L. Hartman, et al, "Continuously Operated AlGaAs Double-Heterostructure Lasers with 70° Lifetimes as Long as 2 years", Appl. Phys. Lett., December 1977, pp. 756-759.

- High efficiency, high yield and low cost
- High efficiency and high optical power output
- Phase-locked laser diode array
- Distributed feedback laser diode for single frequency oscillation.

Even though some work on AlGaAs has continued, the main research and development interests have now shifted to InGaAsP/InP laser diodes which emit at long wavelength (1.3 or 1.5 μm).

The strong index guided structure, including strip-buried, plano-convex buried, planar-buried, buried-crecent (single crecent or double crecent) and ridge-waveguide designs, can confine optical field for reducing threshold current and provide single-transverse mode operation. Buried heterostructure laser diodes operating in the fundamental transverse mode fabricated from wafers, prepared by Molecular Beam Epitaxy (MBE), have CW thresholds as low as 2.5 mA[1], the lowest ever reported in any lasers. Gain-guided proton-bombarded stripe-geometry lasers also show a significant improvement in device performances over lasers fabricated from conventional DH laser wafers also grown by MBE, especially in the symmetry outputs and thresholds.

It has been proved[2] that higher order modes cannot exist in the laser diode when the diode active region width is smaller than the cut-off width (cut-off width is function of active layer thickness and varying with laser diode structure). The Double-Channel Planar Buried-Heterostructure Laser Diode (DC-PBH LD) has been experimented with by NEC for stable fundamental single transverse mode operation up to high excitation level to obtain high output power, active waveguide parameters should satisfy first order mode cutoff condition. Normally, the laser diode requires a Thermoelectric (TE) cooler to extend its lifetime; however, without a TE cooler, the PC-PBH LD has been tested at 5 mW outputs, 70° C ambient temperature over 4000 hours and 10 mW, 50° C over 2000 hours. No increase in the driving current has been observed in all operating conditions up to 70° C at 10 mW.

1. W. T. Tsang, et al, "Ultra-low Threshold, Buided-index Waveguide, Separate Confinement CW Buried-Heterostructure Lasers", Elect. Lett., September 1982, pp. 845-847.

2. K. Kobayashi, Private Communication.

Fundamental transverse mode lasing was maintained and no changes in emission spectrum and pulse response waveform have been observed within measurement accuracy. From the experimental performance of DC-PBH LD, the fiber optic designer can rely on laser diode operation over a wide temperature range without use of the TE cooler.

A laser diode's frequency response depends on the laser current density and the length of laser cavity. Lan and Yariv[1] predicted that the short length laser diode can respond up to 24 GHz.

In addition to the active waveguide and current confinement (narrow active region) structures to improve laser diode power output and efficiency, the mirror reflectivity is also an important factor. The conventional, commonly practiced, cleaved facet mirror reflectivity (30 percent) is not an optimum value. A simple gold layer (reflectivity is estimated approximately 95 percent) is deposited on to the laser diode rear-end facet, and can increase light output power from the front facet by 1.5 times, compared to that without a reflective coating. This technique has been proved by NEC's DC-PBH LD.

High power Continuous Wave (CW) room temperature operation of phase-locked laser diode arrays has been achieved in Xerox Palo Alto Research Center and other institutes in the past several years. The laser array often consists of 10 to 40 3.5 μm wide gain-guided lasers on 10 μm centers, operating simultaneously in a phase-locked manner, to achieve much higher CW output power. Recently, Xeros reported that the 40 laser diode array with coated mirror facets ($R_f = 0.9$, $R_f = 0.12$) has an output power of 2W, a threshold current of 1.25A, and the power conversion efficiency of 16.4 percent. For the short-term future, those high power laser diode arrays may not be suitable for the microwave fiber optic communications.

Stable single-mode lasers are desirable for microwave fiber optic operation. Lasers which emit in a single mode under steady-state conditions tend to break into multimode operation when modulated. Nevertheless, stable single mode operation may be obtained by using the grating feedback technique. Distributed Feedback (DFB) laser diodes and distributed Bragg Reflector (DBR) lasers have been investigated both on GaAlAs/GaAs and InGaAsP/InP laser (from the fabrication point

1. A. Yariv, 1983 Cleo, May 17-20, 1983, Baltimore, Md.

of view, the long wavelength region is more attractive because of the longer grating period). Theoretical threshold for the grating feedback lasers is as low as that of cleaved lasers.[1] Recently, a 1.5 μm DFB InGaAsP laser was constructed whose output remained in a single mode under high speed (500 Mb/s) modulation[2] and 2 GHz[3].

4.1.1 High Speed, Commercially Available Laser Diodes

GaAlAs laser diodes are commercially available from many vendors operating at wavelength between 0.80 to 0.88 μm. Table 4.1.1-1 presents some of the high performance microwave CW laser diodes (majority of the data was collected during November 1 through November 12, 1982). The packages of most of these laser diodes are not designed for microwave applications.

The long wavelength commercially available laser diodes (all of this data was collected during November 1 through November 12, 1982) are presented in Table 4.1.1-2.

4.2 Laser Diode Frequency Response/Resonance-Like Phenomena

The frequency response of laser diode is dependent upon:

- Laser diode intrinsic parameters
- ILD external circuit design
- ILD driving power and modulation frequency
- ILD package

---

1. H. Kogelnik and C. V. Shank, "Stimulated Emission in a Periodic Structure", Appl. Phys. Lett., February 1971, pp. 152-154.

2. K. Sakai, et al, "1.5 μm Range InGaAsP/InP Distributed Feedback Lasers", IEEE J. of QE, August 1982, pp. 1272-1278.

3. Koyama, IEEE J. of QE, June 1983.

4. Kobayashi, et al, "Direct Frequency Modulation in AlGaAs Semiconductor Lasers", IEEE Trans. on MTT, April 1982, pp. 428-441.

Table 4.1.1-1. Commercially Available High Speed, Short Wavelength, CW Laser Diodes

Manufacturer	Model #	Threshold Current (mA)	Operating Current/ Voltage (mA/V)	Power Output (mW)	Beam Spread (Degree)	$\lambda/\Delta\lambda$ (mn)	Band-Width (GHz)	Life Time Hours
OIS	OL2000[1]	100	130	4.5-10	-	800,835/0.1		
General Optronics	GOLS	100	120/1.5	5	10,45	830	3	100,000
Hitachi	HLP-1000	70	95/1.8	15	10,30	830/0.1	1	10,000
	HLP-2000	20	25/1.8	3	25,35	830/0.1	1	10,000
	HLP-3000	35	40/1.8	10	25,30	830/0.1	1	10,000
Northern Telecom	L-5-3	120	145/2.0	5	10,50	840/0.1	2	100
Mitsubishi	ML-2205F[2]	30	40/1.8	3	10,40	830/0.1	2	100,000
	ML-3001	30	40/	3.5	10,40	830/0.1	2	10,000[3]
LDL/MACOM	SCW-21	60	85/1.8	8	10,35	810-860/01	5	10,000
	LCW-10	90	115/2.0	7	10,35	810-860/01	5	10,000
RCA	C86014E	75	100/2.0	10	10,35	820/0.1	2	10,000
Fujitsu	FLD080WA	100	130/1.7	8	10,35	850/1	-	-

1. With Optical Feedback
2. Model with Fiber Pigtail Attached
3. At 50°C

Table 4.1.1-2. Commercially Available Long Wavelength Laser Diodes

MANUFACTURER	MODEL NUMBER	THRESHOLD CURRENT (mA)	OPERATING CURRENT/ VOLTAGE (mA/V)	POWER OUTPUT (mW)	BEAM SPREAD (DEGREE)	$\lambda/\Delta\lambda$ (nm)	RISE TIME (ns)	LIFE TIME HOURS
Lasertron	QL5-1270	100	120/1.4	5	10 x 30	1270/1	1	10,000
	QL5-1300	100	150/1.5	7	10 x 40	1300	-	10,000
	QL5-1500	100	150/1.5	5	10 x 40	1500	-	10,000
LDL/MACOM	QCW-123	250	300/2.0	6	10 x 35	1100-1300	1	10,000
RCA	C86023E	150	250/2.0	7	---	1300/---	1	25,000
Hitachi	LD5201*	50	70/1.5	2	---	1300/1	1	---
Fujitsu	FLDBOWD	20	50/1.2	5	---	1301/1	-	---
General Optronics	GOXL	100	120/1.6	7	---	1300/4	1	10,000

*With 50/125 μm, graded-index pigtail and NA = 0.2.

The large signal ILD dynamic frequency response is a very complicated problem which will not be discussed in this report. Parameters include package capacitance and inductance introduced by the bonding wires. The package parasite reactances seriously limit ILD frequency and may also create resonance-like phenomenon. The package effect will be discussed late in this section, as it is well known that the frequency response and modulation efficiency is a function of temperature.

In a manner similar to that for conventional microwave diodes (such as TED and IMPATT diode), the laser diode (no package parameters are considered) amplitude-phase relations can be obtained from a linearization of the rate equation.[4]

The input current to the laser diode is split into a dc component I_0 and a time-varying component with amplitude i and angular modulation frequency ω:

$$I = I_0 + i \cos \omega t \qquad (4.1)$$

A pair of differential equations defines the modulated photon density and the electron density in terms of the steady-state values. The output optical power can be expressed as:

$$P = P_0 + p \cos (\omega t + 0) \qquad (4.2)$$

where P_0 is the steady-state output, p is the amplitude of the modulated output power, and ϕ is the phase angle of relative to the modulating current. Solving the differential equations, one can get for the modulation depth ρ/P_0 and angle[1,2].

$$\frac{\rho}{P_0} = \frac{A \frac{i}{ev}}{\omega_0^2 - \omega^2 \; j\omega\beta} \qquad (4.3)$$

1. T. L. Paoli and J. E. Ripper, Proc. IEEE pp. 1457, 1970.

2. G. Arnold and P. Russer, Appl. Phys. p. 255, 1977.

$$\phi = \tan^{-1} \frac{-\omega\beta}{\omega_0^2 - \omega^2} \qquad (4.4)$$

with

$$P_0 = \alpha \overline{N}ph \qquad (4.5)$$

$$\alpha = \frac{h \nu V \mu}{\zeta ph} \qquad (4.6)$$

$$W_0 = \frac{A P_p}{ph\ \alpha} = \frac{1}{\zeta sp\ \zeta ph} \quad \frac{Ib - Ith}{Ith} \qquad (4.7)$$

$$\beta = \frac{1}{sp} \cdot \frac{Ib}{Ith} \qquad (4.8)$$

where $\overline{N}ph$ is the internal photon density

α is proportionally factor (Watt cm^3).

μ is a differential efficiency (equal to the product of the differential quantum efficiency and the coupling efficiency laser-fiber-connector).

Ith is the threshold current.

V is the laser cavity volume.

ζsp is the spontaneous emission lifetime of injected carriers.

ζph is the photon lifetime.

ω_0 is the angular resonance frequency.

The phase changes, $\Delta\phi$, in the laser diode were translated into differential delay changes $\Delta \zeta$ using the relationship:

$$\Delta \zeta = \frac{-\Delta\phi}{360.\ f} \qquad (4.9)$$

where f is the modulation frequency.

For small modulation signals biased above threshold, the frequency response is flat up to frequencies close to the "relaxation oscillation" resonance occurs. At low frequencies, $\omega \simeq o$, equation (4.3) reduces to a modulation efficiency γ (watts/amps):

$$\gamma = \frac{\rho}{i} = \frac{h\nu}{e}\mu \qquad (4.10)$$

In this case, μ takes the form of an external quantum efficiency. The output light amplitude may then also be written as:

$$\rho = i\,\frac{\Delta P}{\Delta I} \qquad (4.11)$$

which is obtained from a Taylor Series expansion of the optical output.

The laser diode with modulation frequency in 1 to 4 GHz, the "relaxation-oscillation resonance" frequency, fr, can be calculated from:

$$f_r = \frac{1}{2\pi}\left(\frac{1}{\zeta sp}\;\frac{1}{\zeta ph}\right)^{1/2}\left(\frac{I_o}{I_{th}} - 1\right)^{1/2} \qquad (4.12)$$

For laser diodes to be capable of operating above 4 GHz, the relaxation resource frequency can be expressed more accurately as:

$$f_r = \frac{1}{2\pi}\left(\frac{\Gamma nom\ d}{\zeta\ ph}\;\frac{\zeta ph + 1}{\zeta\ sp}\right)^{1/2}\left(\frac{I_o}{I_{th}} - 1\right)^{1/2} \qquad (4.13)$$

where Γ is the transverse optical confinement factor

Nom is the injected carrier density required for zero gain

d is the thickness of the active region

Also in 1983 CLEO, May 17-20, 1983, Baltimore, Maryland and 1983 IOOC, June 17-30, Tokyo, Japan, A. Yarice expressed the relaxation frequency in a general term as:

$$f_r = \frac{1}{2\pi}\sqrt{\frac{A\quad N_{ph}}{\zeta ph}}$$

where A is the differential gain coefficient, N_{ph} is the photon density in the active region.

At resonance, the modulation depth amplitude, m , normalized to its value at $\omega = o$, then:

$$m = \left| \frac{(p/P)\ \omega = \omega_o}{(p/P_o)\ \omega = \omega_o} \right|$$

$$= \frac{W_o}{\beta}$$

$$= \frac{I_{th}}{I_o} \left(\frac{\zeta sp}{\zeta ph} \right)^{1/2} \left(\frac{I_p}{I_{th}} - 1 \right)^{1/2} \qquad (4.15)$$

For above resonance ($\omega >> \omega_o$), the normalized modulation depth amplitude reduces to:

$$m = (\omega_o/\omega)^2 \qquad (4.16)$$

This corresponds to a 6 -dB/octave slope.

Figures 4.2-1[1], 4.2-2[2], 4.2-3[3], and 4.2-4[4] illustrate experimental small signal modulation response for several different commercially available, packaged, stripe geometry laser diodes. Different resonance-like frequency response displayed at different bias currents. Figueroa[2], et al, also presented the experimental relaxation oscillation resonance frequency as a function of dc bias for the Hitachi CSP laser, model HLP1400 up to $I_o \simeq 2I_{th}$, as depicted in Figure 4.2-5.

Refer to equation (4.4), the phase varies from 0^o at $\omega = o$ to -90^o at resonance $\omega = \omega_o$ and approaches -180^o for $\omega >> \omega_o$. At the last limit, as well as at resonance, the phase is dependent upon the I_o/I_{th} ratio.

1. W. Susaki, et al, "Wideband Frequency Modulation With a Reduced Resonance-Like Peak in TJS Lasers", 1981 IOOC, April 27-29, 1981 San Francisco, Calif.

2. L. Figueroa, C. W. Slayman and H. W. Yen, "High Frequency Characteristics of GaAlAs Injection Lasers", IEEE Trans. on MTT, October 1982, pp. 1706-1715.

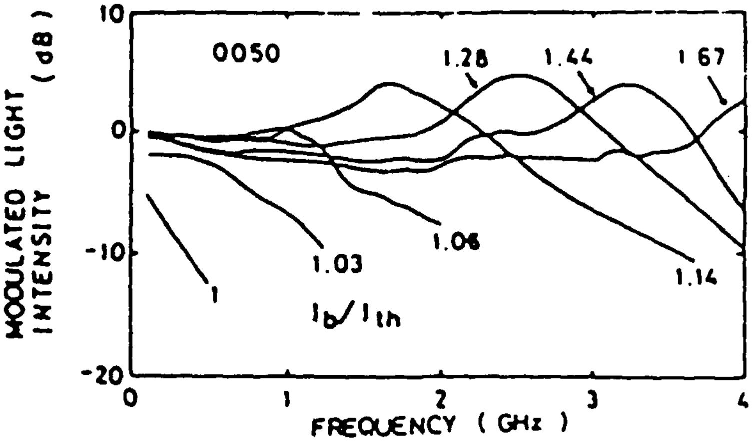

Figure 4.2-1. Frequency Modulation Characteristics of a TJS Laser (after Susaki, et al)

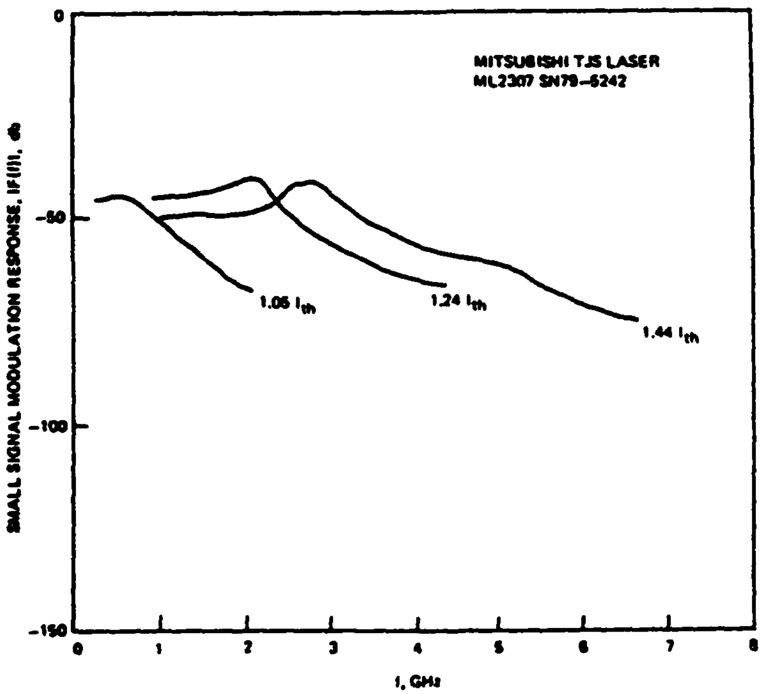

Figure 4.2-2. Experimental Small Signal Modulation Response of Mitsubishi TJS Laser (after Figueroa, Slayman, and Yen)

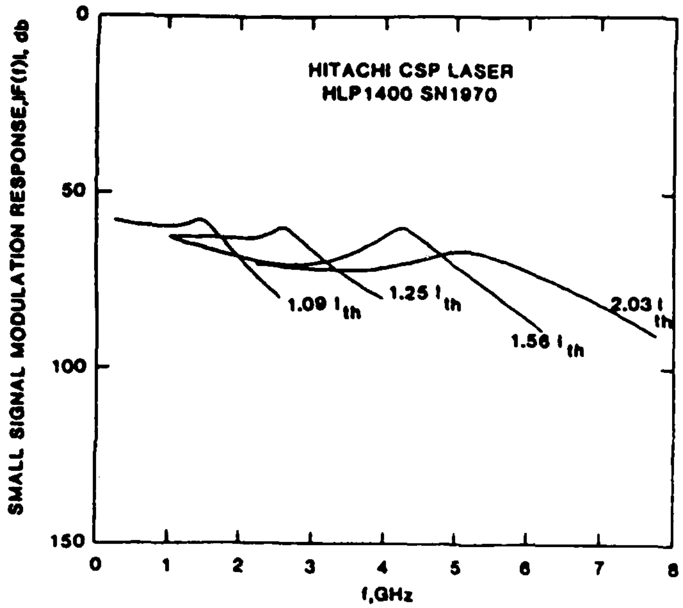

Figure 4.2-3. Experimental Small Signal Modulation Response of the Hitachi CSP Laser (after Figueroa, Slayman, and Yen)

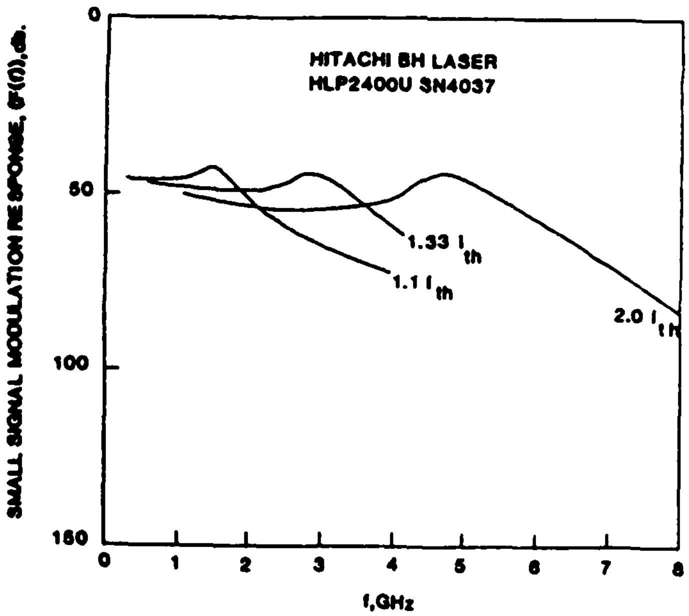

Figure 4.2-4. Experimental Small Signal Modulation Response of the Hitachi BH Laser (after Figueroa, Slayman, and Yen)

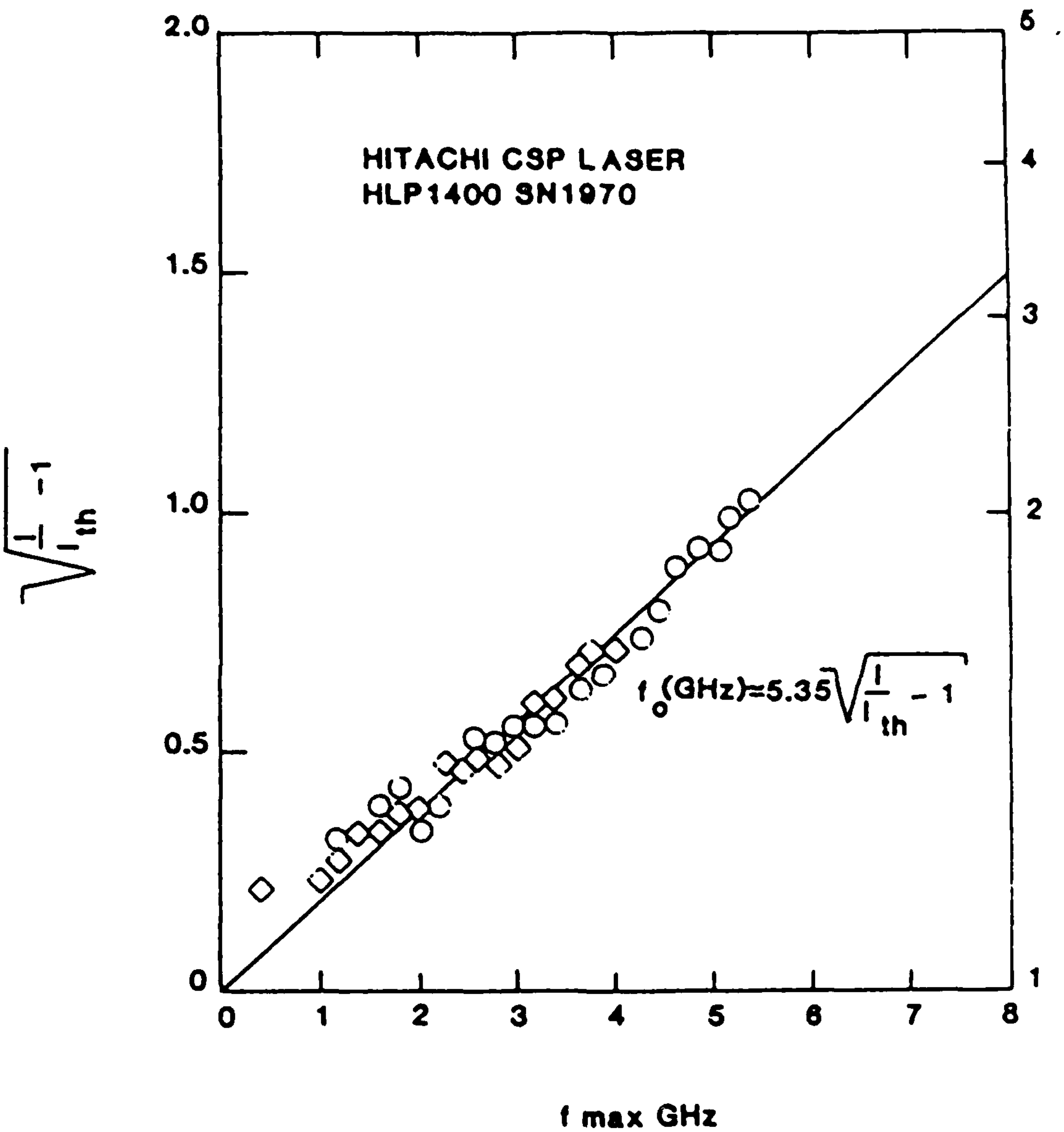

Figure 4.2-5. Experimental Relaxation Oscillation Resonance Frequency as a Function of dc Bias for the Hitachi CSP Laser (after Figueroa, Slayman, and Yen)

When the current passes through the laser diode active region or the ambient temperature (heat sink) changes, the index of refraction within the active region will vary. Also, the carriers and radiation confinement will change accordingly. Furthermore, the effective absorption coefficient may show a temperature dependence and so will the internal quantum efficiency and laser gain factor. Therefore, the threshold current I_{th} is the most temperature-sensitive parameter in the modulation equations. The ζ_{sp} and ζ_{ph} may be affected in a minor way by temperature. As a first approximation, it may be adequate to deal with the temperature dependence of I_{th} only, since the temperature sensitive gain coefficient A can be lumped together with the steady-state output P_0 and expressed as a function of the resonance frequency and the photon life-time as in equation (4.7). The temperature dependence of I_{th} is usually of the form:

$$I_{th} = I_{thRT} \exp\left(\frac{T - T_{RT}}{T_0}\right) \tag{4.17}$$

where I_{thRT} is the threshold current at room temperature, T_0 is 170^0 K and $T_{RT} = 298^0$ K. Therefore, the higher resonance frequencies at lower temperatures due to an increase in I_0/I_{th}.

4.3 Laser Diode Package

As mentioned previously in Section 4.2 that the laser diode frequency response is dependent upon the device package. For direct modulation, the equivalent circuit of the laser diode with the packaging impedance is shown in Figure 4.3-1.[1,2,3,4]

1. J. J. Pan, 1975, unpublished work.

2. M. Maed, et al, "Buried Heterostructure Laser Packaging for Wideband Optical Transmission Systems", IEEE Trans. Communication, 1978, pp. 1076-1081.

3. (a) R. S. Tucker, Private Communications; (b) R. S. Tucker and D. J. Pope, "Circuit Modelling of the Effect of Diffusion on Damping in Narrow-Stripe Semiconductor Lasers", to be published.

4. R. S. Tucker and D. J. Pope, "Microwave Circuit Models of Semiconductor Injection Lasers", IEEE Trans. on MTT, March 1983, pp. 289-294.

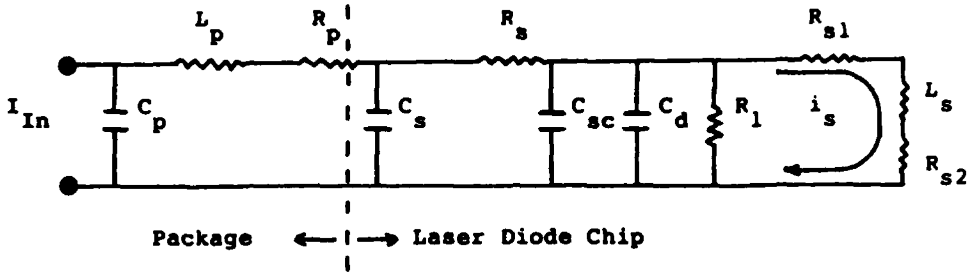

L_p and R_p are bonding wire inductance and resistance, respectively

C_p laser diode package capacitance

R_s is the contact resistance and bulk resistance in the semiconductor chip

C_s is the parasitic capacitance associated with the chip

C_{sc} is the space-change capacitance

C_d is the diode active layer junction capacitance

R_{s1} and R_{s2} are damping resistances due to lateral diffusion and R_{s2} is bias dependent.

R_1 is the small signal, bias dependent, diode junction resistance

Figure 4.3-1. Equivalent Circuit of Laser Diode and its Packaging for High Frequency Modulation

The modulated light output is proportional to the current i_s through the inductor L.[1]

The ratio of i_s to the total current i through the diode is the familiar small signal modulation response of intrinsic laser diode, displaying a resonance at frequency $f = 1/(2\pi\sqrt{LC})$. The combined impedance of the RLC circuit is small compared to the parasitics so that in analyzing the effect of parasitic elements on the modulation performance, the laser diode can be approximated as a short circuit.

1. J. Katz, et al, "The Intrinsic Electrical Equivalent Circuit of a Laser Diode", IEEE J. of QE, January 1981, pp. 4-7.

The circuit elements are described in Figure 4.3-1. Both Figueroa, et al and Tucker observed a roll-off (or a dip) prior to the usual relaxation oscillation resonance. They originally thought that it might be attributed partially to an R-C charging effect. The circuit model depicted in Figure 4.3-1, accurately describes the dip in the frequency response, and the dip can be explained in terms of package and chip parasitics. The stray capacitance C_s and the series resistance R_s are the dominant elements affecting this part of response.

Tucker[1] has evaluated the small-signal model of a buried heterostructure laser, Hitachi HLP-3400, including the package. The shunt package capacitance, C_p, is 0.29 pF, the bonding wire inductance, L_p is 1.42 uH, the wire resistance, R_p is 2 ohms, C_s = 14.1 pF and R_s = 13.1 . The laser diode chip circuit model for the three bias levels (20 mA, 25 mA and 30 mA) is given in Table 4.3. The threshold current of HLP-3400 is 13 mA. The measured and calculated small-signal frequency response is shown in Figure 4.3-2.

Table 4.3. Circuit Element Values for the HLP-3400 Model

I_0(mA)	C_{sc}(pF)	C_d(pF)	R_1(Ω)	R_{s1}(mΩ)	R_{s2}(pΩ)	L_s(pH)
20	10	380	1.23	23.4	34.0	7.07
25	10	381	0.829	24.1	11.8	4.19
30	10	382	0.628	24.7	6.0	3.01

1. Tucker's work to be published.

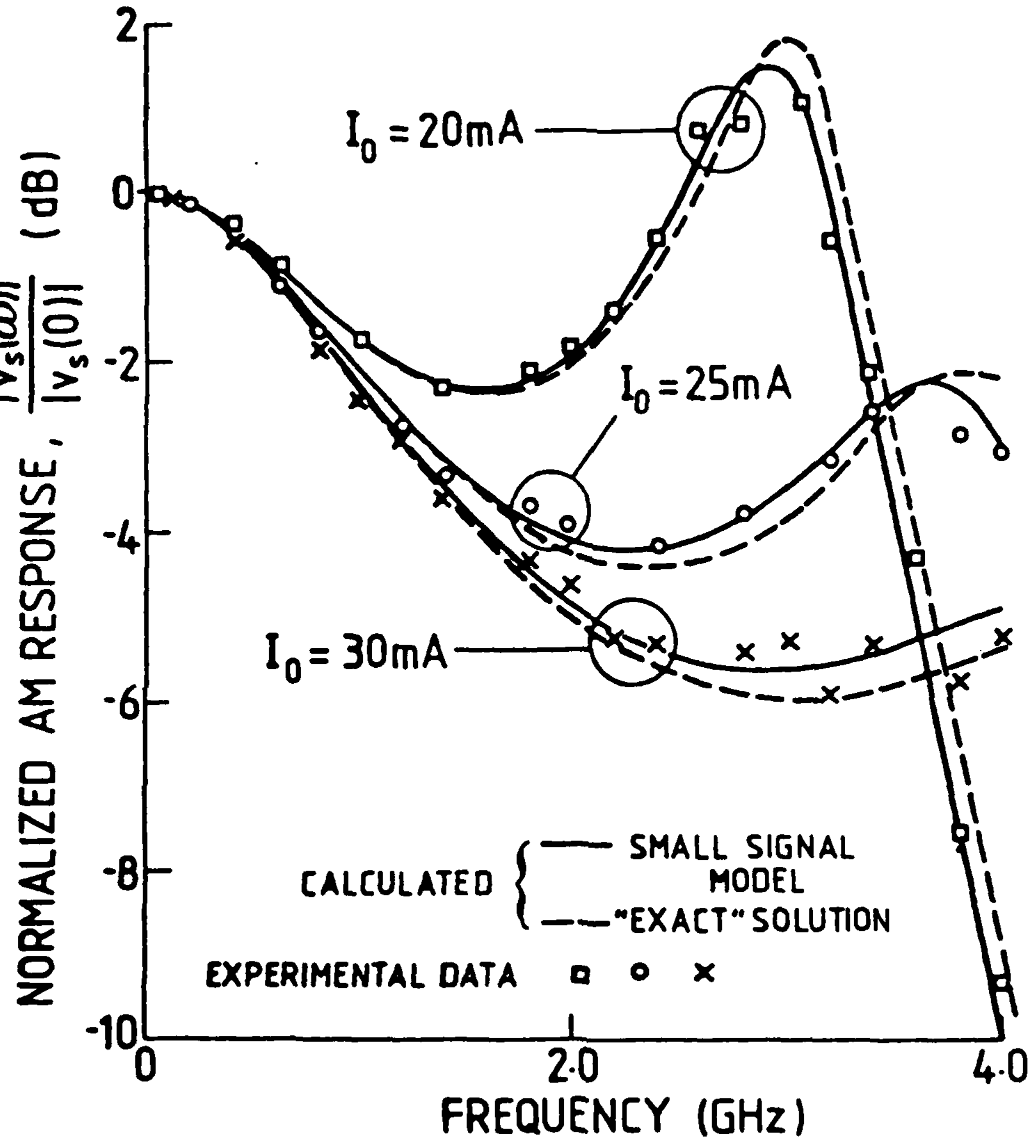

Figure 4.3-2. Measured and Calculated Small-Signal Frequency Response of the Hitachi HLP-3400 Laser Diode for Three Different Values of Biased Current Above Threshold

4.4 LD Nonlinearity and Compensation for Microwave Analog Application

Microwave RF fiber optic systems require very high Signal-to-Noise ratio (S/N) and very low harmonic and Intermodulation Product (IMP) distortions. Nonlinearity will introduce both harmonic and IMP distortions. There are two different groups of nonlinearities:

- Kinks

- Nonlinear junction capacitance, nonlinear relationship between optical power output and driving current, and thermal gradient.

The second group of nonlinearities can be externally compensated or minimized while the device intrinsic kinks cannot. Therefore, the system designer must select the kinks free laser diode.

Most laser diodes have linear P-I curve without "kinks", but some are different. The mechanisms causing "kinks" have been suggested by many authors[1,2] and will not be discussed further here. The nonlinear capacitance compensation techniques have been described in Section 3.1.

4.5 Laser Diode Characterization

To design a wideband microwave laser diode transmitter, the laser diode must, at least be characterized according to the following parameters:

- DC Parameters
  - Capacitance and series resistance
  - Threshold characteristics and optical power versus temperature
  - Kinks

1. C. M. Wang, et al, "Superhigh Differential Quantum Efficiency and Strong Self-Sustained Pulsation in CW Dh Laser Diode", IEEE Trans on MTT, April 1982, pp. 441-447.

2. R. W. Dixson, "Current Direction of GaAs Laser Device Development", BSTJ May/June 1980, pp. 669-722.

- RF Parameters
  - RF impedance
  - Nonlinearity

Normally, the dc and optical parameters are supplied by the laser diode manufacturer. The General Optronics laser diode GOLS-1, selected for 4.4 - 5.0 GHz RF fiber optic link, has the following performance:

Power Output	7 mW
Wavelength	840 nm
Rise Time	0.7 nS
Longitudinal Modes	2-6
Spectral Width	0.3 - 1.3 nm
Emission Angle	$10^{o} \times 38^{o}$
Typical Efficiency	0.3 mW/mA
Spontaneous Emission	0.25 mW
Threshold Current (at 25° C)	50 mA
Forward Voltage	1.7 V
Series Resistance	2 ohm
Capacitance	10 (pF)

Figure 4.5-1 depicts the General Optronics GOLS-1 laser diode optical power versus forward current. Apparently, no kink exists.

The laser diode RF nonlinear characteristics can be observed from harmonics and two-tone IMP measurement. Figure 4.5-2 shows the measurement setup[1] of two-tone IMP for laser diode. The tunable filter and spectrum analyzer (such as HP8566A) are used to measure harmonic components and $2f_1 - f_2$ of third-order

1. C. S. Kim, "Laser Diode Characterizations for Multi-Channel Applications", 1978 IEEE MTT-S International Microwave Symposium Digest, pp. 127-128, Ottawa, Canada.

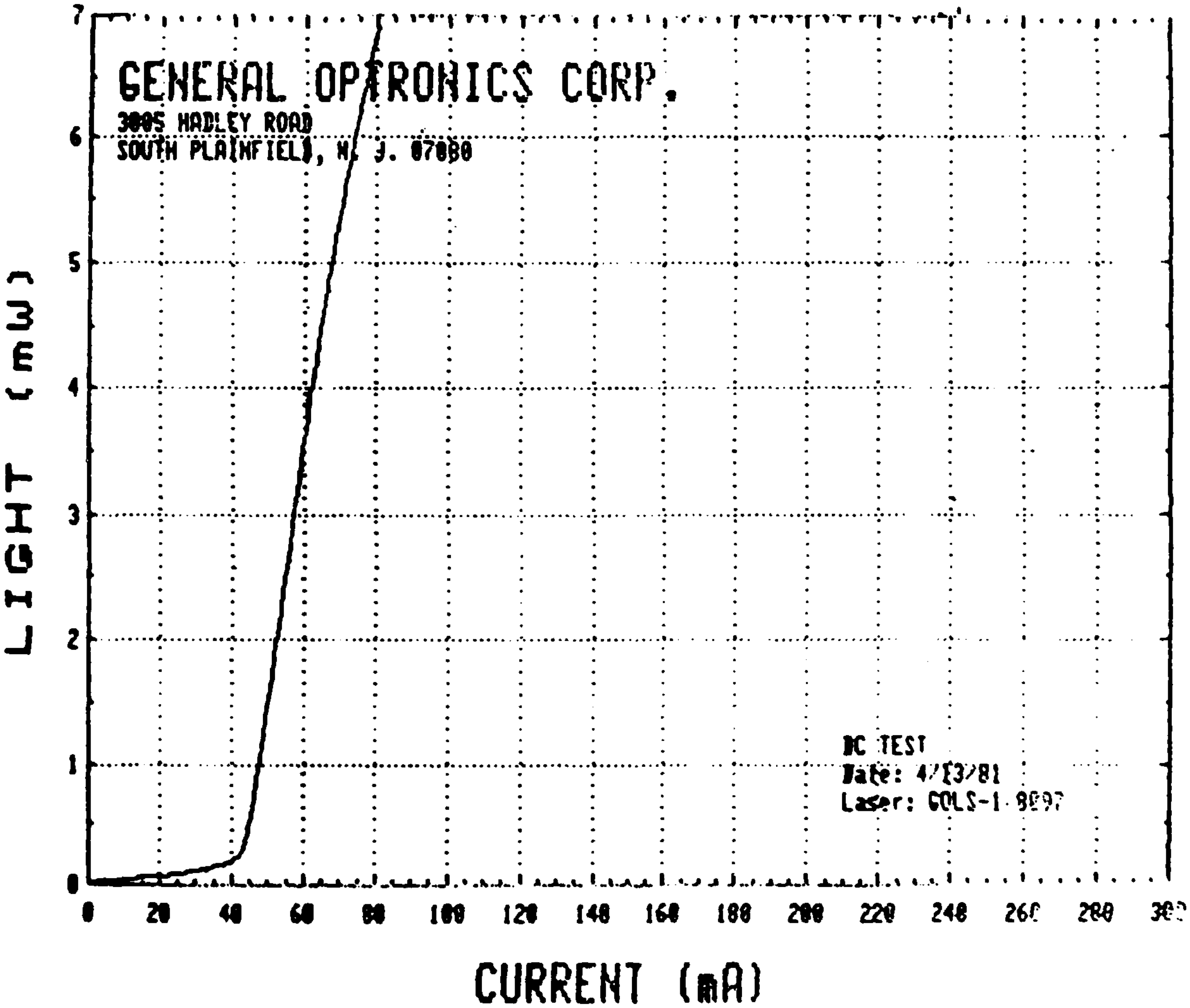

Figure 4.5-1. The Laser Diode (General Optronics GOLS-1) Optical Power Versus Forward Current

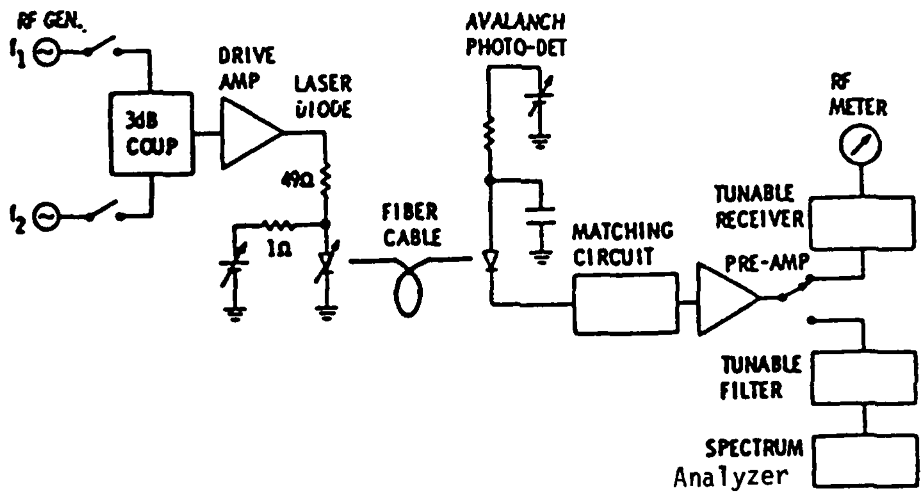

Figure 4.5-2. Measurement Setup for Laser Diode Harmonic and IMP Distortions

distortion components. Other third-order distortion components can be derived from $2f_1 - f_2$.[1]

The laser diode RF impedance versus frequency is extremely important in transmitter circuit design. The impedance matching determines laser diode modulation index, input VSWR, and noise performance. The experimental arrangement used to characterize the RF impedance at room temperature is shown in Figure 4.5-3. Broadband electrical reflection coefficient data referred to the device terminals can be obtained using a network analyzer (such as HP8410C, 8411A, 8412B, and 8746B) or an automatic network analyzer (such as HP9408B). The laser diode can be mounted in a microstrip test fixture. Since the laser diode has a very small resistance (1 to 2 ohms), it is desirable that the test fixture have a lossless impedance taper (transfer 50 ohms to a low impedance) to accurately determine the diode series resistance[2] (avoid the large correction factor required for system loss). Care also must be exercised to ensure that the laser is loosely coupled to the photodetector (photodetector and post detector amplifier must have sufficient bandwidth with a flat frequency response). Loose coupling ensures that the amount of light reflected back into the laser is minimized, while providing sufficient detected signal power for reliable frequency response measurements. The RF impedance of GOLS-1 measured from 1 to 10 GHz, displayed on Smith Chart, is given in Figure 4.5-4. The RF impedances of various laser diodes also have been measured by Tucker and Figueroa, et al. Their measurement results are presented in Figures 4.5-5 and 4.5-6 as reference as well as comparison.

4.6 Laser Diode Transmitter Design

4.6.1 Laser RF Driving Level

The RF input power level to the laser diode affects laser's modulation index, noise level, nonlinear distortions, and frequency response. For feasibility study purposes, a 0 dBm input power feeds the transmitter. Amplifier and

1. K. A. Simons, "The Decibel Relationships Between Amplifier Distortion Products", Proc. IEEE, July 1970.

2. G. D. Vendelin and S. A. Robinson, "A Power Reflection Technique for Characterization of High Quality Varactor Diodes", IEEE Trans. on MTT, December 1966, pp. 603-608.

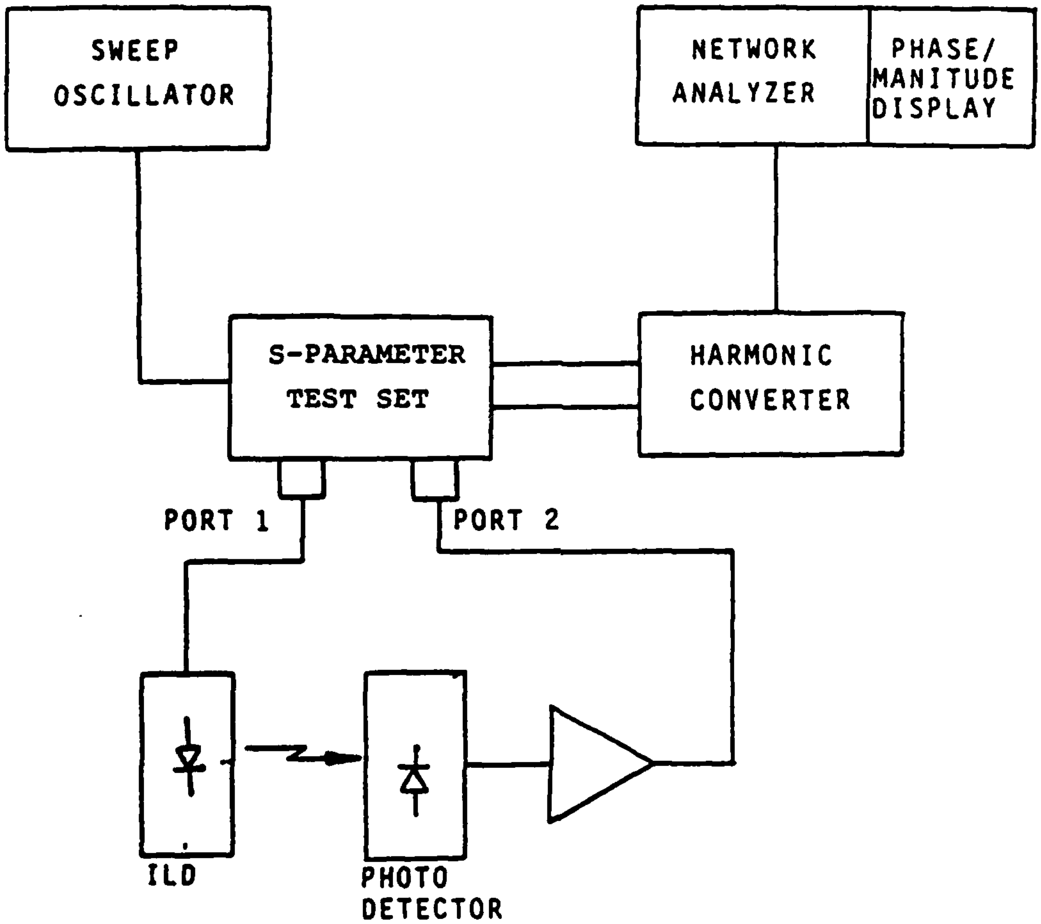

Figure 4.5-3. Measurement Setup of Laser Diode RF Impedances

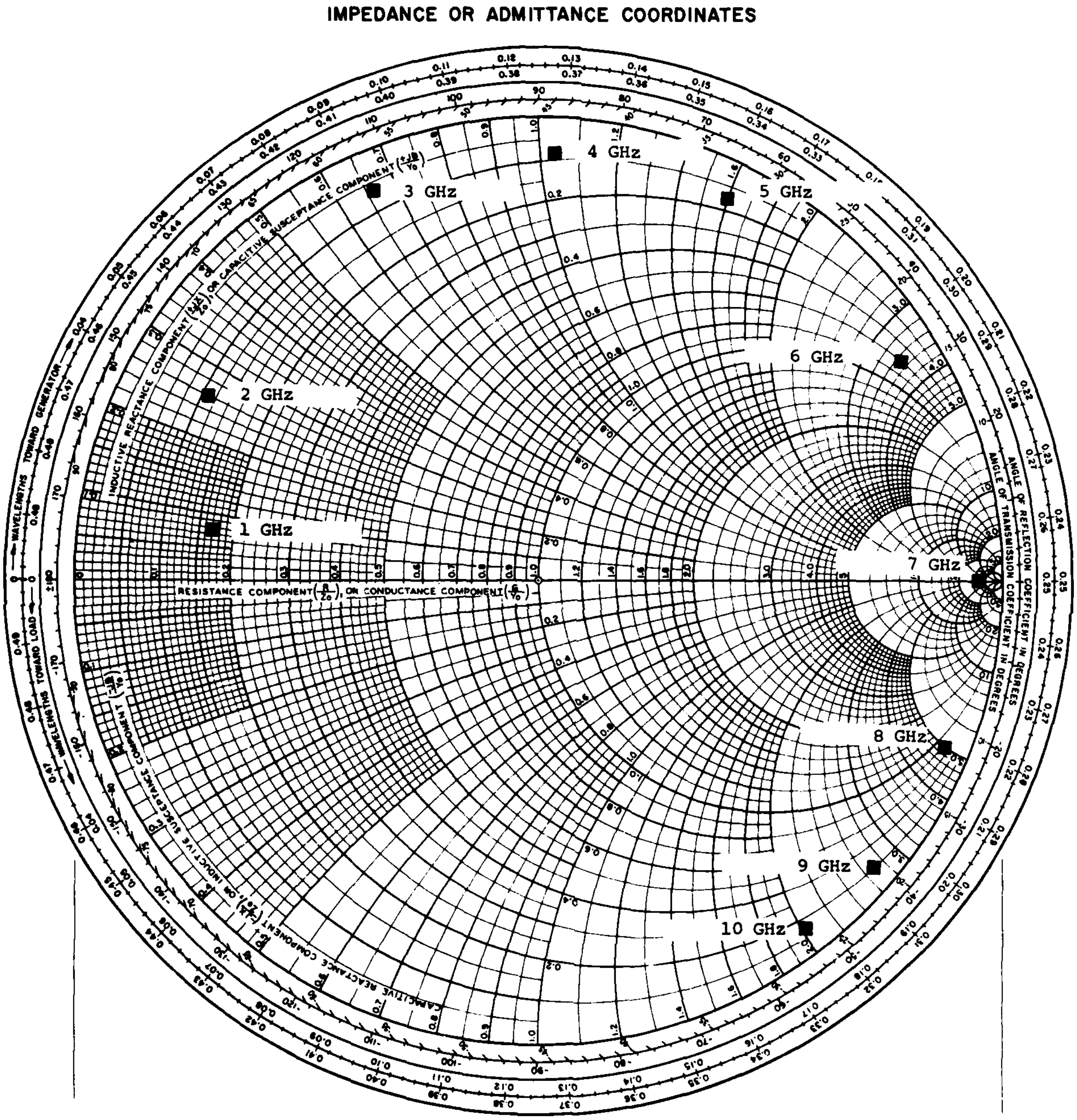

Figure 4.5-4. Measured RF Impedance from 1 to 10 GHz of GOLS-1 Laser Diode Displayed on Smith Chart

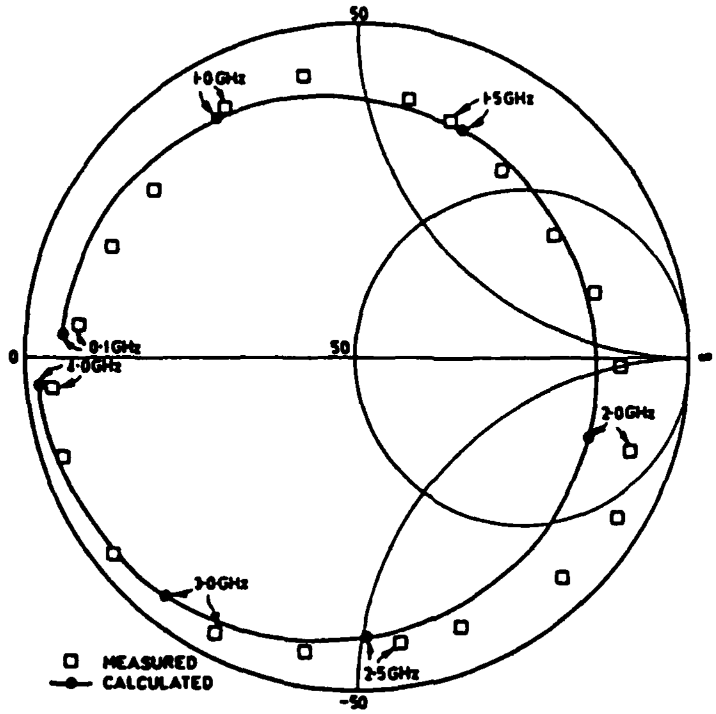

(a)

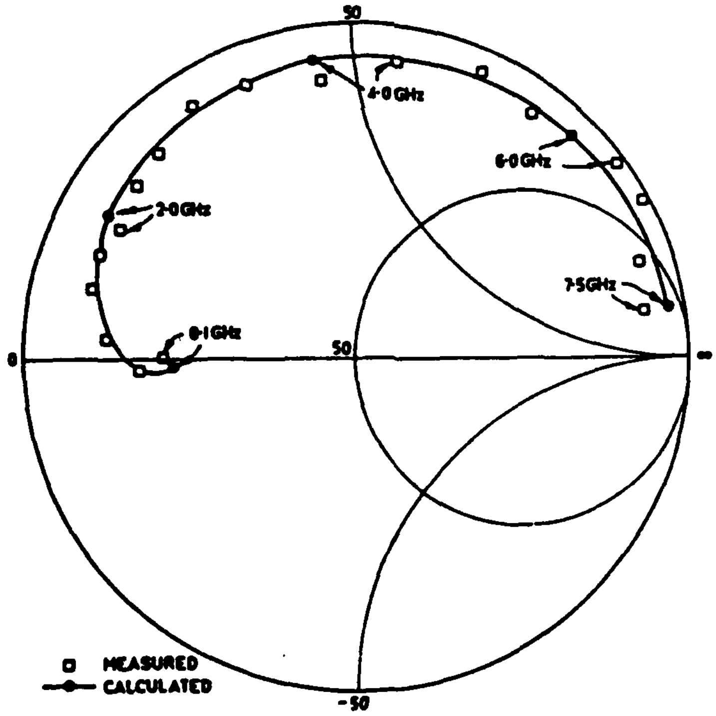

(b)

Figure 4.5-5. Measured and Calculated RF Impedances of (a) Broadstripe Laser (Laser Diode Labs LCW-10) and (b) BH Laser (Hitachi HLP-3400) (after Tucker)

IMPEDANCE OR ADMITTANCE COORDINATES

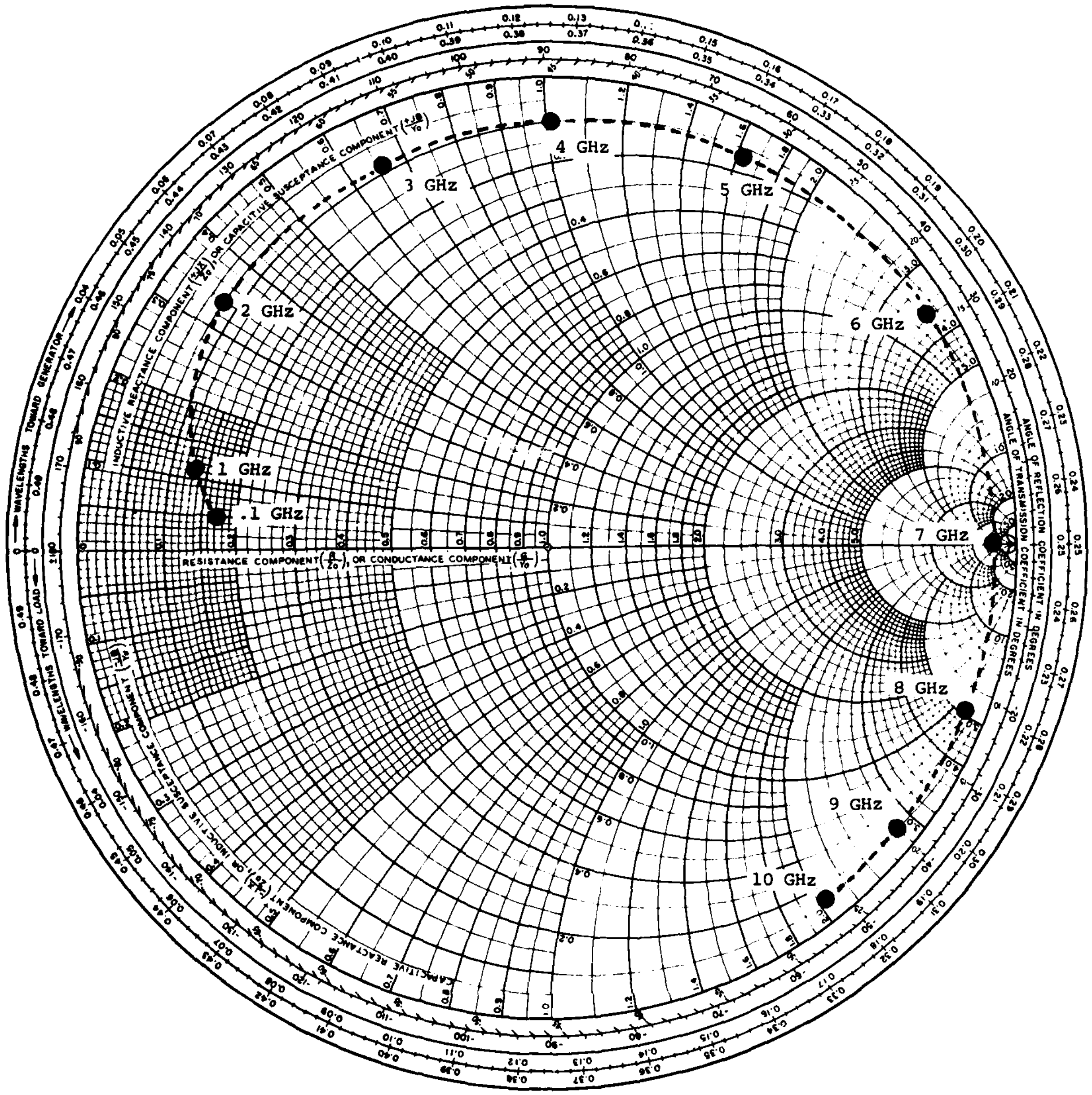

Figure 4.5-6. (a) Experimental Measurements for the Impedance of the Hitachi BH Laser versus Frequency for Frequencies in the Range of 100 MHz - 10 GHz. The Smith Chart is normalized to 50 ohms. The drive current is $I = 1.2\ I_{th}$. (After Figueroa, Slayman and Yen)

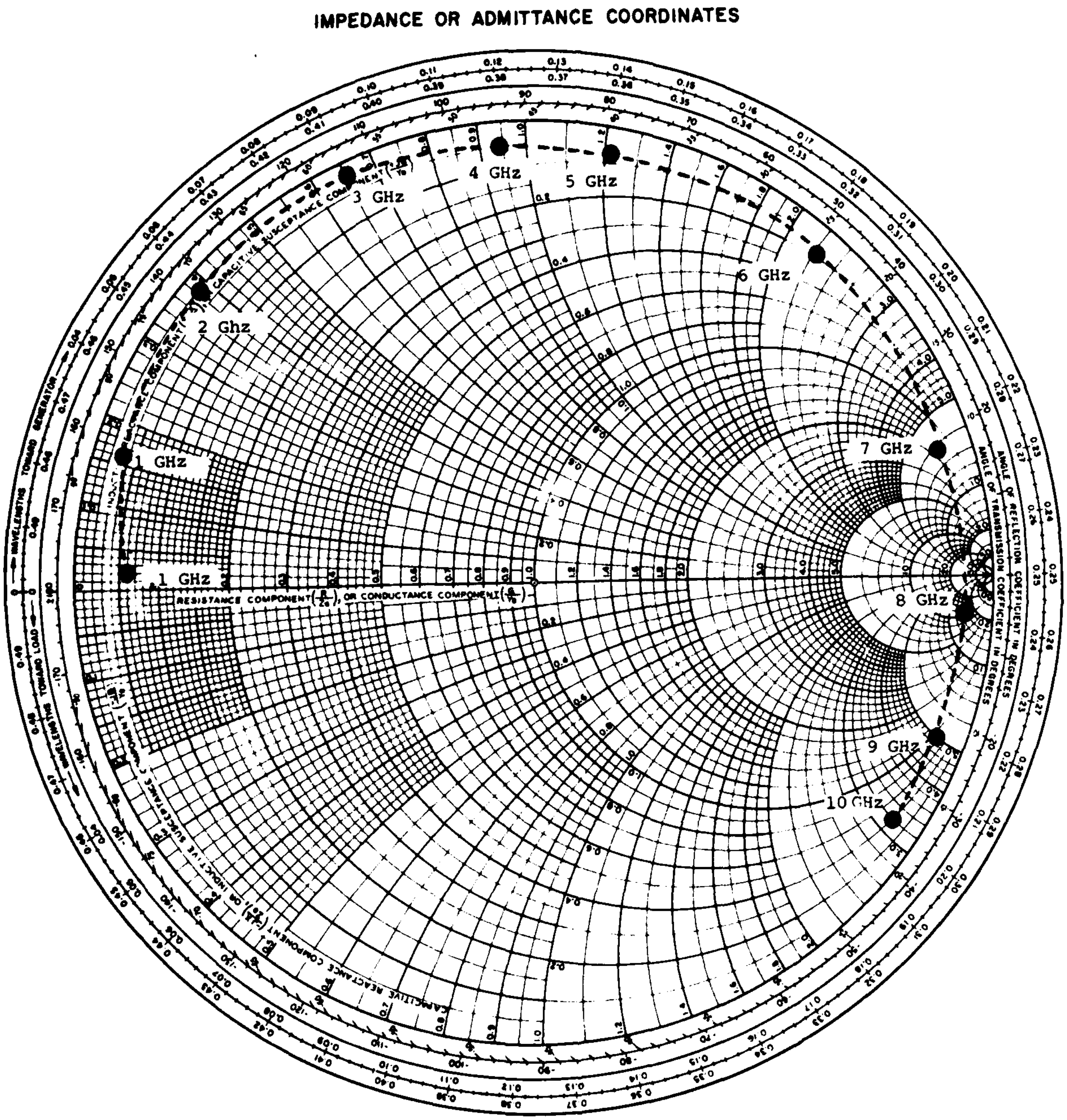

Figure 4.5-6. (b) Experimental Measurements for the Impedance of the Hitachi CSP Laser versus Frequency for Frequencies in the Range of 100 MHz - 10 GHz. The Smith Chart is Normalized to 50 Ohms. The drive current is 1.2 I_{th}. (After Figueroa, Slayman, and Yen)

attenuators, as appropriate, may be used to increase or decrease the input RF power level.

4.6.2 Impedance Matching and Driver Design

The GaAs microwave MESFET is very well suited for direct modulation of a laser diode fiber optic system. Figure 4.6.2-1 shows a schematic diagram of laser transmitter, using a GaAs MESFET as a microwave current-source driver. The low noise MESFET amplifier is used to amplify the RF signal in order to obtain a proper modulation index. Since the laser diode has very low resistance, (approximately 2 ohms) and the amplifier has a 50 ohms output impedance, an impedance transformer must be used. The conventional inductory impedance transformer is not feasible for wideband microwave frequency. However, the MESFET is an attractive candidate for a wideband impedance transformer/amplifier combination for fiber optic communications. Figure 4.6.2-2 depicts an active impedance transformer using a MESFET to match 50 ohm impedance to a laser diode. Mitsubishi medium power FET MGF-2124 was considered because of its power handling capability as well as the minimum nonlinear distortion. A Tee-type microstrip matching was used to achieve the necessary operational bandwidth. Table 4.6.2 illustrates the computer program and computed results. The program instructs the COMPACT[R] program to perform optimization using MGF-2124 S-parameters as input to match 50 ohms to 3 ohms from 4.4 to 5.0 GHz. The results indicated that the matching VSWR (S_{11}) is better than 1.1:1, with a gain (S_{21}) of better than 5 dB and stability factor (K) of larger than 4, over the frequency of 4.4 to 5.0 GHz.

The complete driver can be fabricated in a microstrip configuration on an alumina or a polystyrene substrate. Input and output impedance matching is achieved using microstrip stubs. Figure 4.6.2-3 presents the hardware of laser diode driver fabricated on an alumina substrate. The abbreviations GT, DR, and ILD stand for Gate, Drain, and Injection Laser Diode (between two wires) bias points.

Variations in the threshold current of a laser diode will affect the optic power output, modulation depth, nonlinearity, and delay distortions. One must, therefore, provide a method to compensate for, or to minimize, the threshold current variations. Feedback-control, quasi-feedforward control, adaptive control, and automatic bias control have been used in the past. Each of these methods has its own merits and disadvantages. A simple method using an optical tap (instead of

MICROWAVE FIBER-OPTIC ILD TRANSMITTER

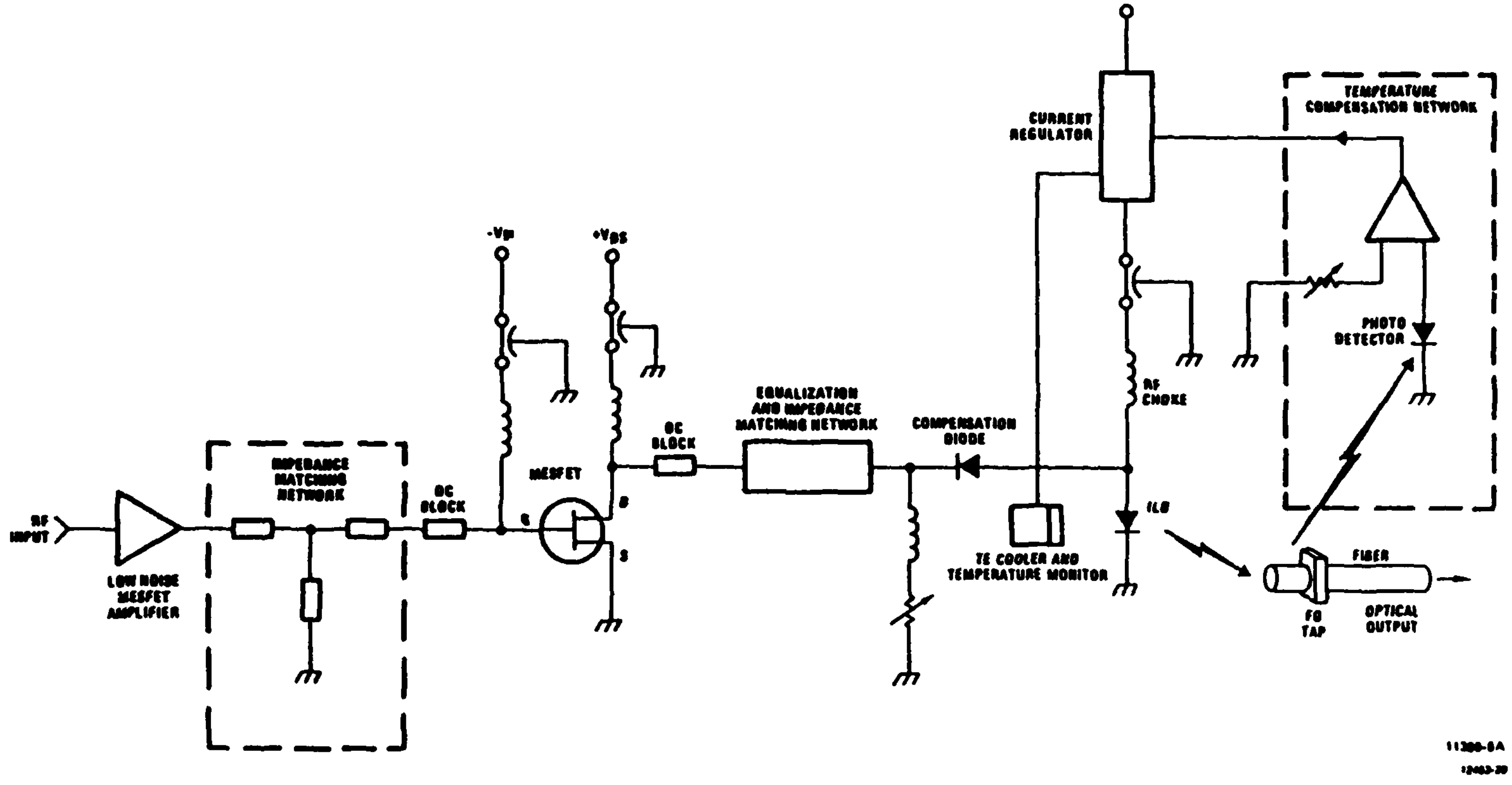

Figure 4.6.2-1. A Schematic Diagram of a Wideband Microwave Laser Diode Driver and Nonlinearity Compensation Network

ACHIEVE LOW OUTPUT IMPEDANCE

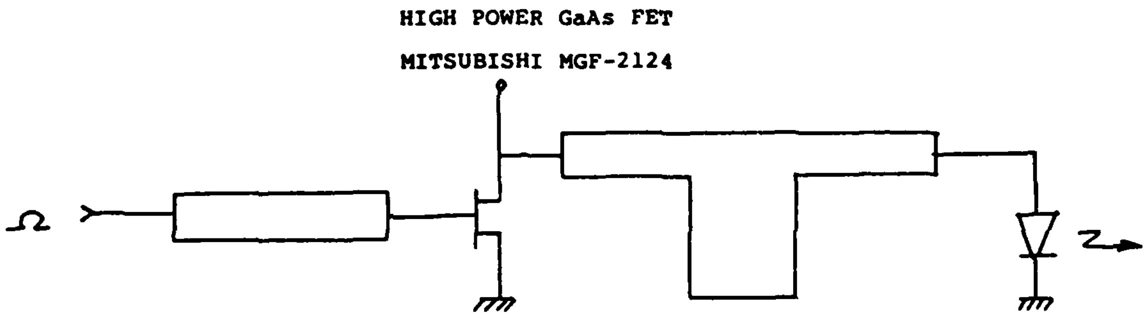

OUTPUT MATCHING USES T-TYPE TRANSFORMER IN MICROSTRIP

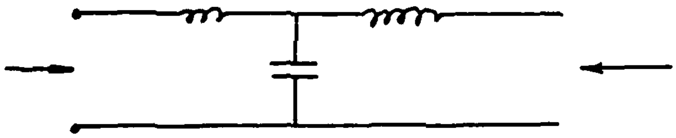

Figure 4.6.2-2. Configuration of Using MESFET as Active Impedance Transformer to Match 50 ohm to Laser Diode

Table 4.6.2. Computer Program and Results to Match 50 ohms to 3 ohms using MGF-2124 MESFET, from 4.4 to 5.0 GHz

```
TRL AA MS - 37.492 - 223.1 9.9 25
TWO BB S3 50
TRL CC MS -3.0234 -12.08 9.9 25
OST DD MS 50 -190.29 9.9 25
EQU EE CC
CAX AA EE
PRI AA S3 50
END
4400 5000 200
END
50 0 3 0
50 0 3 0
50 0 3 0
50 0 3 0
END
.1 175 1.99 30.4 .05 -8.9 .38 -168
.1 166 1.7 23.5 .049 -13.8 .39 -174
END
.1
0 10 0 6
END
```

POLAR S-PARAMETERS WITH COMPLEX LOAD AND SOURCE

FREQ.	SOURCE IMP. (R,JX) OHMS		LOAD IMP. (R,JX) OHMS	
4400.00	(50.00,	0.00)	(3.00,	0.00)
4600.00	(50.00,	0.00)	(3.00,	0.00)
4800.00	(50.00,	0.00)	(3.00,	0.00)
5000.00	(50.00,	0.00)	(3.00,	0.00)

F	S11 (MAGN.	ANGL)	S21 (MAGN.	ANGL)	S12 (MAGN.	ANGL)	S22 (MAGN.	ANGL)	S21 DB	K FACTOR
4400.00	0.06	-158	1.95	-101.2	0.049	-140.5	0.43	-24	5.81	4.27
4600.00	0.09	-158	1.96	-117.8	0.051	-156.7	0.31	-30	5.83	4.51
4800.00	0.11	-168	1.94	-139.7	0.053	-177.9	0.09	-30	5.78	4.77
5000.00	0 .09	-179	1.78	-170.2	0.051	152.5	0.28	105	5.01	5.04

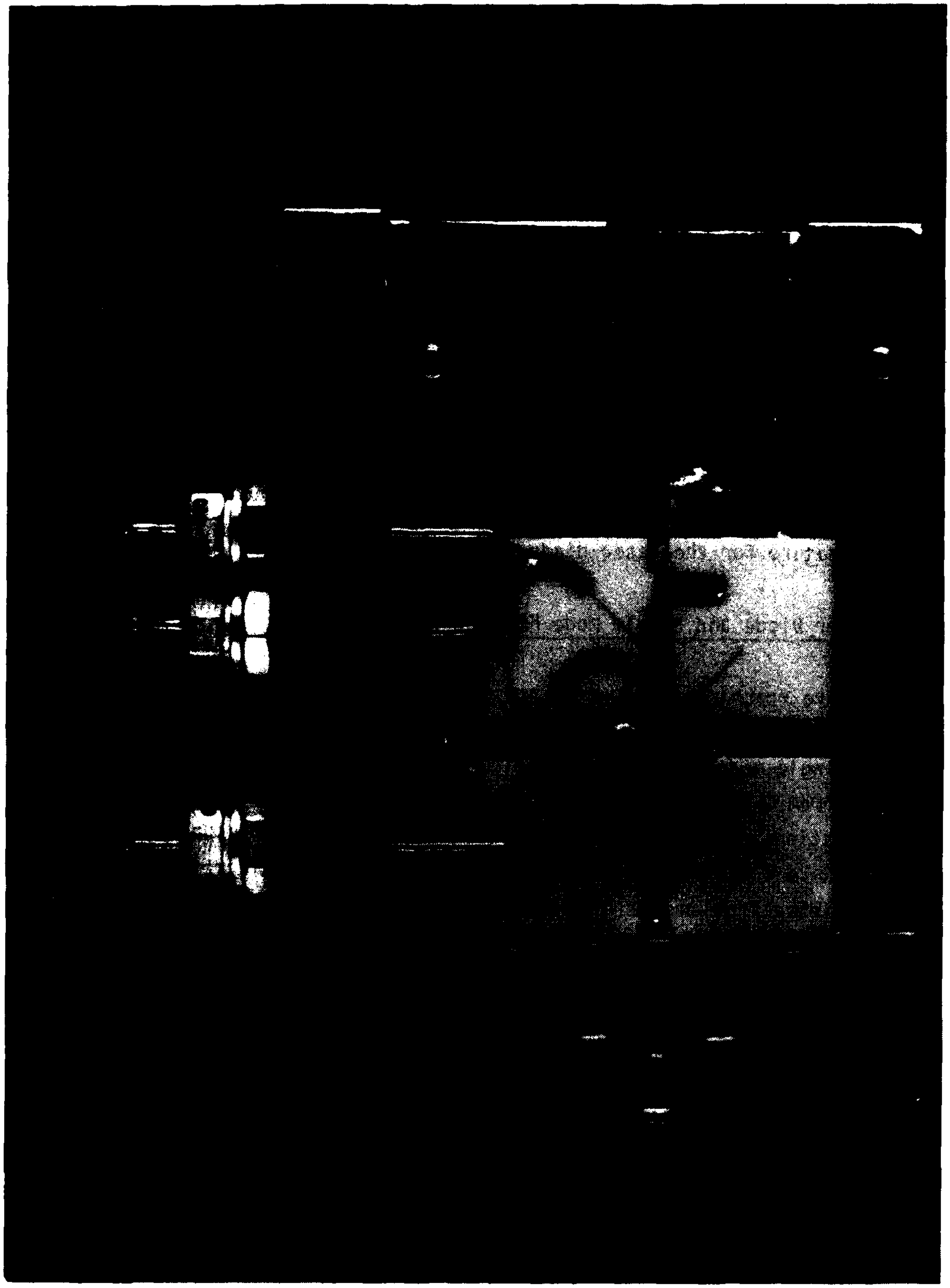

Figure 4.6.2-3 Laser Diode Driver Fabricated on an Alumina Substrate

the back mirror of the ILD) can monitor the actual output power for feedback control. This approach can eliminate the problem of ILD front-to-back mirror mistracking. To preserve the valuable laser output power, the cladding mode optical tap may be used. The tap feeds optical power to the monitor photodetector and the closed loop feedback circuit supply to the dc bias, which is adjusted to maintain the peak light output constant relative to the reference channel. The photodetector can be a PIN photodiode or a low cost phototransistor. For wide temperature range operation, a Thermoelectric cooler (TE) should be used to prolong the LD's lifetime.

A TE cooler control circuit was also developed during this project to enable laser diode transmitter operation at temperatures above 50° C. Figure 4.6.2-4 depicts the hardware of 5.0 GHz laser diode driver, TE cooler control circuit, and feedback circuit. The temperature of laser diode mount is constantly monitored, and then the TE cooler driver current is automatically adjusted to maintain a constant temperature for the laser diode.

4.6.3 Laser Diode and Single Mode Fiber Interface

Before reaching its quantum noise limited performance, the system requires maximizing the received optical power to improve system S/N. The small core size of single mode fiber requires highly precise alignment to couple more optical power from ILD to fiber. Various coupling methods, including different microlens formations, have been investigated for improvement of coupling efficiency. Table 4.6.3 illustrates different techniques for improving the coupling efficiency from an ILD into a single mode fiber. The polished V-shape-fiber-end approach offers a very low coupling loss of 1.1 dB. In the 4.4 - 5.0 GHz RF FO systems, a hemispherical microlens was used at fiber tip to collect more light from the laser diode. A 5 percent coupling efficiency was obtained to minimize laser noise.

One of the major problems when using a single mode fiber with a small core is the precision positioning scheme necessary to maximize optical coupling to the laser diode emission region which is 5 μm by 0.5 μm in size. One solution consists of micrometer controlled, miniature, precision acme threads and slides which have a resolution of approximately 1 μm and are relatively inexpensive,

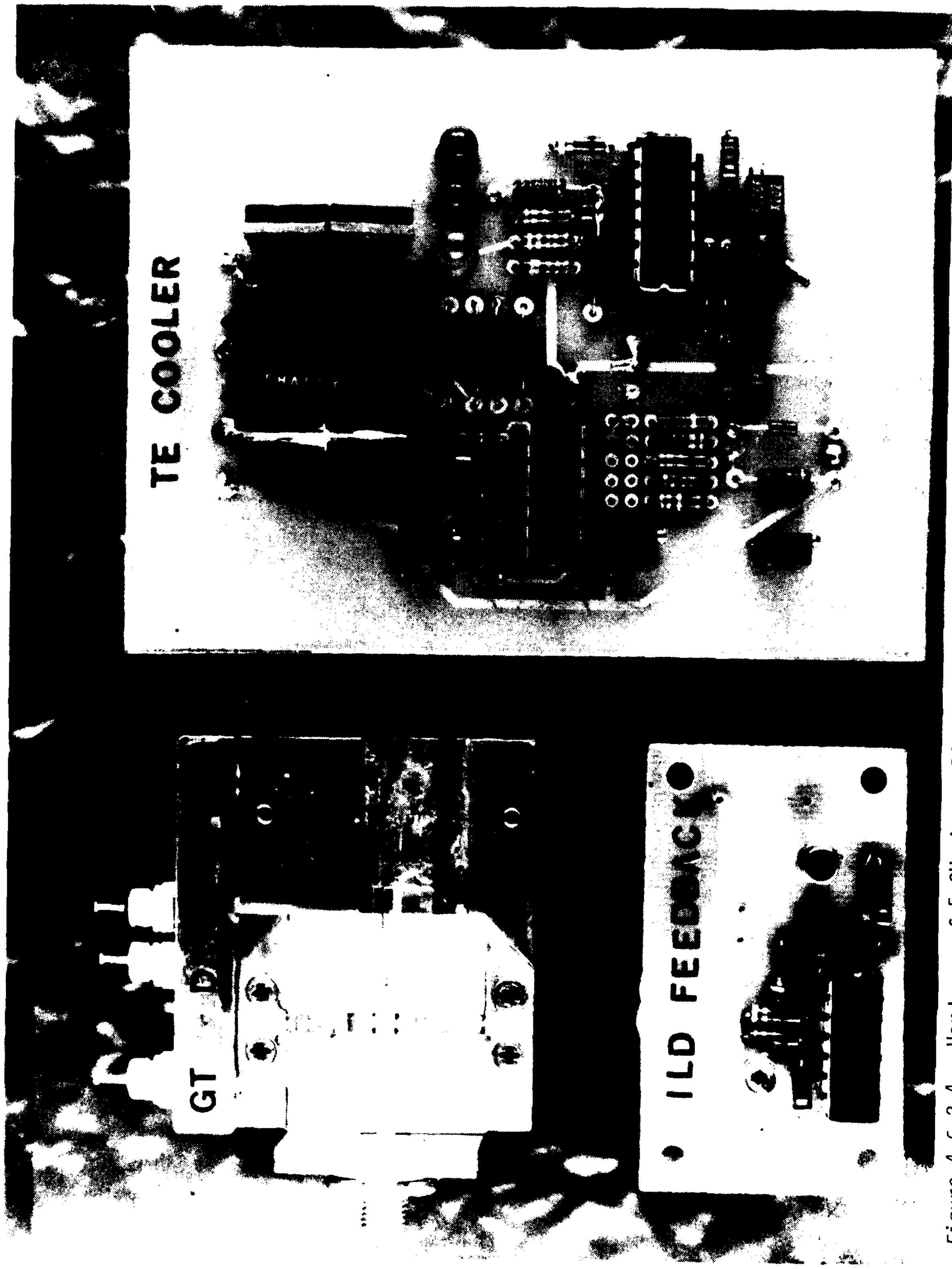

Figure 4.6.2-4. Hardware of 5 GHz Laser Diode Driver, Feedback Circuit and TE Cooler Control Circuit

Table 4.6.3. Insertion Laser Diode - Single Mode Fiber Coupling

COUPLING METHOD	COUPLING LOSS (dB)	INSTITUTE
. Butt Joint	7-12	--
. Miniature Lens (Hemispherical and Hemicylindrical)	0.8-15 (0.8 dB Obtained)	NTT
. Hemispherical Microlens	2.9 - 4.4	NTT
. Two Confocal Lenses	4.5	NTT
. Tapered Fiber	--	--
. Selfoc Lens	--	--
. Hemispherical Lens and Selfoc Lens	--	--
. Bulb-Ended Fiber	--	--
. Polished V-Shape Fiber-End	1.1	Standard Elektrik Lorenz AG,[1] W. Germany
. YIG Sphere	4.7	NTT[2]

1. Laser Focus, Feb. 1982, pp. 103-104
2. IEEE J. of Lightwave Tech., March 1983, pp. 121-130

fairly easy to implement, and would probably handle the job with good repeatability and low drift. To get finer resolution than this would require Piezoelectric translators which are also miniature in size, easy to implement but relatively expensive. The benefits they offer are 0.5 μm resolution, no drift and exceptional repeatability but at the expense of large necessary external controllers. A tradeoff between housing complexity of the two approaches and therefore, cost versus resolution needed should provide the answer as to which scheme would be best.

Recently, a nonreciprocal method for laser diode-to-optical fiber coupling has been described by Sugie and Saruwatari.[1] The coupling component consists of a Yttrium Iron Garnet (YIG) sphere graded-index rod lens and a polarizer. The coupling loss between laser and the single mode fiber (9.9 μm core and 125.5 μm clad) is less than 4.7 dB. However, the YIG sphere also provides a 32 dB isolation between fiber and laser. This nonreciprocal approach will minimize the light reflection from the fiber which may easily deteriorate the laser noise characteristics.

4.6.4 Laser Noise Discussion

Laser intrinsic noise, modal noise, partition noise and delay noise, and its reduction methods have been briefly described in Section 3. In this section, these noises and distortions will be explored a little further.

In order to have a stable transverse single mode operation up to high light output and be suitable for microwave fiber optic application, the stripe widths of both index-guided lasers and gain-guided lasers[2] should be less than

1. T. Sugie and M. Saruwatari, "An Effective Nonreciprocal Circuit for Semiconductor Laser-to-Optical-Fiber Coupling Using a YIG Sphere", IEEE J. of Lightwave Tech., March 1983, pp. 121-130.

2.
- Index-guided laser: a refractive index step is created parallel to the active layer by various technological means.
- Gain-guided laser: the waveguiding parallel to the junction is accomplished only by the lateral distribution of the carrier density which forms a gain profile by which the laser mode is guided.
- Index-guided laser is preferable for microwave fiber optics due to the smooth transition around threshold.

5 μm. Such narrow stripe lasers of both types do not exhibit "kinks", or self-pulsation of their light-output. For a gain-guided laser there is also some curvature in light-current characteristics above threshold. Because of this curvature, gain-guided laser exhibits larger second-order harmonic distortions than index-guided lasers.

The intrinsic noise of a laser diode is governed by the quantum process inside the laser cavity.[1,2] These processes include the shot noise of the junction current, the spontaneous recombination of carriers within the active layer, the light absorption and scattering, and the stimulated emission. No theoretical analysis is given here. Figure 4.6.4-1 depicts measured intrinsic dc Signal-to-Noise ratios (S/N) at 50 MHz for an index-guided laser and a gain-guided laser.[2] The S/N has its minimum value a little bit above threshold and this minimum is much more pronounced for an index-guided laser than for a gain-guided laser. The actual S/N between the modulated signal and the noise is lower than the dc-S/N, depending on the modulation index, m, of laser modulation. Figure 4.6.4-1 shows the extrapolated S/N for m = 0.5 and a bandwidth of 5 MHz. This corresponds to transmission of a single TV with a very satisfactory S/N of 60 - 70 dB. Nonlinear distortions near the relaxation oscillation resonance frequency is high.

The laser diode partition noise strongly depends on the emission spectrum of the laser. If the laser oscillates strictly in a single-longitudinal mode, there is obviously no partition noise at all. On the other hand, a laser emitting in a large number of longitudinal modes and relatively large spontaneous emission may also have low partition noise.

If multimode fibers are fed with laser lignt, interference between the different fiber modes occurs. This interference generates a speckle pattern in a cross section of the fiber core. At nonideal fiber-to-fiber connections (connectors, splices) the coupling efficiency from one fiber section into the next one depends on the speckle pattern at the intersection. Since the speckle pattern

1. D. E. McCumber, "Intensity Fluctuation in the Output of CW Laser Oscillators", Phys. Rev. January 1966, pp. 306-322.

2. K. Perterman and G. Arnold, "Noise and Distortion Characteristics of Semiconductor Lasers in Optical Fiber Communication Systems", IEEE Trans. of MTT, April 1982, pp. 389-401.

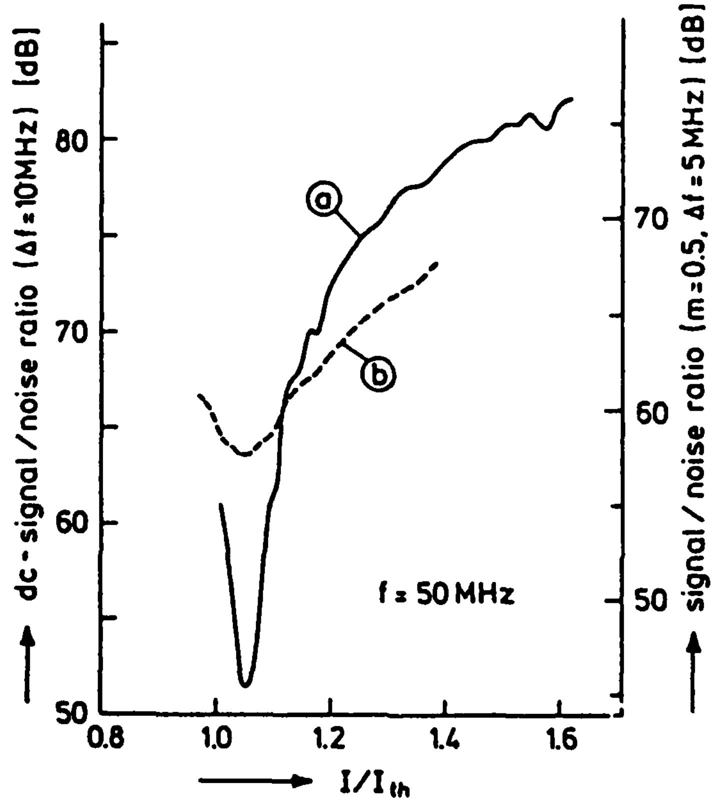

Figure 4.6.4-1. Measured Signal-to-Noise Ratio of (a) Index-Guided Laser and, (b) Gain-Guided Laser (after Perterman and Arnold)

is extremely sensitive to delay/variations of the fiber modes, it is generally not stable and is heavily influenced by mechanical vibrations, temperature changes, and, of course, minor laser wavelength changes. Hence, every practical fiber connection exhibits a varying transmission factor depending on external disturbance. Since direct modulation of a laser diode not only modulates the emitted power but also the wavelength, the occurring speckle pattern is modulated and hence the coupling efficiency, as well. This leads to a nonlinear behavior of the graded-index fiber which gives rise to poor and unstable S/N. The elimination of modal noise problems is only possible by using single mode fibers. A considerable reduction of modal noise is possible by employing gain-guided lasers which transmit many longitudinal modes and partially average the effect of modal noise.

If light is launched into optical fibers, the fiber front face as well as connectors, splices, and the fiber far end scatter light back to the source. Reflected light which gets back into the laser deteriorates laser linearity, spectral stability, and noise behavior.

Because of birefringence in single mode fibers, the two orthogonal fundamental modes propagate with different velocities. This effect leads to polarization mode dispersion (several picoseconds per kilometer), with a decreasing transfer function bandwidth. Also, nonlinear distortions and excess noise are possible. They are of importance for analog as well as digital transmission. To solve these problems, polarization-maintaining fibers were developed with strong birefringence to decouple the two orthogonal modes.

Intensity and frequency fluctuation in semiconductor laser diodes can limit the performance of fiber optic sensors designed to operate at low frequencies ($\leq$10 kHz) as well as microwave fiber optic systems used for injection oscillator locking (in which phase noise near the carrier is very important). Previous measurements have shown that both intensity and frequency noise power spectra in a number of different GaAlAs laser structures decrease with frequency approximately inverse.[1] However, it recently has been found that the low-frequency fluctuation

1. A. Dandridge and A. B. Tveten, "Phase Noise of Single Diode Lasers in Interferometer Systems", Appl. Phys. Lett. pp. 530-532, 1982.

in the intensity of light emitted from the two facets of single mode laser diodes are not perfectly correlated.[1]

Figure 4.6.4-2 shows the frequency dependence of the intensity noise of three lasers, emitting from the front facets of the lasers. The lasers showed a frequency dependence of noise power approximately proportional to 1/f.

5.0 SINGLE MODE OPTICAL FIBER

5.1 Need of Single Mode Fiber

The need to minimize transmission cost, electromagnetic interference, electromagnetic pulse, and size/weight-effectiveness in microwave, high speed, and long haul applications have motivated research and development in single mode optical fiber transmission systems. In recent years, considerable progress has been realized. Single mode optical fibers represent an intrinsically wideband transmission medium which is well suited for large capacity transmission, especially in long wavelength regions where optical transmission loss is low. Terrestrial longhaul, microwave RF, high speed digital and submarine transmissions are demanding the single mode optical fiber.

5.2 Discussion of Fundamental Single Mode Fiber and Operational Parameters

Various refractive index profiles, as depicted in Figure 5.2, have been developed for single mode fibers and are being assessed by manufacturers. They represent different approaches to reduce dispersion. Snyder[2] has used the simple analytic forms for the fields, propagation constant, and other parameters to describe the fundamental mode (HE_{11}) in the Gaussian refractive index and the step refractive index single mode fiber, instead of using the solution of transcendental equations. Table 5.2-1 summarizes the single mode parameters given by Synder, in

1. A. Dandridge and H. F. Taylor, "Correlation of Low-Frequency Intensity and Frequency Fluctuation in GaAlAs Lasers", IEEE Trans on MTT, October 1982, pp. 1726-1738.

2. A. W. Snyder, "Understanding Monomode Optical Fibers", Proc. of IEEE January 1981, pp. 6-13.

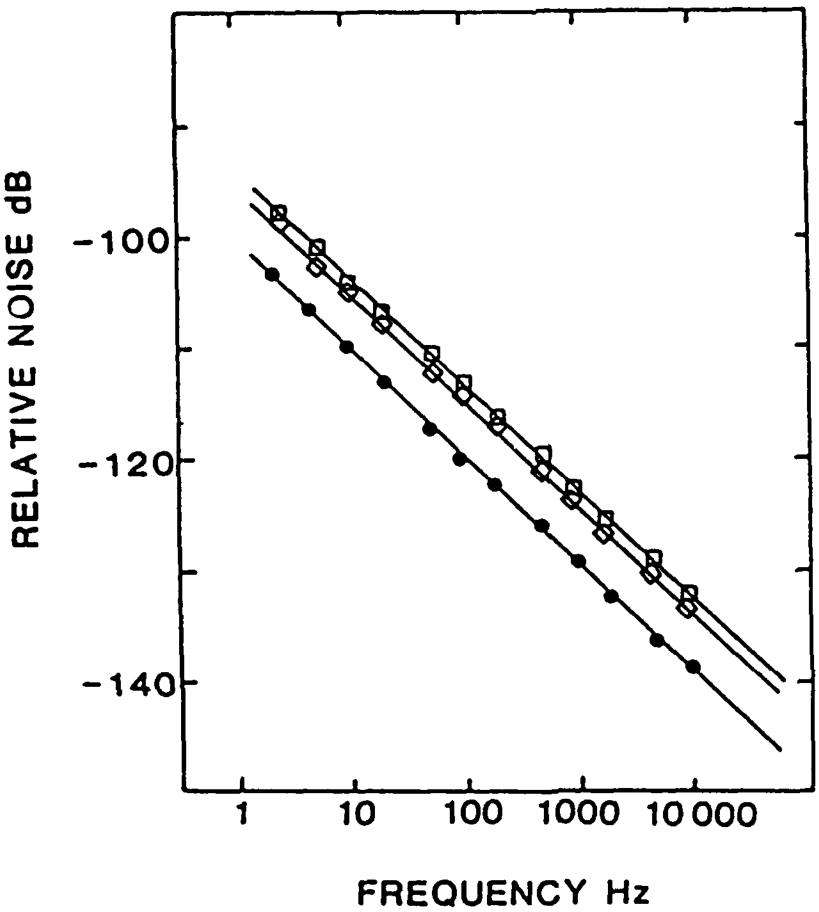

Frequency dependence of the intensity noise (1 Hz B/W) of the three lasers tested: ●, TJS; ◊, CSP; □, BH.

(After Dangridge and Taylor.)

Figure 4.6.4-2.

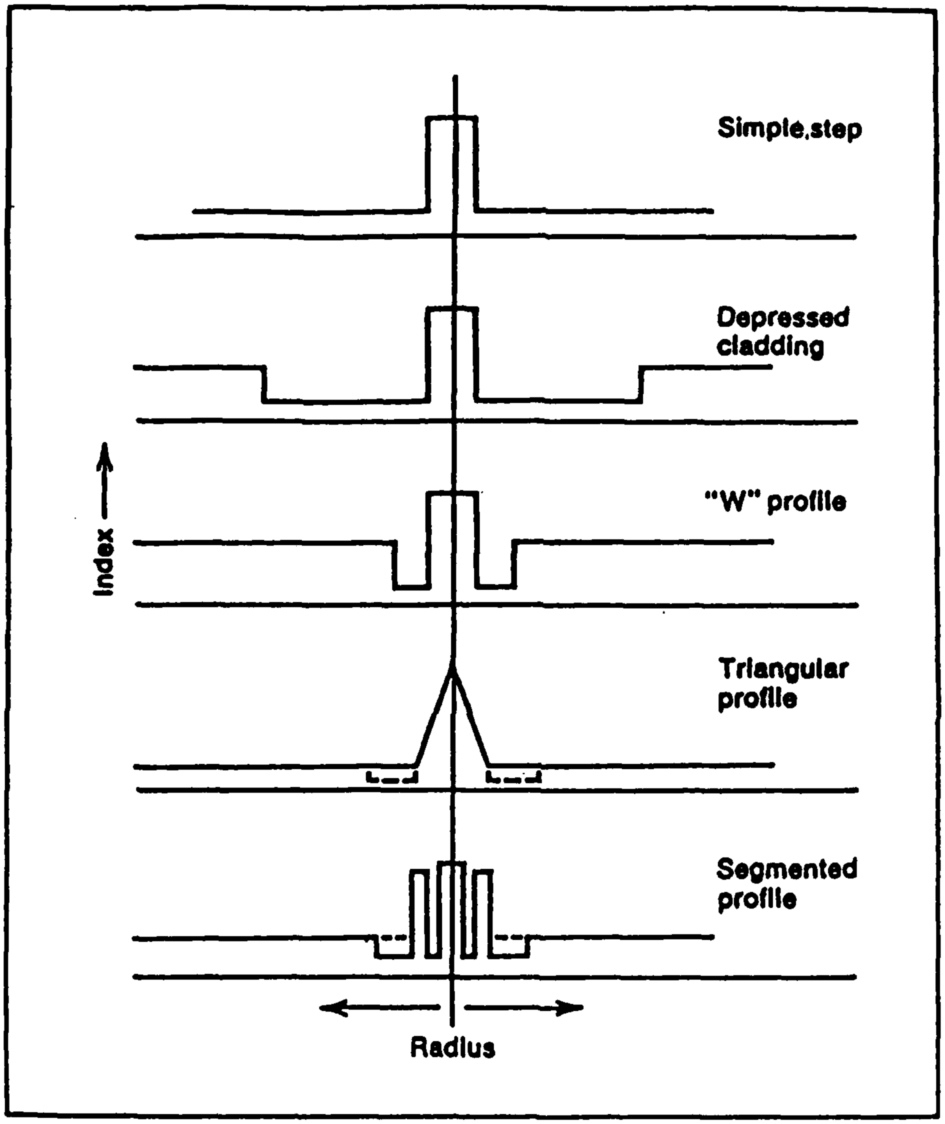

Figure 5.2. Various Refractive Profiles of Single Mode Fiber

Table 5.2-1. Single Mode Fiber Parameters Expressed in Terms of the Spot Size

z-directed power density	$S(r) = \frac{1}{2}E_x H_y^* = \frac{1}{2}(\varepsilon/\mu)^{1/2} e^{-(r/r_o)^2}$
Total power	$P = 2\pi \int_0^r rS(r)\,dr = \frac{\pi}{2}\left(\frac{\varepsilon}{\mu}\right)^{1/2} r_o^2$
Fraction of power within 0 to r	$\eta(r) = \frac{\int_0^r rS(r)\,dr}{\int_0^\infty rS(r)\,dr} = 1 - e^{-(r/r_o)^2}$
(Group velocity)$^{-1}$	$v_g^{-1} = \frac{d\beta}{d\omega} = \frac{\omega\mu\varepsilon_{co}}{\beta}\left\{1 + \left(\frac{\Delta}{Vn_{co}}\right)^2 \left(\frac{\rho^2}{r_o^2} + y\right)\right\}$ $y = (\rho\beta)^2 - (\rho k_{co})^2$
Waveguide dispersion parameter	$D = \frac{1}{\rho\mu\varepsilon_{cl}}\left(\frac{n_{co}}{\Delta}\right)^3 \frac{dv_g^{-1}}{d\omega} \cong \frac{1}{V^3}\left\{V\frac{d}{dV}\left(\frac{\rho}{r_o}\right)^2 - \left(\frac{\rho}{r_o}\right)^2\right\}$ (neglecting terms in Δ)

	Gaussian Profile	Step Profile	"Smoothed Out" Step Profile
$S(r)$ for $V>1$	$\frac{1}{2}\left(\frac{\varepsilon}{\mu}\right)^{1/2} e^{-(r/\rho)^2(V-1)}$	$\frac{1}{2}\left(\frac{\varepsilon}{\mu}\right)^{1/2} e^{-(r/\rho)^2 \ln V^2}$	$\frac{1}{2}\left(\frac{\varepsilon}{\mu}\right)^{1/2} e^{-(r/\rho)^2(m+1)(V^{\frac{2}{m+2}} - 1)}$
P for $V>1$	$\frac{\pi}{2}\left(\frac{\varepsilon}{\mu}\right)^{1/2} \frac{\rho^2}{V-1}$	$\frac{\pi}{2}\left(\frac{\varepsilon}{\mu}\right)^{1/2} \frac{\rho^2}{\ln V^2}$	$\frac{\pi}{2}\left(\frac{\varepsilon}{\mu}\right)^{1/2} \rho^2/(m+1)(V^{\frac{2}{m+2}} - 1)$
$\eta(r)$ for $V>1$	$1 - e^{-(r/\rho)^2(V-1)}$	$1 - e^{-(r/\rho)^2 \ln V^2}$ $= 1 - (1/V)^2, r=\rho$	$1 - e^{-(r/\rho)^2(m+1)(V^{\frac{2}{m+2}} - 1)}$
v_g^{-1} for $V>1$	$\frac{\omega\mu\varepsilon_{co}}{\beta}\left\{1 - \frac{1}{V}\left(\frac{\Delta}{n_{co}}\right)^2\right\}$	$\frac{\omega\mu\varepsilon_{co}}{\beta}\left\{1 + \left(\frac{\Delta}{Vn_{co}}\right)^2\right\}$	$\frac{\omega\mu\varepsilon_{co}}{\beta}\left\{1 - \left(\frac{\Delta}{n_{co}}\right)^2 \left(\frac{1}{V^2}\right)^{\left(\frac{m+1}{m+2}\right)}\right\}$
D for $V>1$	$1/V^3$	$2(1 - \ln V)/V^3$	$\frac{m+1}{V^3}\left\{1 - \left(\frac{m}{m+2}\right)V^{\frac{2}{m+2}}\right\}$

terms of the spot size, v_0. Table 5.2-2 presents the single mode fields for various core index profiles. The spot size is defined as the width to 2/e intensity of the HE_{11} mode or, alternatively, in terms of the spot size of an incident Gaussian beam which gives maximum launching efficiency.

5.3 Trend and Prediction

Figure 5.3-1 shows loss spectra of three state-of-the-art single mode fibers made by MCVD (Modified Chemical Vapor Deposition), OVD (Outside Vapor Disposition), and VAD (Vapor-Phase Axial Deposition) processes. The OVD Process has produced fiber with loss of 0.16 dB/km at 1.5 μm wavelength.[1] The VAD fiber exhibits the lowest OH absorption at 1.39 μm and the MCVD fiber is a depressed-index-cladding type, developed for undersea-cable application, where simultaneous achievement of low loss, bending insensitivity, and minimum dispersion at 1.3 μm was an important consideration.

Adding more cladding layers or index walls can extend the useful range of minimal dispersion and reduce bending loss. Figure 5.3-2 depicts the measured dispersion spectrum of an experimental, low loss, quadruplyclad fiber (with two index walls).[2] Such ultrawideband fibers will alleviate mode partition noise problems associated with the use of multilongitudinal mode lasers.

Near future single mode fiber developments will emphasize the following aspects:

- Polarization-maintaining single mode fiber

1. M. G. Blankenship and C. W. Deneka, "The Outside Vapor Deposition Method of Fabricating Optical Waveguide Fibers", IEEE J. of QE, October 1982, pp. 1418-1423.

2. L. G. Cohen, et al, "Low-Loss Quadruple Clad Single Mode Lightguide with Dispersion Below 2 ps/km . nm over the 1.28 m - 1.65 m Wavelength Range", Elect. Lett. November 1982, pp. 1023-1024.

Table 5.2-2. Fields Distribution of the Single Mode Fiber

$$E_x = e^{-\frac{1}{2}\left(\frac{r}{r_o}\right)^2} e^{i\beta z} \qquad H_y = (\varepsilon/\mu)^{\frac{1}{2}} E_x \tag{II.1}$$

with E_y, H_x, E_z and H_z negligible

$$n^2(r/\rho) = n_{cl}^2 + s(r^2/\rho^2)\Delta^2 \tag{II.2}$$

$$\Delta = (n_{co}^2 - n_{cl}^2)^{\frac{1}{2}} \tag{II.3}$$

$$(\rho\beta)^2 = (\rho k_{co})^2 - \left(\frac{\rho}{r_o}\right)^2 + V^2\left\{\int_0^\infty e^{-c_o x}\frac{ds}{dx}(x)\,dx + s(o) - 1\right\} \tag{II.4}$$

where $k_{co} = 2\pi n_{co}/\lambda$ and $V = 2\pi\rho\Delta/\lambda$ with $x = (r/\rho)^2$ and

$c_o = (\rho/r_o)^2$

$c_o = (\rho/r_o)^2$ is found by solving

$$1 = -V^2 \int_0^\infty x e^{-c_o x}\frac{ds}{dx}(x)\,dx \tag{II.5}$$

	Gaussian Profile	Step Profile	"Smoothed Out" Step Profile
$s(r^2/\rho^2)$	$e^{-(r/\rho)^2}$	$1\ ,\quad r < \rho$ $0\ ,\quad r > \rho$	$\Gamma^{-1}(m+1)\int_a^\infty t^m e^{-t}\,dt \qquad a = (m+1)r^2/\rho^2$
$(\rho/r_o)^2$ for $V > 1$	$V - 1$	$\ln V^2$	$(m+1)(V^{\frac{2}{m+2}} - 1) \underset{m\to\infty}{\sim} \ln V^2 + \frac{(\ln V^2 - 2)\ln V^2}{2m}$
$(\rho\beta)^2$ for $V > 1$	$(\rho k_{co})^2 - 2V + 1$	$(\rho k_{co})^2 - \ln V^2 - 1$	$(\rho k_{co})^2 - (m+2)V^{\frac{2}{m+2}} + (m+1)$ $\underset{m\to\infty}{\sim} (\rho k_{co})^2 - \ln V^2 - 1 - (\ln V^2)^2/2m$

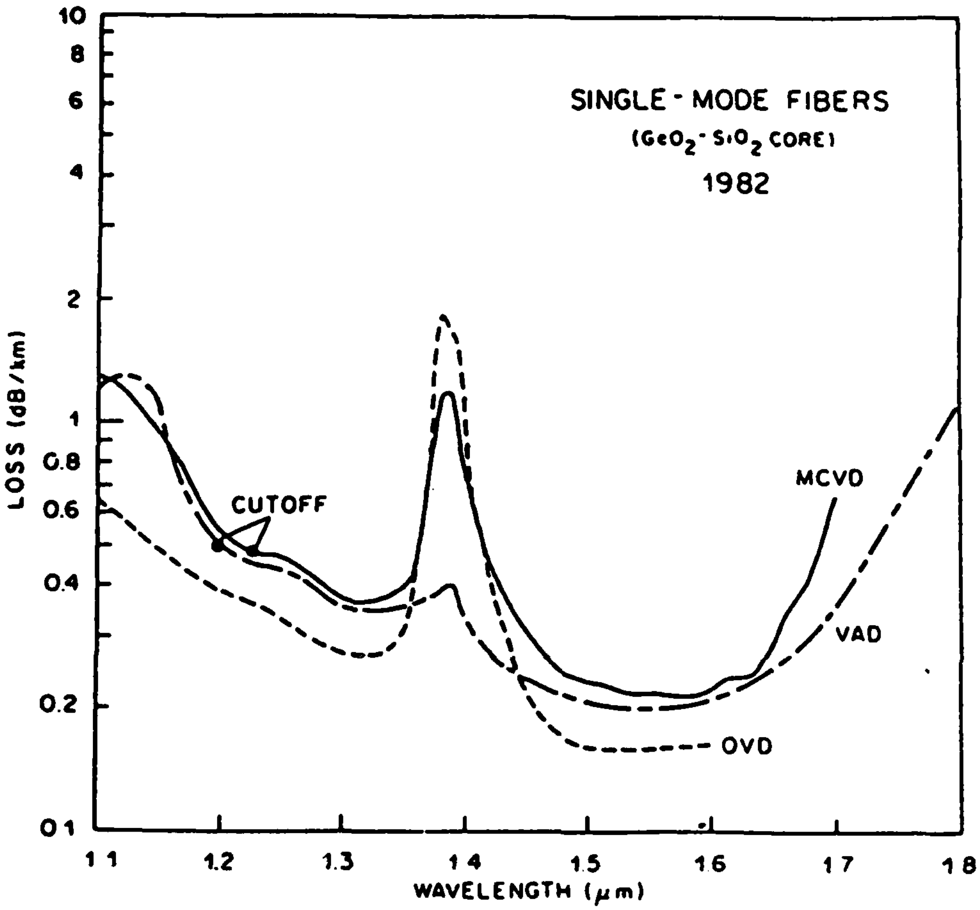

Figure 5.3-1. Loss Spectra of Three State-of-the-Art Single Mode Fibers (After T.Y. LI)

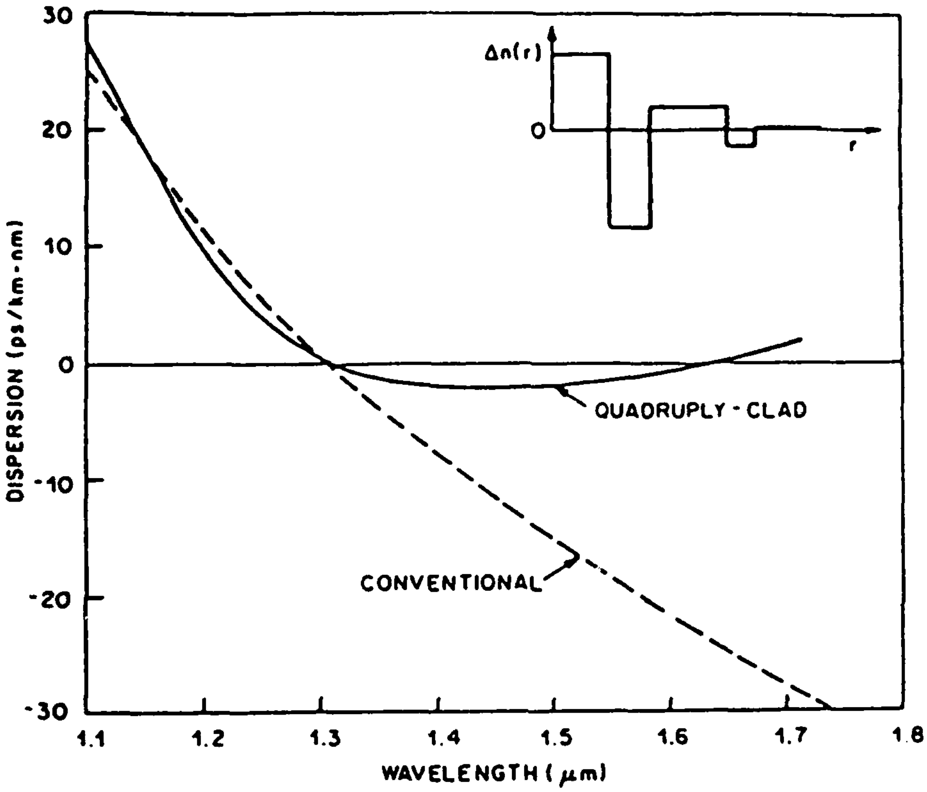

Figure 5.3-2. Chromatic-dispersion spectra of single mode fibers. The Dashed Curve is for a conventional step-index fiber. The solid curve is the measured dispersion of an experimental quadruply-clad fiber with a profile as shown in the upper right corner. (After T.Y. LI)

- Fiber index profile optimization for undersea communications applications

- Single mode fiber manufacturing and cabling techniques improvement

Profile optimization and manufacturing technique improvement will not be discussed in this report. However, the preservation of polarization in single mode fiber is very important for microwave communications and interferometric sensors. Single mode optical fibers do not normally preserve the polarization state of the light propagation along with fiber. In ordinary axially symmetrical optical fibers, the polarization state of the propagated wave is subject to unstable fluctuation when ambient conditions change. An ideal circular fiber can support two independent, degenerate modes of orthogonal polarization, which may be arbitrarily chosen as the horizontal H and the vertical V linear polarizations. Either one of these constitutes the fundamental HE_{11} mode. In general, the electrical field of light propagating along the fiber is a linear superposition of these two polarization eigenmodes. In practical single mode fibers, various imperfections such as asymmetrical lateral stress and a noncircular core break the circular symmetry of the ideal fiber and lift the degeneracy of these two polarization modes. They propagate with different phase velocities, and this difference between their effective refractive indices is called birefringence: $B = n_v - n_v$. The birefringence can result either from a geometrical deformation or from various elasto-optic, magnetic-optic, and electro-optic index changes. These birefringence mechanisms act on the fiber in usually unknown number, strength, orientations, and locations along the fiber. They result from internal defects, cabling, coiling, inadvertent twistings, and stray magnetic and electric fields. Most are sensitive to the environment. The fiber polarization or birefringence change may give rise to the following problems in the single mode fiber systems.

- The received signal level fluctuates when the receiver is sensitive to the polarization.

- The slight elliptical deformation remaining in the fiber separates the propagation constants of two orthogonal HE_{11} modes, and cause the polarization mode dispersion in the group delay.

- Reduction of bandwidth[1,2].

- The polarization instability will deteriorate the measurement accuracy of magneto-optic current sensor of fiber optic gyroscope.

The solution to these is use of the polarization maintaining fiber. High birefringence fibers of different configuration, maintain a polarization state over a long length.

a. Single linear polarization (SLP) fiber.

1. Absolutely SLP fiber: the fiber is designed so that the transmission losses for the horizontally and vertically polarized mode are largely different so that one propagation mode is cut off.

2. Linearly birefringence fibers: Both polarization modes can be propagated, but the propagation constant difference is made as large as possible. The coupling between two modes is effectively reduced by increasing the modal birefringence. Two different fibers have been investigated.

    - Stress-induced linearly birefringence fibers
    - Geometrically birefringence fibers

1. D. N. Payne, A. J. Barlow, and J. J. R. Hansen, "Development of Low- and High - Bifringence Optical Fibers", IEEE Trans. on MTT, April 1982, pp 323-334.

2. T. Katsuyama, et al, "Propagation Characteristics of Single Polarization Fibers", Appl Optics, June 1983, pp 1748-1753.

AD-A148 679 RF FIBER OPTIC LINK(U) HARRIS CORP MELBOURNE FL 2/2
J J PAN JUN 84 RF-001/0161A RADC-TR-84-118
F30602-81-C-0259

UNCLASSIFIED F/G 17/2 NL

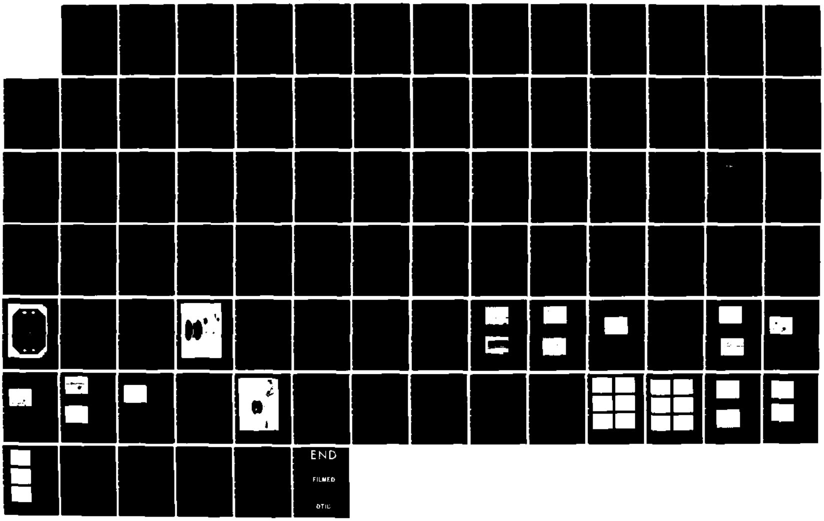

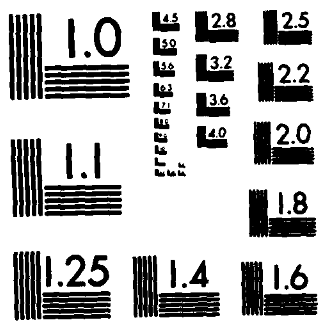

MICROCOPY RESOLUTION TEST CHART
NATIONAL BUREAU OF STANDARDS-1963-A

b. Single Circular Polarization (SCP) fibers. An axially symmetrical fiber is twisted to product a difference in the propagation constants of the clockwise and counter clockwise circulary polarized HE_{11} mode taking advantage of the twist induced optical activity.

The performance[1] comparison of SLP and SCP fibers is given in Table 5.3-3.

Table 5.3-3. Comparison of SLP and SCP Fibers

	SLP fibers	SCP fibers
Fabrication	Difficult	Easy
Polarization stability	Probably better	Probably poorer
Connection	Difficult	Easy
Polarization dispersion	Large	Small
Polarization matching with LO injection	Necessary	Unnecessary

5.4 Survey of Single Mode Fiber Availability and Measurement Technique

5.4.1 Single Mode Fibers

During the 4.4 - 5.0 GHz RF fiber optic link project, only Siecor, Fujikura and Furukawa could commerically supply single mode fibers. The Fujikura single mode fiber, an evaluation sample, has been used in the 4.4 - 5.0 GHz system. Its performance is tabulated in Table 5.4.1-1

1. T. Okoshi, "Heterodyne and Coherent Optical Fiber Communications: Recent Progress", IEEE Trans. of MTT, August 1982, pp 1138-1149.

At the end of the project, single mode fibers were available from:

- Siecor or Corning Glass Works
- Val tec
- Lightwave Technologies
- ITT
- AMFOX
- Sumitomo Electric
- Fujikura
- Furukawa
- Hitachi
- York Technology

The performance of single mode fibers from Lightwave Technologies, ITT, AMFOX, and Sumitomo Electric is summarized in Table 5.4.1-2. (Data collected during period of November 1 through 12, 1982). It is interesting to observe that the core diameter varies from 4 μm to 10 μm of different designs.

5.4.2 Single Mode Fiber Spot Size Measurement

The field distribution in the core and cladding of a single mode fiber is important in characterizing the fiber's optical performance. The width parameter of the best-fit Gaussian function, called beamwidth or spot size, is an appropriate characterization of the field distribution of single-mode fiber. Several spot-size measurement techniques have been investigated during this project. Since these measurement techniques also were discussed by Anderson and Philen[1], and are not central to project objectives, they will not be presented in this report.

1. W. T. William and D. L. Philen, "Spot Size Measurements for Single Mode Fibers - A Comparison of Four Techniques", IEEE J. of Lightwave Technology, March 1982, pp. 20-26.

Table 5.4.1-1. Performance of Fujikura Single Mode Fiber

ITEM	TEST RESULTS	
Length 1,00μm		
Delta	0.30 percent	
Attenuation	2.4 dB/km	0.82μm
	2.1 dB/km	0.84μm
Cutoff Wave Length	0.70μm	
Core Diameter	6μm	
Cladding Diameter	125μm	
Core Non-circularity	0 percent	
Core Cladding Concentricity Error	1μm	

Table 5.4.1-2. Performance Summary of Single Mode Fibers Manufactured by Lightwave Technologies and Sumitomo Electric

Performance Parameters / Manufacturer	Model No.	Core Diameter (um)	Cladding Diameter (um)	Attenuation (dB/Km)	Operation Wavelength (um)	Numerical Aperture
Lightwave Technologies	F0808C F0413C	5.2 ± 0.5 8.2 ± 0.8	47* 76*	4 1	0.82 1.30	0.11 0.11
ITT	PCF-MG1	4.5	80	4	0.85	0.1
AMFOX	3000	4-8	250	6	0.82	0.1
Sumitromo Electric	ES-1/05XX ES-1/07XX ES-1/10XX	10 10 10	125 125 125	0.5 0.7 1.0	1.30 1.30 1.30	0.1 0.1 0.1

* Fiber diameter is 125 ± 3 um.

6.0 SINGLE MODE OPTICAL FIBER COMPONENTS

6.1 Single Mode Fiber Connector

The core diameter of a single mode fiber is, in general, less than 10 μm, and highly precise core axis alignment is required to join fibers. The demountable connector of single mode fibers requires:

- Fiber and hole located exactly at the plug (or ferrule) center.
- Fiber has very good diameter tolerance (1 μm is allowable).
- Fiber core is axially centered (low accentricity).

These requirements sometimes are difficult to meet. Several different single mode connectors have been fabricated and reported. The fabrication methods, performance, and references of these single mode connectors are presented in Table 6.1. The newly developed low insertion and high return loss connectors minimize the reflection light injecting back into laser diode. Consequently, laser diode instability and noises are reduced and system performance improved.

Presently, only Daini Seikosha and Furukawa commercially provide single mode fiber connectors using ceramic capillaries and plug ferrule. The ceramic capillary has a concentricity of less than 1 μm and a hole diameter accuracy of 0 to +1 μm.

For connector assembly the fiber end is required to have an optically smooth surface perpendicular to the axis so that when two terminations are put in a connector, maximum light is transferred without optical scattering. Either clean cleaving or polishing is required for fiber end preparation. If polishing is utilized, the technique requires that the tip of the fiber initially protrudes through the ceramic hole. The plug ferrule end is then polished back to the ceramic surface, leaving an accurately centered fiber with a good surface finish.

Table 6.1. Single Mode Connectors

FABRICATION METHOD	INSERTION LOSS (dB) (Fiber Core/Clad Diameter, μm)	INSTITUTE	REFERENCE
. Ball-bearing array aligned ferrule	0.46 (5.7/150)	NTT	Elect. Lett. Sept. 1978 pp. 612-614
. Tapered Cylindrical Plug, stainless steel	0.47 (8.6/150)	NTT	Elect. Lett. Jan 1979 pp. 28-29
. Precision-made Ceramic Capillary	0.3 (10/125)	NTT	Elect. Lett. Dec. 1979 pp. 809-810
. Plastic Moulded Ferrule	0.48 (10/125)	NTT	Elect. Lett. July 1982 pp. 598-599
. Sapphire Ball Lens	o.54 (3-5/125)	Fujitsu	Appl. Opt., Oct. 1982 pp. 3475-3483
. (a) Physical contact ferrule with treated end	0.13 (with 24 dB return loss) (10/125)	NTT	Appl. Opt., Oct. 1982 pp. 3475-3483
(b) Angle butted ferrule with Obliquely Polished	0.4 (with 40 dB return loss)	NTT	IOOC '83 Digest pp. 126-127
. Transfer-Molded Biconiacal	0.65 (9/110)	Bell Lab	IOOC '81 Digest p. 98
. Transfer-Molded Biconical	0.28 (10/105)	Bell Lab	OFC '83 Digest p. 14

6.2 Single Mode Fiber Splicing

Single mode optical fibers have many advantages for long distance and microwave transmission. The small core sizes, however, cause splicing problems in the same manner as for the connector. In the past several years many precision tools or equipment have been developed to reduce splicing loss and to conquer the operation difficulties. Some of these techniques have been applied to practical field installation. Table 6.2 lists the single mode fiber slicing loss using various techniques. It is interesting to notice that the ultraviolet curable cement approach can achieve an insertion loss of 0.02 dB. The cemented approach eliminates the hazard of potential fire or explosion. The uv splicing tool consists of fusion stages and vacuum chucks which translate and hold the prepared fibers in position. A tube positioning post is used to hold an inner tube by means of a slot and vacuum post mounted on a three axis positioner. A local scattered light detector, as shown in Figure 6.2[1] is used to precisely align fiber cores. The local scattered light detector consists of a PIN Photodetector and a (5 cm) "U" shaped cross-section glass waveguide surrounding a portion of the receiving fiber of the splice. When fiber cores are not precisely aligned, light is launched into the cladding of the adjacent fiber, guided by the "U" shaped waveguide and coupled to the photodiode. This arrangement provides greatly increased sensitivity to slight misalignments. The local detector thus provides an accurate indication of core alignment (minimum signal level) and is calibrated to allow direct measurement of splice loss.

The theoretical analysis of splice loss for step index single mode fiber is studied by Marcuse[2]. In splicing by the core centering automtic fusion machine, the misalignment is neglected and the transmission coefficient T is

$$T = \left(\frac{2\, W_1\, W_2}{W_1^2 + W_2^2} \right)^2 \qquad (6.1)$$

where W is the spot size. The results of UV cured splicing techniques almost reach the theoretical minimum splice loss.

Splice losses are mainly caused by axial and angular displacements. Fiber splices are suprisingly tolerant of longitudinal displacement as compared with the axial displacement. Equation (6.1) derived by Marcuse is fairly accurate,

Table 6.2. Single Mode Fiber Splicing Techniques

SPLICING TECHNIQUE	INSERTION LOSS (dB0 (Fiber Core/Clad Diameter μm)	INSTITUTE	REFERENCE
. Electric arc fusion	0.4 (5.2/125) 0.2 (7/125) 0.1 (10/125)	NTT	IEEE J. of QE, Aug. 1978 p. 614
. Electric Arc Fusion	0.08 (10/125)	Fukikura/Sumitomo/FUrukawa/NTT	Appl. Optics, Jun 1982, p. 1916
. Convex-convex butting and Electric Arc Fusion	0.15-0.6 (4.4/126) (Polarization-Maintaining fiber)	NTT	IEEE J of LT, March 1983 p. 61
. Cl_2-H_2 Flame Fusion	<0.2 (-)	Bell Lab	IOOC '83 Digest p. 96
Ultraviolet Curable Cement	0.02 (-)	Bell Lab	IOOC '83 Digest p. 128

especially when the normalized frequency, v,[1] is small. Murakami and coworkers also derived formulas for the splice losses caused by axial and angular displacements using the series expansion.[2] Their work indicates that the single mode fiber splice loss is normalized frequency dependent and measurement results have excellent agreement with theory.

As mentioned in Section 5, the single mode polarization maintaining fibers are indispensable for applications of coherent optical communications systems, fiber sensors, microwave/millimeter wave wideband fiber optics, and connection between the fiber and the polarization sensitive optical devices such as integrated circuits. Polarization maintaining fibers, including both the stress birefringent fiber and the shape birefringent fiber, have been produced successfully by several manufacturers; however, the splicing of single polarization-maintaining fibers is still in the infant stage. The phase mismatch between eigenmodes in a fiber and the misalignment of linear birefringence axes at the joints (splice) will distort the polarizations in polarization-maintaining fiber. After Monerie[3] analyzed the crosstalk due to joints in circularly polarized eigenstates and linearly polarized eigenstates, Noda, et al[4] reported the splicing alignment techniques consisting of butting the convex profiles of the stress-induced region for single polarization maintaining fibers. The convex profiles were prepared by the mesa etching. Resultant splicing coupling loss was 0.15 - 0.6 dB. Cross-talk changed from -29 to -27 dB in the best case (crosstalk degradation was 1.6 dB).

1. C. M. Miller, "Local Detection Device for Single Mode Fiber Splicing", OFC '82 Digest, pp. 44-45.

2. D. Marcuse, "Loss Analysis of Single Mode Fiber Splices", Bell September Tech. J. 1977, May/June, pp. 703-718.

3. M. Monerie, et al, "Normalized Frequency Dependence of Splice Losses in Single Mode Optical Fibers", Elec. Lett. April 1978, pp. 277-278.

4. J. Noda, et al, "Splicing of Single Polarization Maintaining Fibers", IEEE J of LT, March 1983, pp. 61-66.

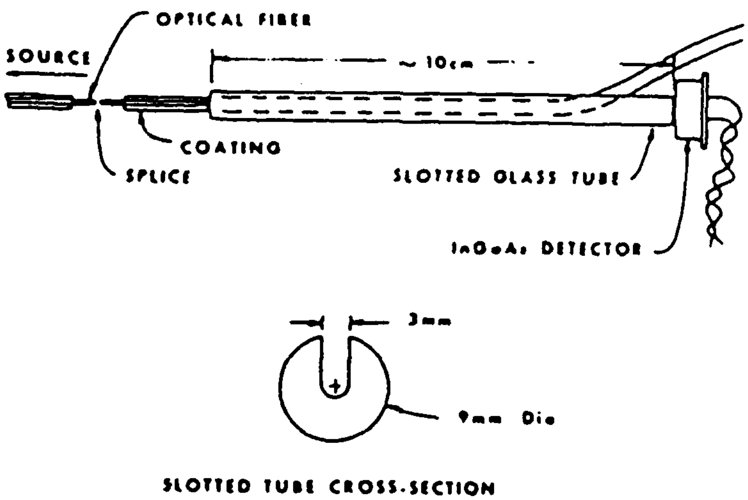

Figure 6.2. Local Detection of Light Lost in a Splice (After Miller)

6.3 Single Mode Fiber Coupler

A single mode fiber optical directional coupler is a very important component in:

- Interferometric sensors
- Duplex communication systems using a single strand fiber
- Monitoring circuit for communication systems
- Wavelength Division Multiplexing (WDM) communication systems
- Optical Time Domain Reflectometric systems

Several fabrication methods, such as etching and twisting or fusing, and polishing have been reported as being used to construct couplers from existing single mode fibers. These couplers are listed in Table 6.3. Couplers can also be formed to drawing preforms with a twin core.[1]

The coupling of light between two single modes is achieved because the electric field propagating in the core of a single mode fiber extends into the cladding region. If the cores of two single mode fibers are brought near each other, the field propagating in one fiber has a finite amplitude in the core of the second fiber. The detailed discussion of optical fiber coupling can be found elsewhere.[2] For the optical fiber with small numerical aperture (i.e., $\Delta n/n_1 = (n_1-n_2)/n_1 \ll 1$), the coupling coefficient, C, of the single mode coupler can be expressed

$$C = \frac{\lambda}{2\pi n_1} \frac{U^2}{a^2V^2} \frac{K_0[W(h/a)]}{K_1^2\ (W)}$$

where λ is the optical signal wavelength, n_1 and n_1 are the core and cladding refractive index of the fiber, respectively, a is the fiber core radius, h is the

1. G. Schiffner, et al, "Double Core Single Mode Optical Fiber as Directional Coupler", J. Appl. Phys. 1980, pp. 41-45.

2. A. W. Snyder, "Coupled Mode Theory for Optical Fibers", J. Opt. Soc. Amer., November 1972, pp. 1267-1277.

Table 6.3. Single Mode Fiber Couplers

COUPLER TYPE	FABRICATION TECHNIQUE	LOSS (dB)/DIRECTIVITY (Core/Clad Diameter, μm)	INSTITUTE	REFERENCE
4-Port	Fused Biconical-Taper	0.2 - 0.5/- (8/110)	Department of Commerce - Canada	Opt. Lett., July 1981 p. 327
4-Port	Bottle	1/- (10-125)	Naval R. Lab	IOOC '81 Digest p. 72
4-Port	Fused Biconical Taper	1 (-)	ITT	OFC '82 Digest p. 36
4-Port	Sapphire Ball Lens	1.5 - 2.5/53 (4.48/62.5)	Fujitsu	Appl. Opt., Oct. 1982, p. 3484
1 X D	Polished and Press Contact	0.18/60 (4/125)	Stanford U.	Opt. Lett., Jan. 1983, p. 60
4-Port	Polished/Adjacent Contact/Cement	0.1/- (-)	Gould	OFC '83, Digest, p. 30
Tunable 4-Port	Polished/Contact	0.15-/60 (4/125)	Stanford U.	IEEE Trans on MTT, April 1982 p. 592
4-Port	Etching/Twist	0.2 (4.7/125) Polarization-Maintaining	Naval R. Lab	IOOC '83 Digest, p. 116

distance between fiber axes, and K_V are the modified Bessel functions of the second kind and of order V. The parameters U and W are the transverse mode propagation constraints in a core and a cladding, respectively, and satisfy $V^2 = U^2 + W^2$ where V is the normalized frequency.

$$V = \frac{2 \pi a}{\lambda} \sqrt{n_1^2 - n_2^2} \tag{6.3}$$

Over a characteristic length called the coupling length L, all energy initially in the first core will be transferred into the second core. The coupling length can be determined from the following equation:

$$L = \frac{n_1}{\lambda} \left(\frac{\pi a V}{U} \right) \frac{K_1^2 (W)}{K_0 (h/a)} \tag{6.4}$$

In a tapered coupler, the V number is reduced in the tapering process because elongation of the fibers decreases the core radius. This is important in a practical sense, because coupling can now be achieved with a greater core-to-core spearation without reducing cladding thickness. The coupling length, L, determines the optical power coupled from one fiber to the other fiber. The optical power is completely transferred from one fiber to the other over a distance of $L \simeq 0.2$ cm.

Using the optical coupling principal, Digonnet and Shaw[1] have demonstrated a polishing technique in the fabrication of a tunable single mode fiber directional coupler. By controlling the fiber core separation by means of micropositioners, a fine, smooth adjustment of the coupler splitting ratio can be varied.

Similar to the single polarization maintaining splicing, the polarization preserving single mode fiber coupler is a very important component for interferometric sensors and coherent communications to minimize system noise. Birefringence corrected couplers[2] and polarization preserving couplers fabricated by

1. M. J. F. Digonnet and H. J. Shaw, "Analysis of a Tunable Single Mode Optical Fiber Coupler", IEEE Trans. on MTT, April 1982, pp. 592-600.

2. C. A. Villarruel, M. Abebe, and W. K. Burns, "Birefringence Correction for Single Mode Fiber Couplers", Opt. Lett. December 1982, pp. 626-628.

etch fusion technique[1] have progressed in the past several years; however, many concepts still need to be explored.

7.0 MICROWAVE PHOTODETECTORS AND RF FIBER OPTIC RECEIVER

7.1 General Discussion

7.1.1 Short Wavelength versus Long Wavelength: Photodetector Viewpoint

It is well known that the intrinsic low dispersion property of single mode fibers makes them attractive for high frequency, high data rate, long-haul lightwave systems, especially in the wavelength region between 1.1 and 1.7 μm, in addition to providing high radiation resistance. During the beginning of this project, there was no microwave Ge APD, InGaAs P APD or PIN PD commercially available for long wavelength application above 4.4 GHz. Therefore, we selected the short wavelength hardware design for the present system, but investigated the long wavelength operation for the future system.

7.1.2 Gain and Bandwidth of Photodetectors

The gain, G, of the photodetector is defined as the photocurrent, I, drawn in respect to the photocurrent, I_0, created by the extraction of one electron hole pair per incident photon.

$$G = \frac{I}{I_0} = \frac{h\nu}{q} \cdot \frac{I}{\mu_i \, Pabs} \tag{7.1}$$

where $h\nu$ is the photon energy, q the electronic charge, Pabs absorbed optical power and μ_i inner quantum efficiency.

For high frequency photodetection, the photodetector frequency response and bandwidth are important in the receiver design. The photodetector bandwidth is defined as:

$$B = \frac{1}{2\pi \, \mu \, eff} \tag{7.2}$$

1. C. A. Villarruel, M. Abebe, and W. K. Burns, "Polarization Preserving Single Mode Fiber Coupler", IOOC 1983 Digest, pp. 116-117.

For high frequency photodetection, the photodetector frequency response and bandwidth are important in the receiver design. The photodetector bandwidth is defined as:

$$B = \frac{1}{2\pi \mu \; eff} \tag{7.2}$$

Where μ eff the effective lifetime of the device. Assuming a RC like low pass behavior, the rise time τ_r of the electrical response is directly correlated to the bandwidth. Then:

$$\tau_r = \frac{0.36}{B} \tag{7.3}$$

for the 10- to 90- percent turn on time, if the detector is activated by a steplike light pulse. The same time $\tau f = \tau_r$ is the full time, if the device shows no storage behavior.

7.1.3 Various Photodetectors Response

7.1.3.1 P-N Junction Diode

The reverse biased P-N diode, with or without a heterojunction, is a conventional detector where the light enters from the p- or the n- side of the device. The bandwidth of P-N junction diode is:

$$B = \frac{1}{2\pi} \quad \frac{1}{t_1 + t_2} \tag{7.4}$$

where

$$t_1 = (R_L + R_S)\, C \tag{7.5}$$

R_L is load resistance

R_S is diode series resistance

C is depletion layer capacitance

t_2 is transit time

For well designed very small devices, the time constant t_1, becomes very small for 50 ohm load resistance because the internal capacitance C is only a few femtofarad. If fully depleted the, equation (7.4) becomes

$$B = \frac{1}{2\pi t2} \tag{7.6}$$

If surface recombination effects can be neglected the PN diode is a unity gain device; then, the gain bandwidth product is

$$GB = \frac{1}{2\pi\ t_2}$$

For devices with an active area of 5 mm x 5 mm, then the GF will be in the vicinity of 1.2 to 1.5 GHz. It is barely feasible for low end microwave application. However, the electronic field developed at the surface barrier of a Schottky diode allows one to use the device up to 16 GHz or higher frequency.

7.1.3.2 Phototransistor

The phototransistor is a bipolar transistor in common emitter connection without any external connection to the base. The "base" the device, a steady state illumination has to be applied. The transistor then is biased in the action portion of the I-V characteristics yielding higher and more linear amplification and a shorter rise time than without biasing. The bandwidth of phototransistor is:

$$B = f_c = \frac{1}{2\pi\ \tau eff} \tag{7.7}$$

$$\simeq \frac{1}{2\pi\ \tau} \tag{7.8}$$

Where τ is the volume lifetime of the minority carrier in the base. The gain factor is:

$$G = 1 + \beta \tag{7.9}$$

Where β is the transistor current amplification factor.

The transistor which has a base width of 0.5 μm may achieve B = 80 MHz and GB products may vary from 800 MHz to 16 GHz. Therefore, at the present time, the phototransistor is not suitable for microwave fiber optic application.

7.1.3.3 MESFET

A 0.25 μm gate GaAs MESFET has demonstrated a 6 dB gain at 45 GHz. Also, the modulation-doped AlGaAs/GaAs MESFET's grown by molecular beam epitaxy have shown faster switching times than standard GaAs devices. Recently, AlGaAs FET's performed as ultrahigh speed picosecond photodetectors, exhibit a high responsivity.[1] The rise time of the FET pulse response was less than 10 ps. Therefore a bandwidth is:

$$B = \frac{0.36}{10 \times 10 - 12} = 36 \text{ GHz}$$

7.1.4 Noise Sources and Penalty of Optoelectronic Receiver

The noise sources associated with receiver are:

- Intrinsic quantum noise
- Shot noise due to the detector dark (leakage) current
- Excess noise of avalanching process if an APD is used
- Shot noise due to gate leakage current of FET or base bias current of bipolar transistor
- Thermal or shot noise of active components in receiver
- Thermal noise due to feedback on shunt resistor

These noises are summarized in Table 7.1.4. The major task in design of a low noise optoelectronic receiver is to select appropriate photodetector and active devices. The receiver noise performance is also associated with other system parameters. For example, the quantum shot noise of optical sources cannot be

1. C. G. Bethea, et al, "Picosecond $Al_xGa_{1-x}As$ Modulation Doped Optical Field Effect Transistor Sampling Gate", Appl. Phys. Lett. April 1983, pp 682-683.

Table 7.1.4. Component Noises in Optoelectronic Receiver

NOISE	SOURCE OF NOISE	CHARACTERISTICS
Quantum Noise	Detector	Fundamental Noise
Leakage Current Shot Noise	Detector	
Excess Noise	Detector	Dominant for Avalanche Photodiode
Thermal Noise of Resistance	Bias or Feedback Resistance	
Thermal Noise or Shot Noise of Active Components	Bipolar Transistor or Field Effect Transistor	

controlled by receiver design and will result in degradation of the optical sensitivity. Laser diode partition noise and modal noise, enhanced by the dispersion properties of transmission medium, also cause a power penalty in optical sensitivity. Futhermore, the finite bandwidth of the optical source and the fiber will also result in a power penalty. However, the partition noise can be optimized together with receiver noise since this noise is closely associated with receiver filter response.

7.1.5 Comparison of Photodetectors

As mentioned in Paragraph 3.1.4 selection of the photodetector is a key task of designing a high frequency and high data rate fiber optic receiver. In addition to the gain and bandwidth selection, noise parameters, quantum efficiency and operating wavelength of the photodetector should also be considered. Various photodetectors at both short and long wavelengths are tabulated in Table 7.1.5 Si, GaAs and Ge materials have been used to fabricate photodetectors. The Si device only responds up to 1.1 μm wavelength. The Ge diode has high dark current (100 - 500 nA). At present, the most promising materials used for photodetectors are from the InGaAsP alloy system, which is epitaxially grown on bulk InP substrates. The atomic fractions of the constituent elements of In, Ga, As, and P can be varied to form a series of alloys with bandgaps that range continuously from 1.35 eV (InP) to 0.73 eV ($In_{0.53}Ga_{0.47}AS$). This range in bandgaps results in the absorption wavelengths below 1.7 μm, with the specific absorption edge wavelength depending on the alloy composition chosen.

The InGaAsP alloy system is advantageous in the long wavelength region for three main reasons. First, a broad spectral sensitivity is obtainable from the wide choise of alloys. Second, the absorbing alloy is grown on InP substrates of relatively high quality. Only those compositions that are lattice matched to the InP substrates are chosen for epitaxial growth. In this way, the quality of the substrate can be maintained in the epitaxial layers without introducing crystalline imperfections that are caused by mismatches in spacing between atoms in the expitaxial layers and those in the substrate. Third, the InP substrates are transparent to long wavelength radiation, absorbing at wavelengths below 0.95 μm. It is thus possible to make detectors so that light absorption occurs far from semiconductor surfaces, thereby minimizing losses due to surface recombination of photogenerated carriers.

Table 7.1.5. Comparison of Photodetectors

PHOTODETECTOR	TYPE	CAPACITANCE (PF)	LEAKAGE CURRENT (nA)	EXCESS NOISE FACTOR	WAVELENGTH (μm)	QUANTUM EFFICIENCY (%)
APD	GE	0.5-2	100-500	0.7	0.5-1.5	0.8/1.3/1.5 m 60/1-/-
	Si	0.5-2	0.2-20	0.3	0.4-1.1	70/-/-
	GaAs	1.2-2	10-50	0.3	0.4-0.9	70/-/-
	Ge	1.5-2	100-500	0.7	0.9-1.5	-/50/20
	Ge - Reach Through	1.5-2	100-500	0.7	0.9-16	-/50/50
	InGaAsP/InP	0.5-1.5	10-50	0.2-0.4	0.9-1.4	-/60/-
	InGaAs/InP	0.5-1.5	100	0.4	0.9-1.3	-/60/-
	HgCdTe	1	150	-	0.9-1.3	-/50/-
	GaAlAsSb/GaAlSb	1-2	1-40	2.1	1.0-1.4	-/90/-
PN*	Schottky-Barrier GaAs	0.1-	10-50 (estimated)	-	0.6-0.85	26-/-
PIN	Ge	10-30	5000		0.9-1.5	-/75/-
	Si	0.5-	0.2-10	-	0.4-101	75/-/-
	InGaAs/InP	0.3-0.5	10	-	0.9-1.6	-/70/70
PHOTOTRANSISTOR	InGaAs/InP	0.3-0.5	50-100		0.9-1.6	-/50/50

* S.Y. Wang, D.M. Bloom and D.M. Collins, "20 GHz Bandwidth GaAs Photodiode," Appl. Phys Lett., Jan. 1983 pp. 190-192

7.1.6 Transistors for Post Detector Amplifier

The post detector amplifier requires low noise, stable transistors for gain amplification. Low noise Si bipolar transistors are suggested for the frequencies below 4.5 GHz and GaAs MESFET for frequencies of 5 MHz to 40 GHz. The GaAs MESFET is not recommended for frequencies below 5 MHz because of its high 1/f (flicker) noise. The low noise Si pipolar transistor has relative high noise figure (3 - 6 dB) above 2 GHz.

7.1.7 Fiber Optic Receiver Circuit Design Considerations

The performance of a fiber optic system, either analog or digital, mainly depends on the total system signal-to-noise ratio (S/N), nonlinearity, and the transient behavior. The system nonlinearity generates harmonic, intermodulation, and cross-modulation distortions which degrade the analog system more severely than the digital one. However, nonlinearity due to photodiodes, not including the postdetector amplifier, is sufficiently low not to be a major obstacle for the realization of high quality analog transmission. The S/N of a fiber optic system is practically determined by the modulation depth, received optical power, operational bandwidth, gain factor of the detector, and noise characteristics of the detector and post-detector amplifier.[1,2] Particularly, the noise performance of the receiver plays the key role of determining the sensitivity of the system. During the receiver design, the following considerations are recommended.

- Select a proper photodetector according to system S/N requirement, available optical source and fiber cable, information bandwidth, data rate, operational wavelength, fiber size, detector package, bias availability, device capacitance, responsibivity, noise equivalent power, and cost limitation. The performance and tradeoff guideline amont the MESFET, APD, and PIN photodiode have been described in the previous sections.

1. Pan, J. J. and D.E. Halley, "Fiber Optic Links for Microwave and Satellite Communication Terminals", 1976 National Telecommunication Conference, December 1976, Dallas, Texas.
2. Pan, J. J., "Temperature Effects on Military Fiber Optic Systems", Military Electronics Expo 1978, November 1978, Anaheim, California.

- Characterize the selected photodiode using an adequate circuit. Product a set of initial values of impedance matching between PD and post-detector amplifier over the complete bandwidth at the desired bias condition.

- Select a proper AGC scheme, a temperature compensation network, and a suitable stabilized bias supply.

- Minimize circuit parasitics and poor groundings for high frequency and high data rate systems.

- Select the proper transistor for post-detector amplifier.

Then the computer-aided optimization, techniques, such as pattern search, should be used to optimize the receiver over the desired bandwidth and temperature range, according to the detector admittance, optimized noise source admittance, frequency and temperature dependent gain factor, and the post-detector amplifier performance (gain, bandwidth, transistor noise figure, and input and output impedance).

7.2 APD

7.2.1 Availability of a High Speed APD (0.8 - 0.9 μm)

Table 7.2.1-1 lists commercially available high-speed APDs. All Mitsubishi, Ford Aerospace and AEG-Telefunken APDs are feasible for 1-8 GHz application. The AEG-Telefunken S171P Si APD has been used in this study and proved to be adequate for 5 GHz operation. The performance characteristics of S171P is listed in Table 7.2.1-2.

Table 7.2.1-1. Avalanche Phototector (APD) for 0.8 - 0.9 μm Fiber Optic Applications

MANUFACTURER	MODEL NO.	BREAKDOWN VOLTAGE (V)	NEP $(W/\sqrt{Hz})$	RESPONSITIVITY (A/W)	CAPACITANCE (pF)	RISE TIME (ns)	DIAMETER OF ACTIVE AREA (mm^2)
RCA	C30902E	180/250	3.0×10^{-15}	77	1.6	0.5	0.5
	C30908E		3.5×10^{-15}	77	1.6	0.5	0.5
	C30921E		3.5×10^{-15}	77	1.6	0.5	0.5
Mitsubishi	PD-1302*	180	1×10^{-14}	--	<0.5	0.15	0.03
Ford Aerospace	L-4501	--	10^{-16}	0.5	--	10^{-3}	0.003
	L-4502	--	10^{-16}	0.5	--	10^{-2}	0.003
AEG-Telefunken	S171P	170	--	QE=50% at 840 nm	0.85	0.2	0.2

* Gain Bandwidth Product = 800 GHz and rise time of 0.15 ns.

Table 7.2.1-2. AGE - Telefunken High Speed Si APD

Model No.: S171P

Package: Microwave

Active Diameter: 0.2 mm

Rise Time for 50 Load: 200 PS

Capacitance: 0.85 PF

Reverse Dark Current at M=100: 1 nA

V_{BR}: 170 V

Efficiency: 30%

Temperature Coefficient: 0.2 5/°C

Spectral Response: 450 to 950 nM

7.2.2 Long Wavelength APD/PIN Photodiodes

Silicon photodetectors, both PIN and avalanche, are normally used in the 0.8 - 0.8 μm spectral region and are extendable to 1.1 μm wavelength at the expense of a lower quantum efficiency. The photodiodes fabricated using direct-bandgap, III-V semiconductor alloys, either ternary or quarternary, such as InGaAs, InGaAsP and AlGaAsSb, are very attractive for 1.0 - 1.6 μm fiber optic applications.[1,2] These III-V long wavelength photodetectors have quantum efficiencies of 50 percent to 90 percent. However, the developed devices are operating at frequencies under 1 GHz modulation and are presently not commercially available.

InGaAsP PIN photodiodes are available from Plessey, RCA, Lasertron, etc., (at time of November, 1982). Unfortunately, these devices have rise times equal to or larger than 1 ns and are not suitable for microwave fiber optic systems.

Indirect-bandgap Ge (Germanium) diodes have the disadvantage of relatively higher dark current than direct-bandgap photodiodes. However, they have been satisfactorily used in many long wavelength (1.3 and 1.55 μm), long distance (up to 105 km) digital telephone links (46 Mb/s and 840 Mb/s). Table 7.2.2 presents some high speed, high performance Ge photodiodes from various vendors. The rise time range from 0.3 ns to 0.08 ns, and are capable of responding to frequencies higher than 10 GHz.

7.2.3 Noise Optimization

Applications of the APD in a fiber optic system is a well developed technique. However, for a wideband or high data rate application, the relation between multiplication noise and quantum efficiency is a tradeoff at a certain

1. J.J. Pan, "Advanced Photodetectors for Fiber Optic Communications Systems", 1979 NEPCON Proceedings pp 161-166, February 1979, Anaheim, CA.
2. G.E. Stillman, et al, "Long Wavelength (1.3 to 1.6 μm) Detectors for Fiber Optical Communications", IEEE Trans. on ED, September 1982, pp 1355-1371.

Table 7.2.2. Microwave Frequency Germanium Photodetectors for Long Wavelength Fiber Optic Communications (November 1982)

Performance Parameters / Manufacturer	Model No.	Spectral Range (um) Low	High	NEP $W/\sqrt{Hz}$	Responsivity (A/W at um)	Rise Time (ns)	Active Area (mm)	Unit Cost ($)
Opto-Electronics	PD20	0.5	1.8	$1X10^{-10}$	0.15 @ 1.5	0.08	0.0086	3275
	PD25	0.5	1.8	$1X10^{-10}$	0.25 @ 1.5	0.05	0.0086	4375
Ford Aerospace	L-4520	0.5	1.8	$1X10^{-16}$	0.7 @ 1.55	0.11	0.03	
	L-4521	0.5	1.8	$1X10^{-12}$	0.97 @ 1.55	0.32	0.81	
	Custom	0.5	1.8	$1X10^{-12}$	0.97 @ 1.55	0.3	0.0062	
Judson Infrared	J-16LD	0.5	1.8	$1X10^{-11}$	0.7 @ 1.5	0.3	0.01	160
Photon Kinetics	30	0.6	1.6	$1X10^{-11}$	—	0.25	0.1	1950

breakdown voltage. It is desired to provide optimum properties for obtaining high performance optical receivers. As is well known, the S/N shown in Equation (3.2) also can be expressed in terms of the excess noise factor of an APD,

$$S/N = \frac{(2I_0M)^2/B_n}{2qI_0M^2F + 4kBTF/R} \tag{7.10}$$

and

$$F = M\,[1-(1-k)\,(M-1)^2/M^2] \tag{7.11}$$

where I_0 is the photo current generated in the detector; M is the multiplication factor; B_n is the effective noise bandwidth and R is the load resistance.

The maximum S/N can be evaluated as:

$$(S/N)\max = -\frac{P_0}{h\nu B_n}[1.8899\,(k_B\ TF\ hV/4q^2P_0R)^{1/3}$$
$$(k/y^2)^{\ 2/3} + \frac{1-k}{y}]^{\ -1} \tag{7.12}$$

7.2.4 APD Response Time and Bandwidth

With the assistance of the APD equivalent circuit, the response time and operational bandwidth of the APD can be analyzed. The simple APD equivalent circuit, without package parasitics, is depicted in Figure 7.2.4 where R_{sc} is the space charge resistance, R_s is the spreading resistance and C_d is the junction capacitance. The dependence on the bias voltage of the phase shift occuring in the APD arises from the contributions of the voltage dependent diode capacitance and the avalanche buildup time. The output voltage V (ω) across the load resistor R_L is given by:

$$V(\omega) = \frac{R_L}{1 + j\omega C_d\,(R_s + R_L)} \cdot \frac{ip\ M_0}{1 + j\omega\,\tau_1 M_0} \exp\ -j\ (\omega\,\tau_1 M_0/2) \tag{7.13}$$

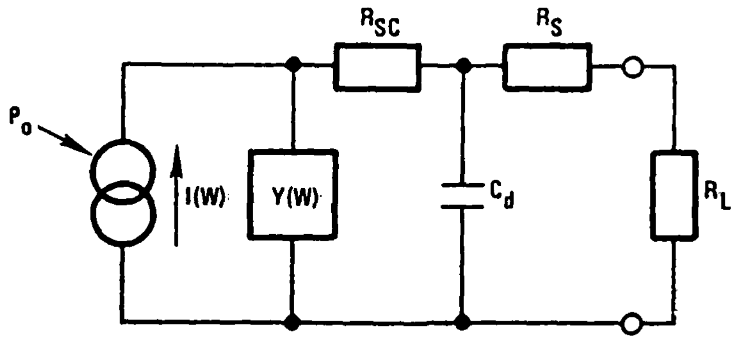

$I(\omega) = (i_o M/1+\omega \tau_1)\ \mathrm{EXP}\ (-j\ \omega \tau_1 M/2)$

$Y(\omega) = gP_o/1+j\ \omega \tau_1 M_o$

$i_o = \eta q\ P_o/h\nu$

11386-3

Figure 7.2.4. APD Equivalent Circuit

where ip is the photocurrent without multiplication and τ_1 is the intrinsic response time in the avalanche region. The transfer function of APD also was investigated by Anderson, et al[1] using noise spectrum measurement.

7.2.5 APD Measurements

7.2.5.1 Noise Measurement

The excess noise factor of APD is a function of multiplication of both hole and electron; therefore, it is a function of bias voltage. The APD noise measurement setup have been discussed elsewhere.[2,3] The noise photocurrent can be determined by measuring the voltage drop across a load resistor with a lock-in amplifier calibration of laser diode noise.

7.2.5.2 APD RF Impedance Measurement

The APD RF impedance measurement versus frequency and bias voltage can be achieved using a network analyzer. The measurement setup and test fixture are similar to the one described in laser diode measurement.

7.2.6 APD Optimum Operation Condition

An optimum value of avalanche gain, Gopt, exists which maximizes the system S/N at a given received power level, and

$$Gopt = \left[\frac{2\{(i_A{}^2/2qBn)\} + Is}{2(rP_R + I_b)}\right]^{1/(2+2)} \qquad (7.14)$$

1. T. Anderson, et al, "Temporal and Frequency Response of Avalanche Photodiodes from Noise Measurements", Appl. Opt., October 1980, pp 3496-3499.

2. H. Ando, et al, "Characteristics of Germanium APD in the Wavelength Region of 1 - 1.6 μm", IEEE J of QE., November 1978, p 804.

3. G.E. Stillman, et al, "Long Wavelength (1.3 - 1.6 μm) Detectors for Fiber Optical Communications", IEEE Trans on ED, September 1982, pp 1355-1371.

7.2.7 APD Temperature Effect

The APD quantum efficiency, noise equivalent power (NEP), responsivity, transit time, frequency response, and linearity are all related to the avalanche multiplication factor which changes with temperature. Under constant voltage bias condition, the temperature variation of M can be expressed as:

$$M(T) = 1 - (1 - M_0^{-1}) [\exp - \gamma (T - T_0)]^{-1} \tag{7.15}$$

where M_0 is the value of M at $T = T_0$ and γ is a constant determined by materials the diode physical parameters depending upon junction profiles.

7.2.8 APD Reliability

The ultimate decision of whether or not the APD will be employed in a transmission system will depend on its reliability, which at present, is unknown. The APD breakdown voltage, dark current, multiplication gain, and reliability are dependent upon:

- APD structure
- Ambient Conditions
- Layer thickness and doping
- Insulating layer/semiconductor interface

Unlike the PIN detector, the insulating, or "passivating" layer in the APD is in contact with the semiconductor gain region which is maintained at very high electric fields. Thus, surface states or other interfacial imperfections are expected to lead to large dark currents or long term degradation of device quality. Extensive research into the nature of the insulator/III-V interface must be done to predict the ultimate reliability of APDs.

Although the problems facing APD's, especially the long wavelength devices, are formidable, the potential increase in system sensitivity that they offer makes them very attractive in fiber optic communications. They are, therefore, the subject of considerable research.

7.3 MESFET

7.3.1 Comparison of GaAs MESFET and Si APD for Microwave Optical Detection

Both Si APD and GaAs low noise microwave MESFETs are feasible for microwave optical demodulation. The MESFET with a gate length of less than 1.0 μm, has a demonstrated noise figure between 0.7 and 2.0 dB at frequencies of 2-6 GHz, and 1.7 to 3.0 dB at 12 GHz. The MESFET, for optical detection, has been proven to be equal or superior to the APD performance at frequencies of 1-6 GHz.[1,2,3,4,5,6]

The MESFET offers the following attractive advantages over the APD:

- Low noise
- Nearly restrictive output impedance thereby providing wideband operation capability
- A frequency response well above X-band
- Low bias voltage required (4-6 V instead of 160 V)
- Provides amplification gain
- Good temperature stability
- Low cost

1. J.J. Pan, "GaAs MESFET for High Speed Optical Detection", 22nd SPIE International Symposium, San Diego, August 1978.
2. J.C. Gammel and J.M Ballantyne, "The OPFET: A New High Speed Optical Detector", IEEE Intl. Elec. Device Meeting, Washington, D.C., December 1978.
3. J.M. Osterwalder and B.J. Rickett, "GaAs MESFET Demodulates Gb/s Signal Rates from GaAlAs Injection Laser", IEEE Proc. June 1979, pp 966-967.
4. E.H. Hara and R.I. MacDonald, "A Broadband Optielectric Microwave Switch", IEEE Trans. on MTT June 1980, pp 667-669.
5. R.I. MacDonald, "High Gain Optical Detection with GaAs FETs", Appl. Opt. 1981, pp 591-594.
6. C.G. Bethea, et al, "Picosecond AlxGal-xAs Modulation Doped Optical Field Effect Transistor Sampling Gate", Appl. Phys. Lett. April 1983, pp 682-683.

Some of the MESFET and APD performances are compared in Table 7.3.1. The receiving sensitivity comparison between the GaAs MESFET and Si APD, at the same RF modulation power of +7 dBm indicates that the MESFET has a more sensitive response than the APD.

7.3.2 Brief Description of GaAs MESFET for High Speed Optical Detection

An advanced low noise GaAs MESFET has a gate length less than 1.0 μm and gate source capacitance less than 0.2 pF. The conduction electrons in GaAs have a six times larger mobility and a two times larger peak drift velocity than they have in silicon. The electrons in GaAs derive a device cutoff frequency reaching well beyond 80 GHz. The drain current variation of the MESFET is proportional to the input optic intensity and is capable of detecting the high speed subcarrier, if the light is modulated. The detected optical signal will be internally amplified by the MESFET through the device transconductance, and it provides a good optical responsiveness over a very wide spectral range, from visible to near-infrared wavelengths. Since the GaAs MESFET has 1) a high purity buffer layer between the substrate and the active layer; 2) a high doping level in the active n-layer; 3) a small source and gate metal resistance; and 4) a short, gate length, all those factors give the device a very low noise figure. Inherently, the device has a wide dynamic range in comparison with other diode photodetectors. The measured S_{22} indicates that the output impedance is almost resistive rather than capacitive, which makes the art of matching wideband impedance to the load relatively easy.

7.3.2.1 GaAs MESFET Principal of Operation

7.3.2.1.1 MESFET Without Light Illumination

Device Description: In most cases, the GaAs microwave MESFET consists of a thin (0.15 μm thick) and highly doped (2.5 x 10^{17} cm^{-3}) n-type active layer, a high resistivity buffer layer (5 μm thick and 1 x 10^{-13} cm^{-3} concentration), a chromium-doped semi-insulating substrate as depicted in Figure 7.2 (a). The source, gate, and drain are fabricated on the active layer. A 0.5 μm thick aluminum-film or Ti/Pt/Au multicomponents are patterned to form a good gate

Table 7.3.1. Performance Comparison of MESFET and APD

Performance \ Device	APD	MESFET
. Response Time (presently avail. device without equilization	3.5-10 GHz	18 GHz
. Distortion	Low	Very Low
. Bandwidth	3 HGz	10 GHz
. Dynamic Range	40-60 dB	60 dB
. Noise	Low	Very Low
. Environmental Effect	Poor	Good
. Bias Condition	160-380 V	4-6 V
. Output Impedance	Reactive, Low Impedance	Resistive, Medium Impedance
. Nuclear Radiation Resistance	Fair	Good
. Cost (each)	$140 - $260	$40 - $125

Schottky contact to n-GaAs with a low resistivity. Low resistance source and drain ohmic contacts are realized by alloying a eutectic composition of Au/Ge. In/Au/Ge, Ni/Au/Ge, and Pt/Au/Ge also have been utilized for various devices. The 0.5 μm single gate device operating at X-band normally has the gate length of 1.0 μm, gate width of 300-500 μm, source gate separation of 1.0 μm, and gate drain separation of 3.0 μm.

Operation Principle: When the MESFET is biased, the metal-to-semiconductor gate between source and drain generates a layer in the semiconductor that is completely depleted of free-carrier electrons. The depletion layer acts as an insulating region and constricts the cross section available for current flow in the active layer. The relationship among the electronic field, the electronic velocity, and the bias condition determines the width of depletion layer and the current flow between drain and source. The depletion region widening is the effect of a field or voltage applied between the gate and the channel of the transistor. The biased MESFET as shown in Figure 7.3.1 (a), the widest depletion layer or the narrowest channel cross section, is located under the drain end of the gate. A typical drain voltage current characteristic at various gate voltage is illustrated in Figure 7.3.1 (b). The electric field, electron drift velocity, and space charge distribution in the channel of a 3 μm MESFET operated in the current saturated region are illustrated in Figure 7.3.1 (c), (d), and (e), respectively.

Unlike silicon, the equilibrium electron velocity of GaAs versus the electric field reaches a peak value (the threshold field) and then decreases and levels off at a saturated velocity. Since the gate length of a microwave MESFET is so short, less than 3 μm, the electrons do not reach equilibrium transport conditions in the high field region of the channel. The electrons remain in equilibrium condition as long as the electric field, E, is below the threshold field, E_p. However, when the electrons enter a high field region ($E>E_p$), they are accelerated to a higher velocity before relaxing to the equilibrium velocity. This acceleration effect shortens the electron transit time through the high field region and shifts the accumulation layer into the gap between and drain.

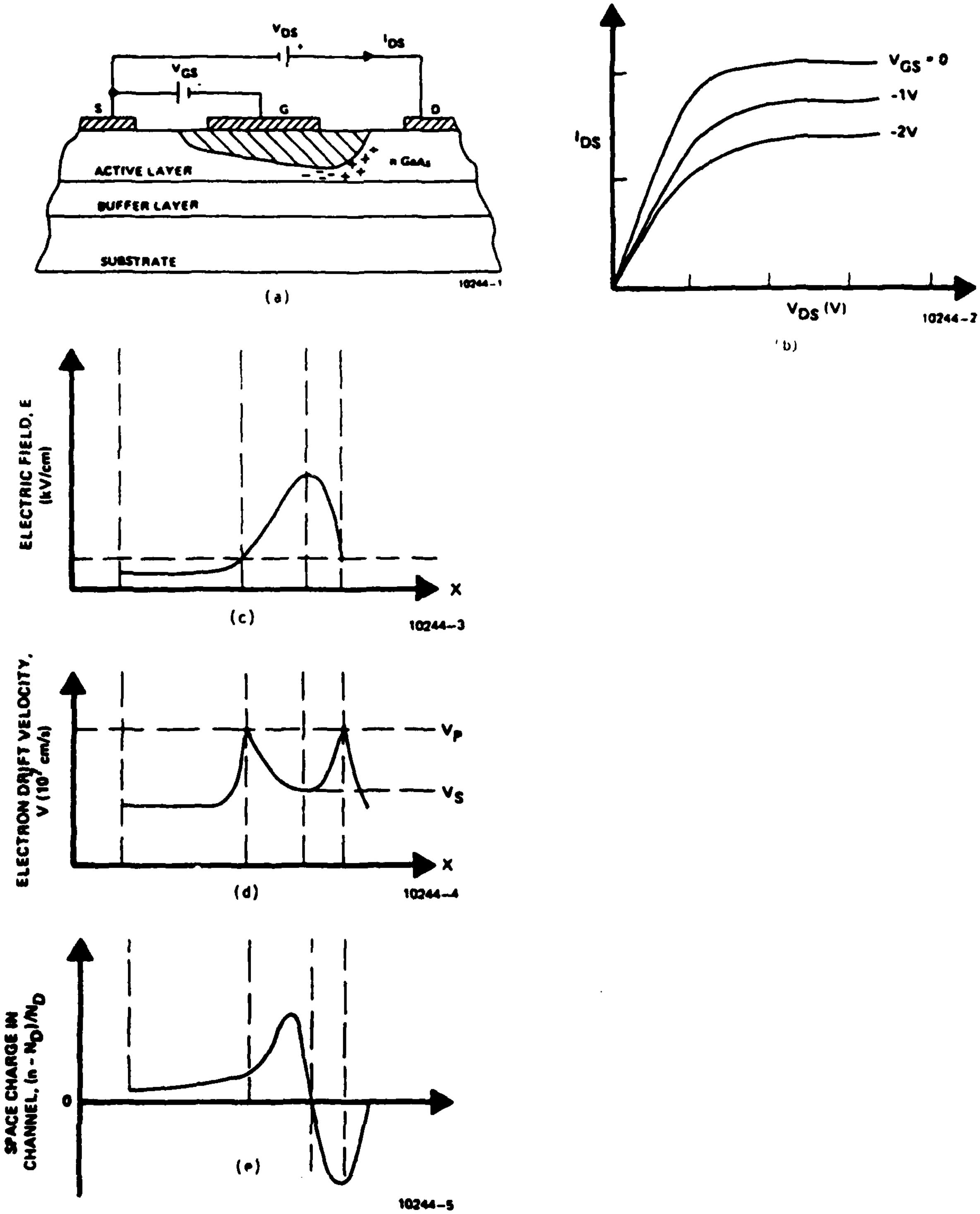

Figure 7.3.1. The Geometry, V-I Curves, Electrical Field, Electron Drift Velocity and Space Charge Distribution of Common Source GaAs MESFET Operator in the Current Saturation Region.

7.3.2.1.2 MESFET with Light Illumination

A drain current of a GaAs MESFET changes when the light illuminates on the gate region of the transistor. Following, are two possible mechanisms causing the drain current variation:

1. The source gate and drain gate photoconductivities change with the incident light intensity.

2. The width of depletion layer varies with light intensity.

When the light illuminates the MESFET gate region, the photoflux penetrates into the active GaAs n-layer at the source gate and drain gate separation gaps, and decays exponentially. Presumably, the light transmittance through the gate metallization is negligible since its thickness is well above 1,000A. The depth of penetration in the gaps may extend farther into the buffer and semiconducting layers depending on the incident light energy, wavelength, and the radiation absorption coefficient of the semiconduct, . This deep penetration is less important to the photo current variation because the carrier concentrations are much smaller in these layers than in the active layer. The optical energy produces the excess carriers and causes the carrier densities and the photoconductivity change in the gaps. The photoconductivity, $\Delta\sigma$, may be approximately calculated from:

$$\Delta\sigma = q \cdot \mu \cdot \zeta \, (1-R) \cdot \alpha \cdot Q \cdot \frac{w_e}{w} \cdot \Psi(t) \qquad (7.16)$$

where q is the electronic charge, μ is the surface mobilities, ζ is the quantum yield of the internal photoelectric effect, R is the surface reflectivity, and Q is the photon flux density. w_e is the effective gap width, w is the gap width and $\Psi(t)$ is the time dependent optical intensity function. Q can be computed from the irradiance and the wavelength. Then the photoconductance of the illuminated gap is obtained as:

$$G = k \, \Delta\sigma \, (Wg/\alpha \, . \, W) \qquad (7.17)$$

where k is a constant and Wg the width of the gap. Practically, only the material with high mobility and short lifetime, such as GaAs, can provide a fast, time dependent, photoconductance variation.

The photoconductive concept of GaAs MESFET optical response has been verified by S-parameter measurement. Figure 7.3.2.1.2-1 depicted the S_{21} result at various illumination conditions of a common gate MESFET driven at V_{dg} = 0V, I_{gs} = 0mA and V_{gs} = -4.6 V, measured from 1 GHz to 2 GHz. A 50 ohm two port test fixture was utilized in the test.

If the modulated light shines in the neighborhood of the gate region, electron-hole pairs are created from the valence band to the conduction band. This increases the carrier concentration, narrows the depletion layer, and raises the current flow between drain and source. Besides the increase of the I_{ds}, the effective capacitance of the depletion layer also increases sharply by illumination from the side of MESFET or by the polarized light shining directly onto the device. It is easy to obtain a more than sevenfold capacitance variation simply by turning on and off the filtered room light.

Equivalent Circuit: The equivalent circuit for operation in the saturated current region in common source configuration and in the location of the lumped elements in the transistor structure are illustrated in Figures 7.7.3.2.1.2-2 (a) and 7.3.2.1.2-2 (b). The optical illumination, causing the MESFET photoconductance change and the width variation of the depletion layer, changes some of these element's values. C_{gs}, C_{dg}, R_s, R_j, R_d, and i_{ds}, marked by the arrowheads, are optical sensitive elements. The analysis of the equivalent circuit will yield many useful circuit design parameters such as the cutoff frequency, device stability factor, maximum available gain, input and output impedances, and others. These circuit parameters also can provide information for device fabrication optimization.

7.3.2.2 GaAs MESFET Optical Response

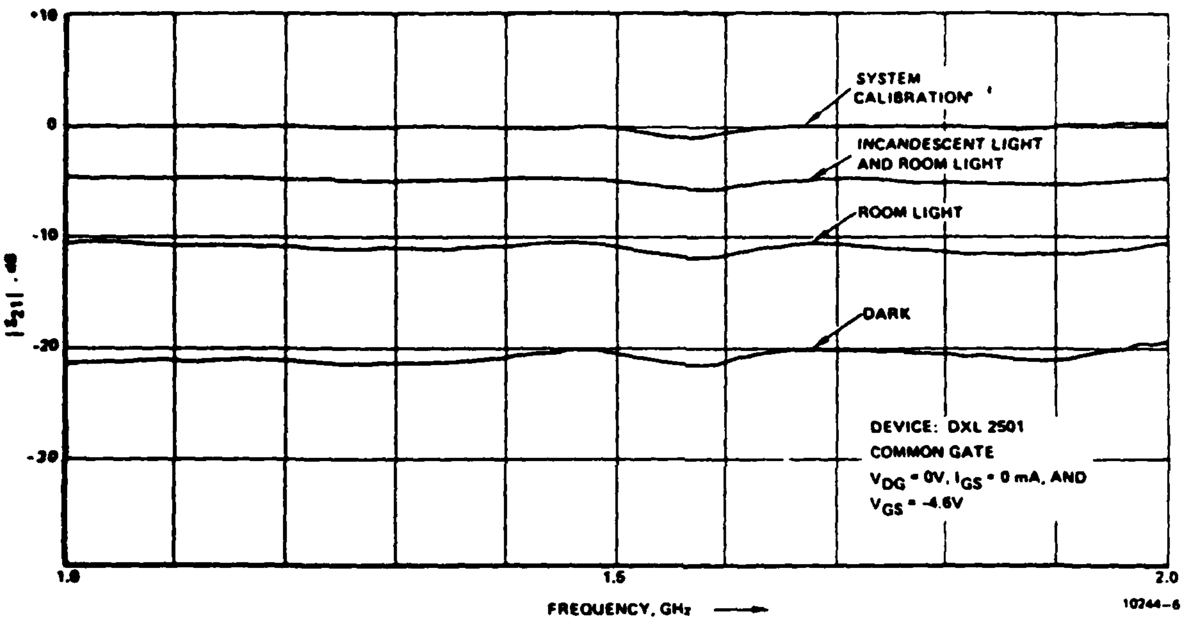

Figure 7.3.2.1.2-1. S_{21} Versus Frequency at Various Illuminations

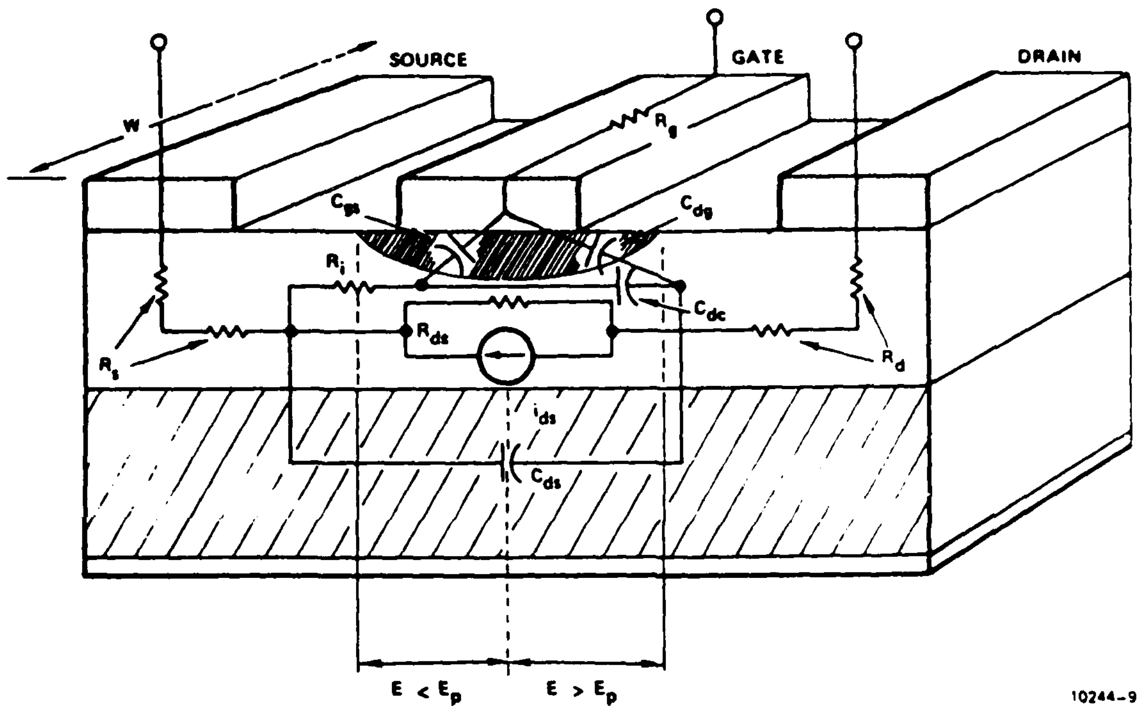

Figure 7.3.2.1.2-2a. Common Source MESFET Equivalent Circuit

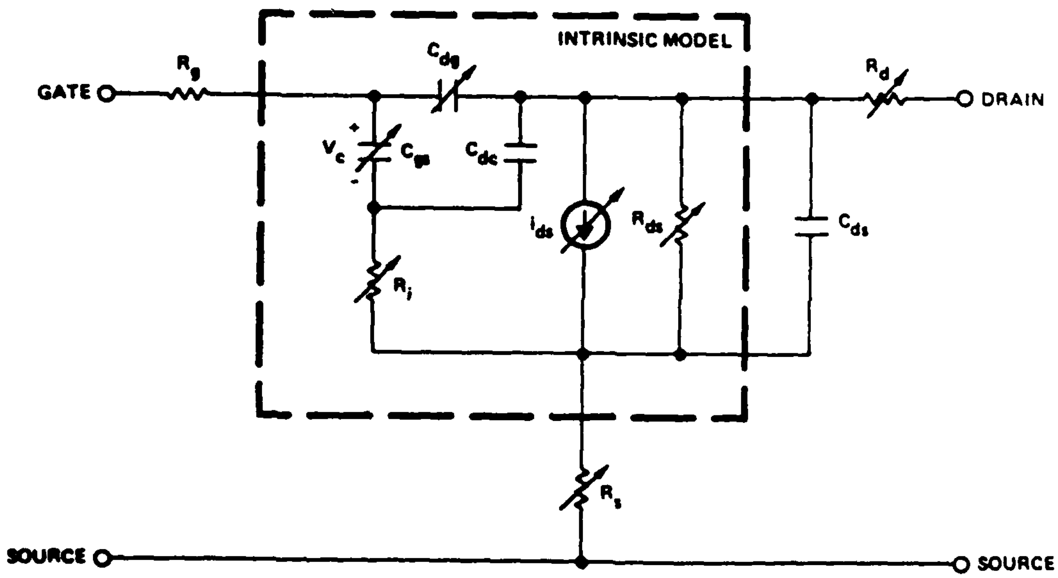

Figure 7.3.2.1.2-2b. Common Source MESFET Equivalent Circuit

7.3.2.2.1 DC Characteristics

As described previously, the drain source current and capacitance change with light illumination. The capacitance variation is sensitive to the incident angle and light polarization. The quantum efficiency of 1 μm gate MESFET, at a desired bias condition and 0.85 μm wavelength, varies from 26 to 42 percent depending on the individual device. The quantum efficiency is sensitive to the bias conditions and less sensitive to the incident light wavelength over a wide spectral range. The spectral response has not been formally measured; however, it was observed that the MESFET does respond from visible wavelengths up to 0.9 μm infrared using sources available in the laboratory.

7.3.2.2.2 Noise Performance and Responsiveness

The low noise, microwave GaAs MESFET has the following possible noise sources:

- Thermal noise in the channel
- Hot electron noise
- Internally scattering noise
- High field diffusion noise
- Noise voltage generated locally in the channel, causes a fluctuation in the depletion layer width
- Contact resistors noise
- Low frequency noise due to carrier fluctuation such as generation recombination, flicker (1/f noise) or diffusion noise

Besides the flicker noise source, exhibiting an 1/f like character at low frequency, all other noise sources are discussed in detail elsewhere. For microwave applications, these noise sources have been minimized to a total device noise temperature of $59^{o}K$ (NF = 0.8 dB) at 2 GHz and $97^{o}K$ (NF = 1.25 dB) at 5 GHz. For fiber optic communications, the low frequency flicker noise becomes interesting for many systems. The amplitude of the flicker noise mainly depends on the device

fabrication process; nevertheless, the circuit design may also affect its performance. Currently, a flicker noise of less than 55°K (NF = 0.75 dB) at 25 MHz has been achieved. It is also verified that flicker noise is not very sensitive to temperature.

When the MESFET is utilized as an optical detector, the noise model described in Reference 4 can be directly applied, except for the increase of an excess gate noise current generated by carrier fluctuation in the depletion layer due to illumination effect. Any increase of C_{gs}, C_{dg}, i_{ds}, R_d and R_s, should be included in the computation. The bias dependent MESFET responsivity is approximately given as:

$$R = \frac{\text{Drain Source Current Change Due to Photoeffect}}{\text{Incident Photon Energy}}$$

$$\simeq \frac{\Delta I_{ds\,max}}{h\,\omega\,\phi\,A_{eff}} \quad \text{A/W} \tag{7.18}$$

where $h\nu$ is the photon energy, ϕ is the incident photon flux and A_{eff} is the effective gate area. In order to obtain high responsivity, a large transconductance device has to be chosen. From the responsivity, operational bandwidth and the total noise current, the noise equivalent power (NEP) of the MESFET is easy to calculate. The device dark leakage current, the most concerned engineering problem, depends on the individual transistor as well as the bias condition. It may vary from several pA to several nA, according to the device selection. Figure 7.3.2.2.2 illustrates an example of the leakage current change of a common-gate device operating as a diode mode versus bias current.

7.3.3 MESFET Availability

7.3.3.1 GaAs MESFET for 0.8 - 0.9 μm Optical Detection

With today's submicron technology, the GaAs MESFET has a cut-off frequency as high as 100 GHz. Consequently, the device can have the capability to optically demodulate frequencies up to 40 GHz with 4 - 5 dB amplification gain.

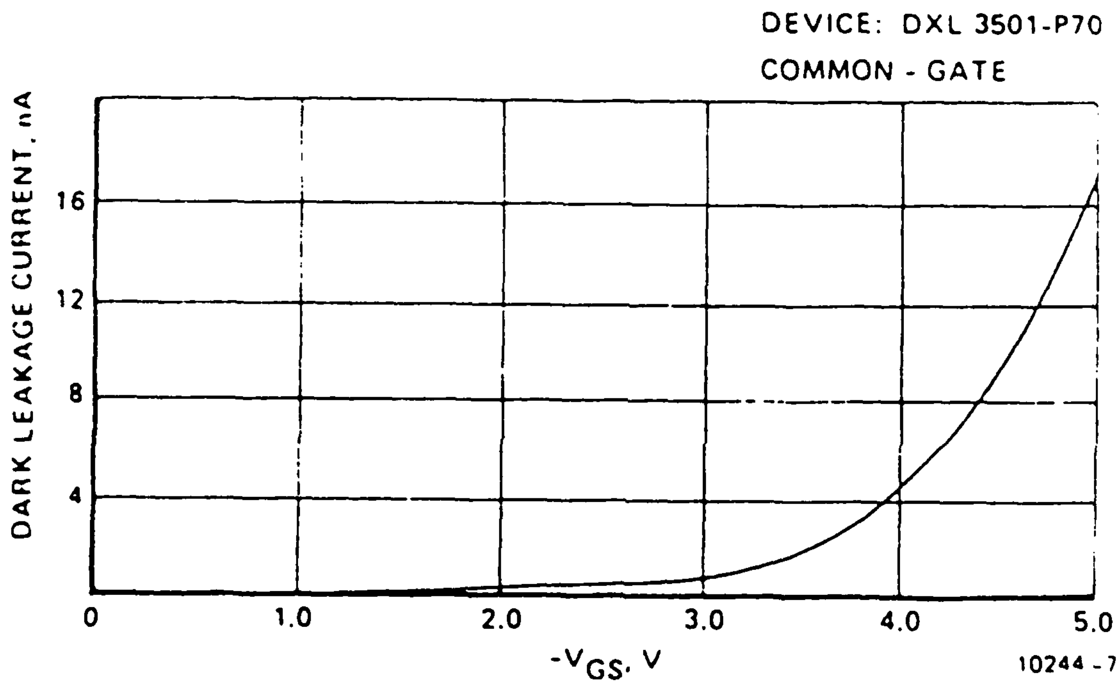

Figure 7.3.2.2.2. Dark Leakage Current Between Source and Gate

Presently, there are more than 20 vendors producing GaAs MESFET with low noise performance. Table 7.3.3.1 lists the commercially available low noise MESFETs at 4 GHz range (some data was taken in November 1982).

7.3.3.2 Long Wavelength MESFET Photodetector

Besides GaAs for 0.8 - 0.9 μm operations, other materials, such as InP, InGaAs and InGaAs/InP, also can be utilized to fabricate MESFETs when they are optimized for desirable, long wavelength. For example, InP/InGaAs MESFET has a better optical response from 1.1 μm to 1.3 μm.[1] Although, the InP MESFET is not commercially available yet, it has been investigated by many institutes.[2,3,4] For example, the Naval Research Laborary[2] has produced an InP MESFET with an impressive noise figure of 3 dB and gain of 9 dB at 10 GHz.

7.3.4 MESFET Characterization

7.3.4.1 DC and RF Parameters Without Illumination

The DC and RF parameters of GaAs MESFET without illumination normally are supplied by device manufacturers. The RF characteristics are given in terms of S-parameters and frequencies.

7.3.4.2 S-Parameter with Illumination

Both common source and common gate configurations are feasible for photo detector and amplifier applications. The latter configuration provides lower input impedance, lower amplification gain, lower responsivity, broader bandwidth, and

1. J.J. Pan, "Advanced Photodetector for Fiber Optic Communication System", 1979 NEPCON, February 1979, Anaheim, California.

2. H. Morkoc, et al, "Schottky Barriers and Ohmic Contacts on N-type InP Based Compound Semiconductors for Microwave FETs", IEEE Trans. on ED, January 1981, pp 1-5.

3. K.J. Sleger, et al, "Low Noise Ion-Implanted InP FET's", IEEE Trans. on ED, September 1981, pp 1031-1034.

4. C.Y. Chen, Bell Lab., Private Communication.

Table 7.3.3.1. Low Noise MESFETs at 4 GHz

Manufacturer	Model Number	Minimum Noise Figure (dB)	Associated Gain (dB)	Maximum Available Gain (dB)
NEC	NE137	0.6	15.5	18.5
NEC	NE218	0.9	13	16.5
Mitsubishi	MGF-1412	0.8	13	18
Dexcel	DXL2503B1	0.9	13	17
	DXL2502A	1.4	12	17
HP	HFET-2204	1.0	13.6	17
	HFET-2202	1.1	13.6	17
Plessey	GAT 6	1.0	14	18.5
Raytheon	LNX835 (Chip)	1.5	13	16
Alpha	ALF 1003	1.5*	12	16
Avantek	8110	1.3	12	--

* Noise Figure of 0.9 dB at 2 GHz (Ga = 14 dB)

similar noise figures when compared with the common source configuration. Besides the photocurrent measurements, the S-parameter of the MESFET was characterized to provide information for RF circuit design. The S-parameter variation caused by the device is strongly bias dependent. Table 7.3.4.1.1-1 and 7.3.4.1.1-1 are examples of MESFET S-parameter measurement results at dark and illuminated conditions from 20 MHz to 1,300 MHz. The negative sign of S_{21} magnitude indicates the gain. The S_{22} phase shows that the device has a nearly resistive output impedance over a wide frequency range. Figure 7.3.4.1 is S_{21} measurement between 7.0 GHz and 10.5 GHz.

7.4 4.4 - 5.0 GHz Fiber Optic Receiver Design

The block diagram of 4.4 to 5.0 GHz fiber optic receiver is shown in Figure 7.7. The GaAs MESFET was selected in post-detector amplifier because the microwave MESFET has many advantages over Si bipolar transistors, such as:

- Low noise
- Wide Operational bandwidth
- High Dynamic range

7.4.1 Receiver RF Circuit Design

RF design considerations of the wideband microwave fiber optic receivers are briefly described as follows:

a. Optimum Noise Performance/Source Admittance of the MESFET. The minimum noise figure of the MESFET does not occur at the source admittance for best gain. An optimum source impedance has to be selected to terminate the transistor input terminal for best gain noise figure performance.

b. Stability Factor Calculation. The stability factor should be constantly evaluated from the initial design until final optimization to ensure that no oscillation takes place. When the device terminates at a desirable input impedance and a 50 ohm load, the transistor S-parameter determines the stability factor as:

Table 7.3.4.1-1. Common Source GaAs Optical Response S-Parameter Measurement

DXL 3501, V_{gs} = 1.5 V, V_{ds} = 2.0 V, I_d = $\frac{6.0}{7.0}$ mA

S-Parameter / Freq.	Darkened								Illuminated							
	S_{11}		S_{21}		S_{12}		S_{22}		S_{11}		S_{21}		S_{12}		S_{22}	
(MHz)	Mag	Ang	Mag	Ang	Mag	Ang	Mag	Ang	Mag	Ang	Mag	Ang	Mag	Ang	Mag	Ang
20	0	-0.7	-10.7	178.9	61.0	74.2	2.5	-0.5	0	-0.7	-11.0	178.2	59.7	83.8	2.7	-2.1
100	0.1	-2.4	-10.7	176.8	48.2	85.6	2.5	-0.4	0	-2.5	-10.9	176.6	47.5	82.3	2.9	-1.0
200	0.1	-3.6	-10.8	174.6	43.1	81.1	2.5	0.4	0.1	-3.8	-10.9	174.2	42.7	81.6	2.9	-0.1
400	0.3	-9.0	-10.7	170.1	37.8	84.9	2.7	-0.7	0.2	-9.4	-10.8	169.8	37.8	84.4	3.1	-1.0
600	0.5	-12.5	-10.5	164.4	34.9	82.5	2.8	-1.0	0.5	-13.2	-10.7	164.0	34.5	83.9	3.2	-1.2
800	0.7	-17.3	-10.4	160.9	32.8	84.0	3.0	-1.2	0.7	-18.1	-10.5	160.4	32.6	81.7	3.4	-1.7
1,000	0.9	-20.5	-10.2	156.1	31.5	84.3	3.0	-1.1	0.9	-21.5	-10.4	155.6	31.1	83.4	3.5	-1.4
1,200	1.2	-24.5	- 9.7	150.7	30.5	83.9	3.2	-0.5	1.3	-25.7	- 9.9	150.4	30.0	85.3	3.7	-0.8
1,300	1.4	-25.4	- 9.6	150.5	30.2	84.6	3.4	0.6	1.4	-26.5	- 9.8	150.0	29.4	85.6	3.8	0.3

Table 7.3.4.1-2. Common Source GaAs MESFET Optical Response S-Parameter Measurement

DXL 3501, V_{gs} = 2.3 V, V_{ds} = 5.0 V, I_d = $\frac{5}{8.7}$ mA

S-Parameter / Frequency	Darkened								Illuminated							
	S_{11}		S_{21}		S_{12}		S_{22}		S_{11}		S_{21}		S_{12}		S_{22}	
(MHz)	Mag	Ang	Mag	Ang	Mag	Ang	Mag	Ang	Mag	Ang	Mag	Ang	Mag	Ang	Mag	Ang
20	0.1	-1.0	-5.9	179	61.7	53.3	1.1	-0.2	0.2	-1.1	-8.1	178.6	57.7	78.1	1.9	-1.2
100	0.2	-1.3	-5.9	177.9	49.3	84.4	1.2	-0.2	0.2	-1.3	-8.1	177.6	47.4	81.1	2.1	-0.7
200	0.2	-1.7	-6.0	175.7	44.0	83.8	1.1	0.8	0.3	-1.8	-8.1	175.7	41.8	83.6	2.0	0.4
400	0.3	-6.0	-6.0	171.6	38.7	85.6	1.2	-0.1	0.3	-6.6	-8.1	171.3	36.4	84.5	2.2	-0.7
600	0.4	-8.1	-5.9	167.0	35.5	83.6	1.4	-0.1	0.4	-9.0	-7.9	166.5	33.6	84.9	2.3	-1.0
800	0.6	-12.3	-5.7	163.9	33.8	81.5	1.5	-0.3	0.7	-13.5	-7.8	163.4	31.3	82.0	2.5	-1.4
1,000	0.6	-14.8	-5.7	159.8	32.0	81.0	1.5	-0.3	0.7	-16.3	-7.7	159.0	29.8	82.1	2.5	-1.7
1,200	0.9	-18.3	-5.3	154.6	31.3	81.2	1.7	0.2	1.0	-20.0	-7.3	153.7	28.8	81.7	2.8	-1.3
1,300	0.9	-19.0	-5.3	154.5	31.1	79.9	1.7	1.5	1.1	-20.9	-7.3	153.7	28.4	80.8	2.8	-0.2

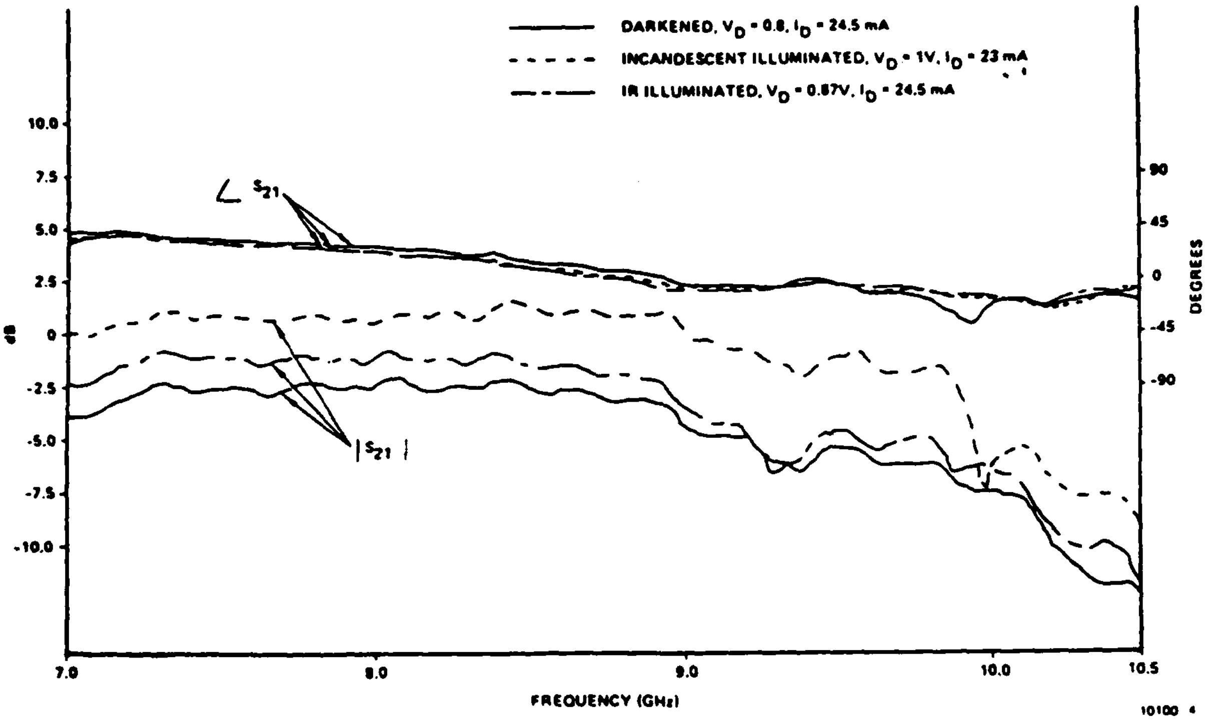

Figure 7.3.4.1. MESFET S_{21} Measurement in X-Band Under Illumination Conditions

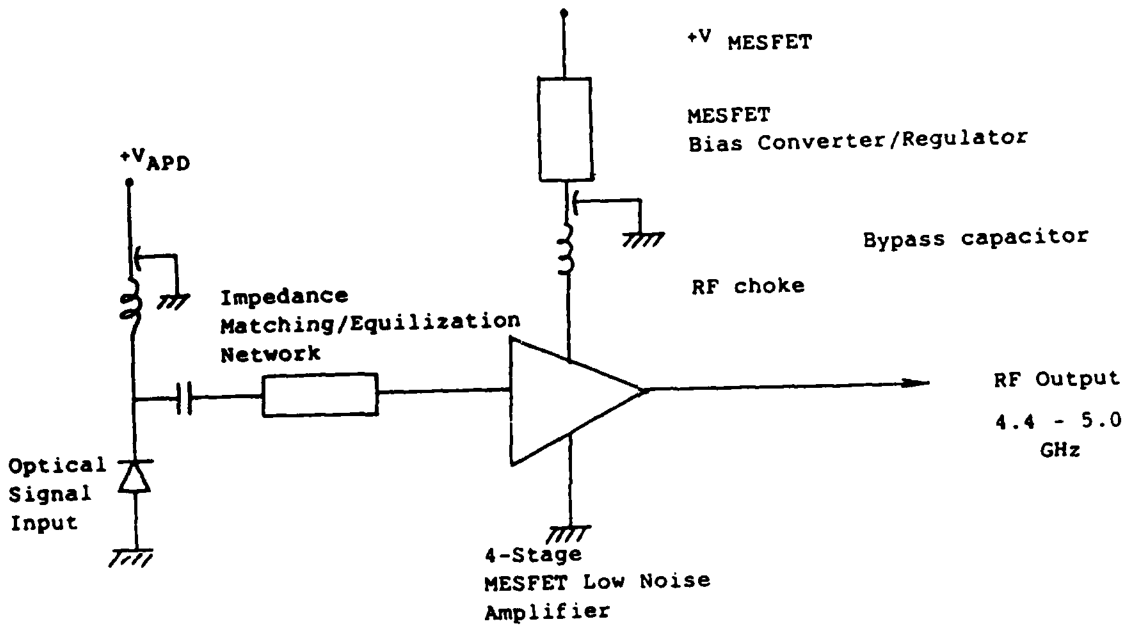

Figure 7.4. Block Diagram of 4.4 to 5.0 GHz Fiber Optic Receiver

$$k = \frac{1 + \left| S_{11} S_{22} - S_{12} S_{21} \right|^2 - \left| S_{11} \right|^2 - \left| S_{22} \right|^2}{2 \; S_{12} \; S_{21}} \qquad (7.19)$$

where S_{22}' is output reflection coefficient with an arbitrary source impedance, Γs, and

$$S_{22} = S_{22}' + \frac{S_{12} \; S_{21} \; \Gamma s}{1 - S_{11} \; \Gamma_s} \qquad (7.20)$$

c. Wideband Output Impedance Matching. The APD has an impedance, with a low real part (1-3 ohms) and a capacitive imaginary part (1-2 pf), while the MESFET has high resistive output impedance (200 to 450 ohms). To match these photodetectors to the 50 ohm post detector amplifier, a proper impedance matching network is required in order to obtain the desired bandwidth.

d. Gain/Noise/Stability Tradeoff. The gain and stability factor of a MESFET can be computed directly from the device S-parameters and displayed on a Smith chart; the optimized noise source admittance also can be plotted on the Smith chart. To ensure stable operation of an LNA with sufficient amplification gain, one should tradeoff these three parameters and determine the best input and output impedances for the MESFET.

e. Optimization. The "Super-COMPACT" or "COMPACT" computer program can be utilized to optimize the receiver noise performance, gain, gain flatness, input/output VSWR, and phase linearity. Each of these parameters has an assigned weighting factor based on the desired circuit requirements.

f. Band Pass Design. In order to minimize the wideband noise and reduce the out of band interference, band pass impedance matching should be used for the cascaded multi-stage amplifier. With the computer aided design approach, one can design a microwave pass band matching network to match 50 ohm to any desired source/load impedances (determined by S_{11} and S_{22}) with a 0.4 dB ripple.

g. Circuit Configuration. The 4.4 - 5.0 GHz microwave fiber optic receiver was fabricated in microstrip configuration. It is well known that this design provides fabrication simplicity while providing small size and weight.

h. Temperature Stabilization. The variation of the APD multiplication gain with temperature is caused by the change of ionization rates and the APD terminal voltage. Both the MESFET noise and amplification gain exhibit changes as a function of temperature. A 2 dB gain variation has been observed in the temperature range of -25^{o}C to +75^{o}C. The gain variation also strongly depends on the gate source bias condition. To minimize gain variation, one should investigate an AGC approach.

7.4.2 Low Noise Post-Detector Amplifier Design Philosphy

The post-detector LNA's shall have the characteristics of high stability, bandpass amplification, flat frequency response, low group delay, good phase linearity, low input/output VSWRs and high reproducibility. The MESFET is the selected candidate for the 4.4 - 5.0 GHz impedance transformer/amplifier. However, the MESFET's intrinsic input/output impedances cause the MESFET amplifier to have high input and output VSWRs and instability over a wide frequency range. High VSWRs increase amplifier mismatching power loss and noise figure and, potentially, would cause oscillation and spurious outputs. Circulators and balanced configurations have been used to overcome the poor VSWRs. However, the balanced amplifier requires two 3 dB quadrature couplers and twice the amount of active devices and power consumption. Both circulator and balanced amplifier approaches degrade overall gain, noise figure, bandwidth, size, and cost.

Recently, microwave amplifier designers have used the classical resistor (or combination of resistor and inductor) feedback[1,2,3] as depicted in Figure 7.4.2 (a) to improve amplifier bandwidth, VSWRs, and stability. The main drawback to using the classical feedback approach is the additional thermal noise generated by the feedback resistor which is amplified and added directly to the amplifier noise figure. This degradation of amplifier noise reduces system sensitivity and dynamic range. Furthermore, the finite size of the feedback

resistor, attached between the MESFET gate and drain, often disturbs the MESFET input/output matching networks. Consequently, it causes deviation from the optimum designed values of gain, noise figure, VSWRs, etc.

To minimize the added thermal noise generated by the feedback resistor and to achieve low VSWRs, wide bandwidth, good gain flatness, low group distortion, and good phase linearity, the RF feedback consists of two sets of $\lambda/4$ low and high impedance lines which prevent thermal noise feedback from the resistor being applied to the input. The low impedance $\lambda/4$ lines bypass the noise as well as the RF signal to ground. These lines also isolate the RF interaction between drain and gate, thereby promoting excellent stability in the amplifier. The circuit scheme of RF feedback MESFET amplifiers is illustrated in Figure 7.8 (b).

In addition to the previously mentioned attractive advantages, the RF feedback technique also provides the following benefits:

- Insensitivity to device S-parameter variations resulting in excellent device interchangeability

- Reduced dependence upon optimum noise figure source admittance matching

- Decreased harmonic and intermodulation distortions

(The detailed discussion of RF feedback amplifier is given in Appendix B). Therefore, the RF feedback amplifier was used in the 4.4 - 5.0 GHz RF fiber optic link receiver design.

1. K.G. Niclar, et al, "The Matched Feedback Amplifier: Ultrawideband Microwave Amplification with GaAs MESFETs", IEEE Trans. on MTT, April 1980, pp 285-294.

2. F. Perez and V. Oretega, "A Graphical Method for the Design of Feedback Networks for Microwave Transistor Amplifiers: Theory and Applications", IEEE Trans. on MTT, October 1981, pp 1019-1026.

3. K.B. Niclas, "Noise in Broadband GaAs MESFET Amplifiers with Parallel Feedback", IEEE Trans. on MTT, January 1982, pp 63-70.

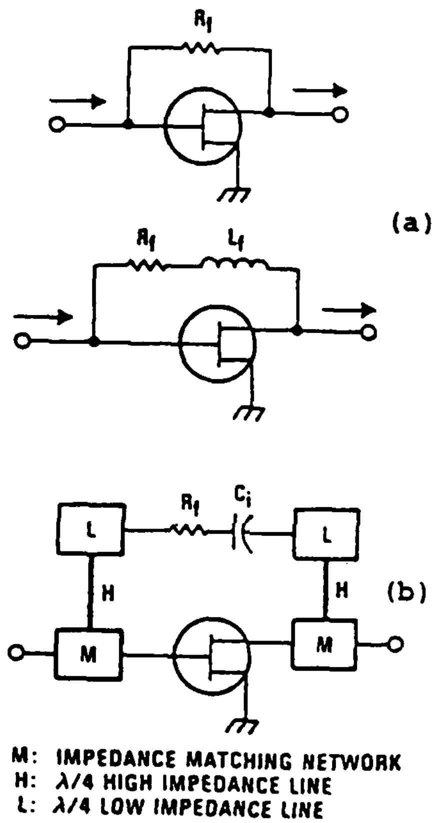

Figure 7.4.2 (a). Classical Feedback MESFET Amplifier Using a Resistor or a Resistor and Inductor Combination;

(b) New RF Feedback MESFET Amplifier

7.4.3 4.4 - 5.0 GHz LNA Design and Optimization

The NEC NE218 was chosen for the 4.4 - 5.0 GHz feedback LNA design and optimization. The computer design/optimization program and optimized results of the single-stage LNA are presented in Table 7.4.3. The LNA configuration is shown in Figure 7.4.2 (b).

7.4.4 Amplifier Fabrication

The 4.4 - 5.0 GHz feedback amplifiers were fabricated on alumina substrates which are 0.025-inch thick metallized chrome-gold. Both substrates and carrier were designed to accommodate packaged devices from other manufacturers.

Bias is supplied to both gate and drain via feed-through filters and RF to DC isolation is provided through the series of high-low-high impedance lines, each $\lambda/4$ in length. As shown in Figure 7.4.4, a short section of 50 Ohm line on Epsilan-10 is used to connect the gate and drain through a resistor and capacitor in the RF feedback loop. The input and output DC blocks were achieved with chip capacitors chosen for their compatibility with the line widths involved.

7.4.5 Performance and Measurement Results

The gain, gain flatness, and VSWR of the amplifiers were evaluated and output VSWRs were 1.16:1 and 1.19:1, respectively, with typical stability factors about 1.47. Six LNA's were fabricated and measured from different MESFET lots as shown in Table 7.4.5. The input and output VSWR's follow the computer predicted values, while gains are higher than calculated.

In order to determine the noise figures and the various amplifiers, a Hewlett-Packard noise figure meter was employed. Results show a typical noise figure of 1.83 dB for the overall amplifier, which is quite impressive considering that the noise figure of the device (NE21889) itself is 1.50 dB. This small difference is caused by the insertion loss of the coaxial-to-micro-strip launcher, DC blocking capacitor, and input impedance matching network.

Table 7.4.3. Computer Design/Optimization Program and Optimized Results of a Single-Stage LNA Using NE 218

(A) Computer Design and Optimization Program

```
1.  TRL AH MS -21.64 -261.9 9.9 25
2.  SST BB MS -37.25 -127.9 9.9 25
3.  TWO CC S3 50
4.  SST DD MS -5.9 -135.4 9.9 25
5.  TRL EE MS -13.4 -266 9.9 25
6.  CAX AA EE
7.  PRI AA S1 50
8.  END
9.  4400 5000 200
10. END
11. .53 -107 1.88 97.9 .137 -15.9 .42 -48
12. .58 -115 1.88 82.9 .102 -36.3 .58 -53
13. END
14. .1
15. 0 0 10 8
16. END
EDF..
EDT..
COMPACT
```

(B) Optimized Results

CIRCUIT OPTIMIZATION WITH 8 VARIABLES

INITIAL CIRCUIT ANALYSIS

POLAR S-PARAMETERS IN 50.0 OHM SYSTEM

FREQ.	S11		S21		S12		S22		S21	K
	(MAGN	ANGL)	(MAGN	ANGL)	(MAGN	ANGL)	(MAGN	ANGL)	DB	FACT
4400.00	0.01	32	2.40	-25.5	0.175	-139.3	0.01	-151	7.61	1.40
4600.00	0.05	45	2.44	-43.8	0 162	-158.1	0 04	147	7.74	1.46
4800.00	0.09	45	2.49	-61.8	0.149	-177.9	0.10	137	7.92	1.50
5000.00	0.13	44	2.55	-79.8	0.139	161.0	0.18	128	8.15	1.52

INPUT SWR_{max} 1.3:1

OUTPUT SWR_{max} 1.44:1

GAIN FLATNESS = .54 db

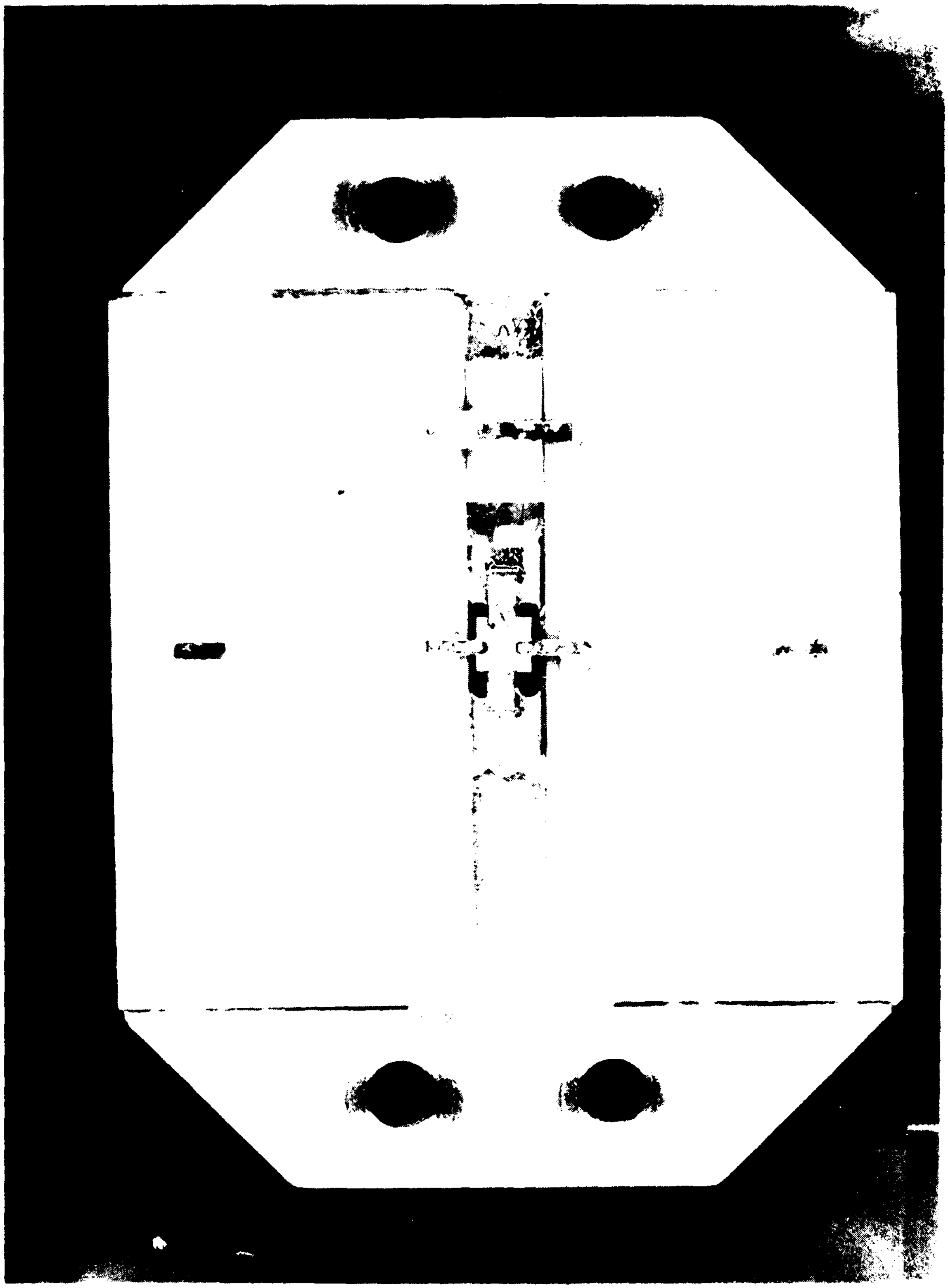

Figure 7.4.4. 4.4 - 5.0 GHz Low Noise Feedback MESFET Amplifier

Table 7.4.5. 4.4 - 5.0 GHz RF Feedback LNA Using NE 218

AMPLIFIER NUMBER	INPUT VSWR	OUTPUT VSWR	GAIN
1	1.03:1 - 1.17:1	1.08:1 - 1.28:1	9 dB
2	1.03:1 - 1.25:1	1.28:1 - 1.92:1	8 dB
3	1.12:1 - 1.28:1	1.02:1 - 1.43:1	9 ±1 dB
4	1.04:1 - 1.22:1	1.04:1 - 1.44:1	11 ±0.5 dB
5	1.11:1 - 1.34:1	1.04:1 - 1.48:1	11.5 ±0.5 dB
6	1.10:1 - 1.23:1	1.12:1 - 1.36:1	10.25 ±0.25 dB

* Amplifiers Number 1,2,3 were fabricated on May 11, 1982; Number 4,5,6 on May 19, 1982.

** Amplifier Number 4 and 5 have 1 dB gain slope between 4.4 to 5.0 GHz which are tuned to compensate ILD frequency roll-off.

7.4.6 APD Receiver

The ADP receiver consisting of a Telefunken APD, a r-stage MESFET LNA, and a demountable single-mode connector is shown in Figure 7.4.6 (package at right).

8.0 LINK TEST AND EVALUATION

The 4.4 and 5.0 GHz fiber otpic systems using 1 Km single mode fiber is shown in Figure 7.4.6. The laser diode transmitter is shown on the left, APD receiver on the right, and the one-stage RF feedback amplifier at front. Tests have been done in the laboratory environment before and during the acceptance test. The data presented in this section was taken during acceptance.

8.1 Test Parameters

The following system parameters of 4.4 - 5.0 GHz, 1-Km fiber optic link were subjected to be tested:

- S/N
- S/N over 4.4 - 5.0 GHz Band
- Harmonic Distortion
- Two-tone, third-order IMP's (intermodulation product)
- Input and Output VSWR's
- Gain Flatness
- Phase
- Laser diode to single-mode fiber coupling efficiency

8.2 Test Setup

The signal-to-noise and frequency response measurements setup is depicted in Figure 8.2-1. The 10 dB directional coupler is used to monitor the RF signal power level. To minimize any possible interaction or interference between the measurement equipment, the signal generator, FO transmitter, and its power supply were located inside of a screen room while the receiver was put outside the screen room.

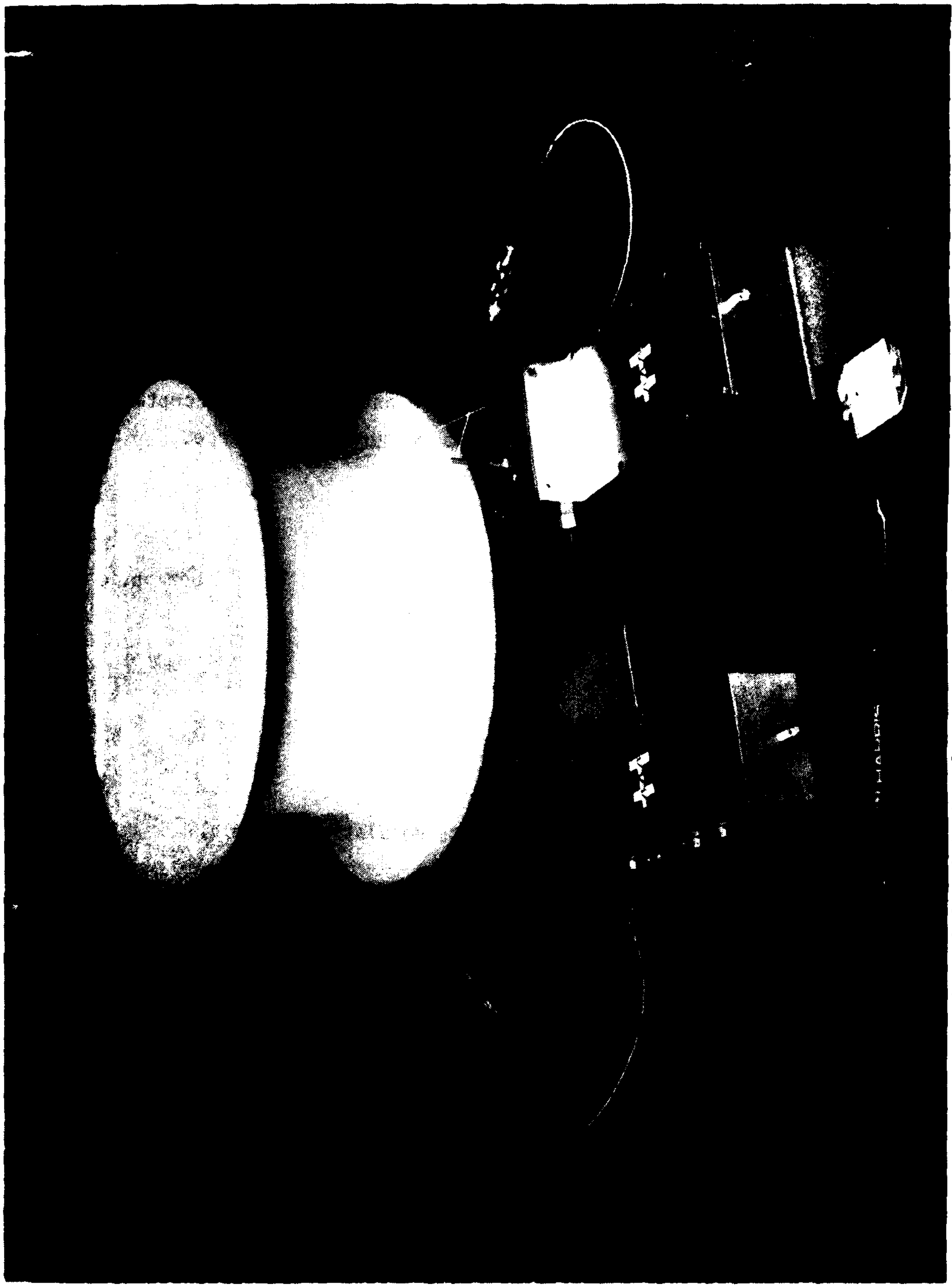

Figure 7.4.6. 4.4 - 5.0 GHz, 1 km Fiber Optic Link; ILD Transmitter on Left and ADP Receiver on Right

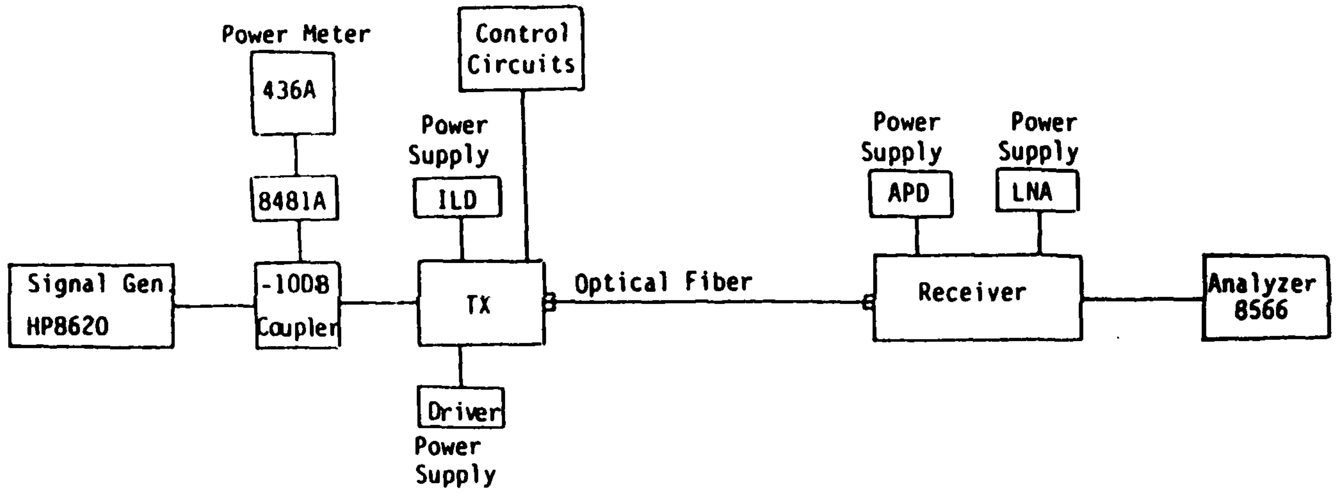

Figure 8.2-1. Test Setup for 4.4 - 5.0 GHz FO Link S/N and Frequency Response Measurements

The third-order, two-time IMP test setup is shown in Figure 8.2-2. Two signal generators can be independently adjusted for frequency and power level. Again, the fiber optic transmitter and related equipment were located inside the screen room.

The coupling coefficient of laser-fiber measurement is presented in Figure 8.2-3.

8.3 Test Results

8.3.1 Signal to Noise Ratio (S/N) Measurement

Figure 8.3.1 displays the S/N's at frequencies of 4.4 to 5.0 GHz at 100 MHz interval. The system showed a S/N of better than 48 dB over 4.4 to 5.0 GHz for a 300 kHz measurement window.

8.3.2 Frequency Response

Figure 8.3.2 illustrates the frequency response result. The flatness over 4.4 to 5.0 GHz is ± 1.34 dB.

8.3.3 Harmonic Distortion

Since both laser diode driver and MESFET amplifiers were designed to have bandpass characteristics, there were no second and third harmonics. Swept from 4 to 10 GHz, Figure 8.3-3 demonstrates that no second harmonics exist. The signals on left of photo are the fundamental signals (+10 dBm) 4.4 to 5.0 GHz at 100 MHz intervals.

8.3.4 Third-Order, Two-Tone IMP Test Results

Several third-order, two-tone IMP's have been tested. When the input signals levels were 0 dBm, no IMP's were observed. When the signals increased to +10 dBm or +5dBm, the following IMP results occurred:

a. +10 dBm each tone, 20 MHz apart: -30 dBc (Figure 8.4-1)

b. +5 dBm each tone, 20 MHz apart: -45 dBc (Figure 8.4-2)

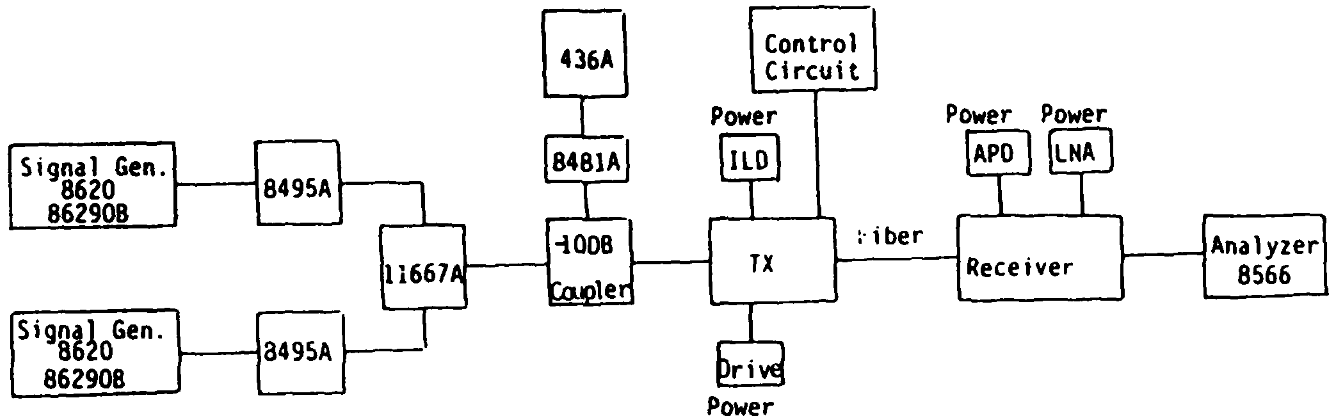

Figure 8.2-2. Test Setup for Two-Tone IMP Measurement

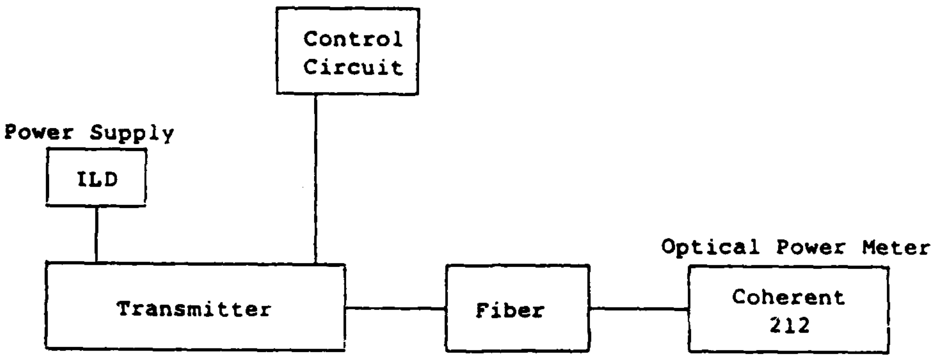

Figure 8.2-3. Test Setup for Laser Diode to Single Mode Fiber Coupling Coefficient Measurement

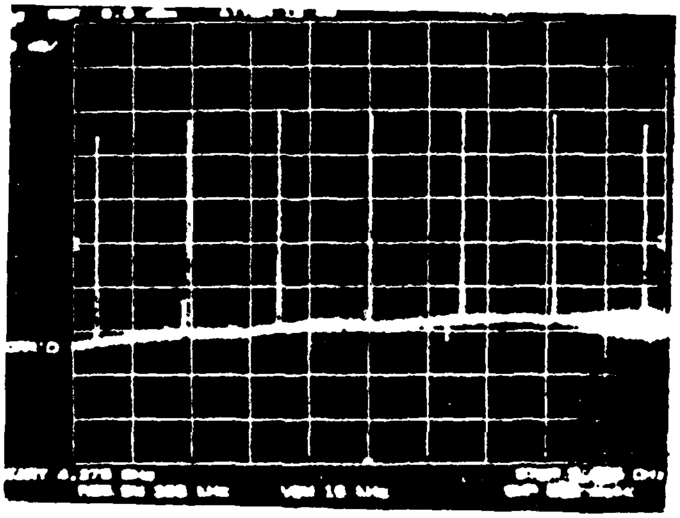

Figure 8.3-1. S/N Measurement Results from 4.4 to 5.0 GHz at 100 MHz Intervals

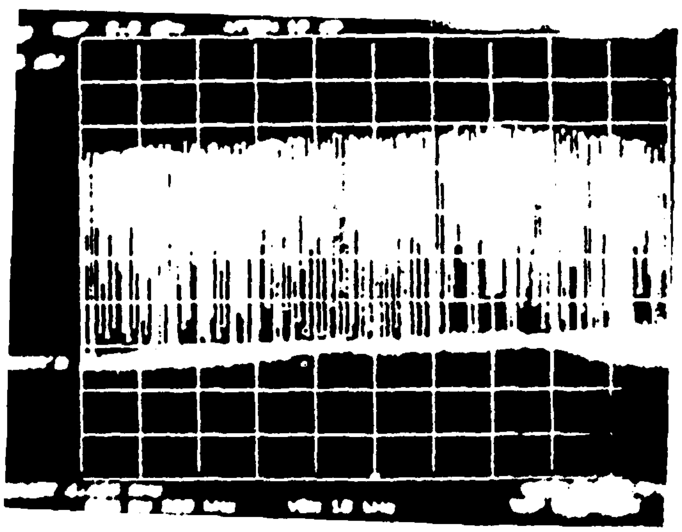

Figure 8.3-2. Frequency Response of 1 km FO Link Over 4.4 to 5.0 GHz

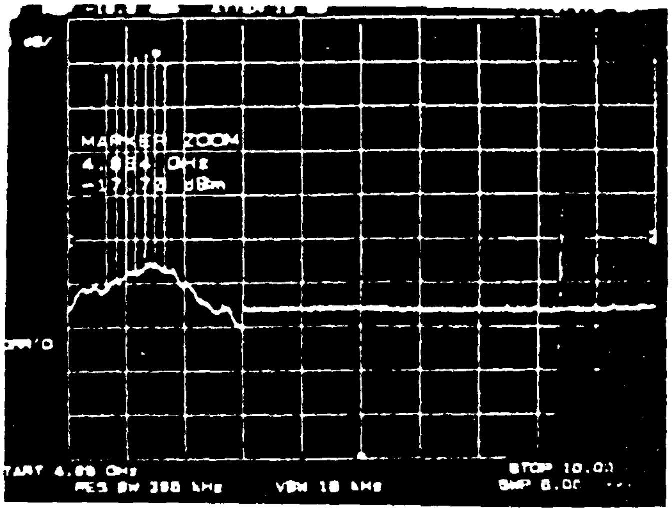

Figure 8.3-3. The Fundamental Signals are From 4.4 - 5.0 GHz at 100 MHz Interval. No Second Harmonics is Observed. Sweeping Frequency from 4 to 10 GHz

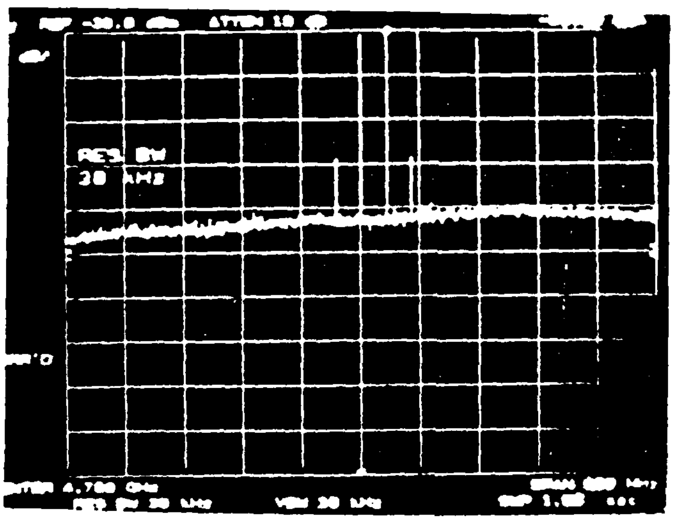

Figure 8.3.4-1. Two-Tone, Third-Order IMP's (4.70 and 4.72 GHz at +10 dBm each)

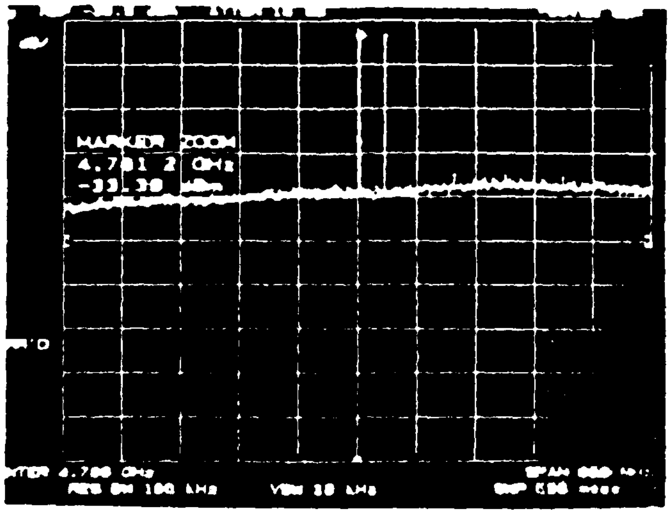

Figure 8.3.4-2. Two-Tone, Third-Order IMP's (4.70 and 4.72 GHz at +5 dBm each)

c. +10 dBm each tone, 250 MHz apart: -45 dBc (Figure 8.4-3)

d. +10 dBm each tone, 64 kHz apart: -20 dBc (Figure 8.4-4)

(signal partially distorted due to interaction between two signal generators)

The magnitude of two-tone IMP will be reduced considerably when the amplitudes of the input signals drop. Normally, 3 dB IMP improvement results for every 1 dB input signal reductions.

8.3.5 Input and Output VSWR's

The input and output VSWR's of the 4.4 - 5.0 GHz FO link were measured by measuring the return losses. Figure 8.3.5-1 is the result of Input VSWR measurements. The VSWR varies from 1.0:1 to 1.58:1 over 4.4 to 5.0 GHz. Figure 8.3.5-2 depicts the output VSWRs which varies from 1.0:1 to 1.22:1.

8.3.6 Gain Flatness of Post-Detector Amplifier

Figure 8.3.6-1 and Figure 8.3.6-2 represent the gain flatness of single-stage and four-stage RF feedback amplifier, respectively.

Figure 8.3.6-3 depicts the phase of a four-stage amplifier over 4.4 to 5.0 GHz. The amplifier phase is linearly varying.

8.3.7 Laser Diode-to-Single Mode Fiber Coupling Coefficient Measurement

The laser diode-to-single mode fiber coupling coefficient measurement was accomplished by the following procedure:

The optical power output of the laser diode (biased at 60 mA) and a 3-foot graded-index fiber

= -1.3 dBm

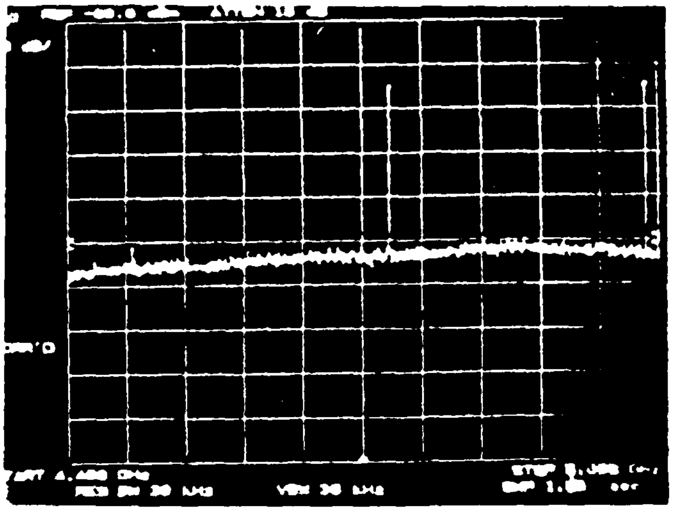

Figure 8.3.4-3. +10 dBm each tone, 250 MHz apart Third-Order IMP Measurement

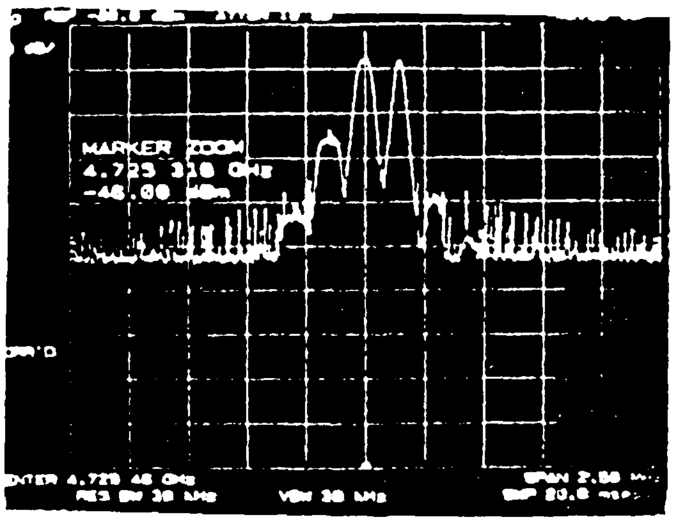

Figure 8.3.4-4. +10 dBm each tone, 64 kHz apart Two-Tone, Third-Order IMP

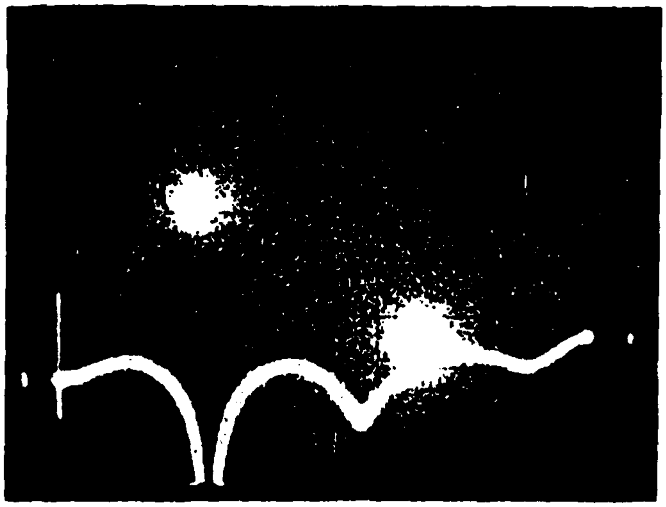

Figure 8.3.5-1. 4.4 - 5.0 GHz FO Link Input VSWR
(1.0:1 to 1.58:1 Over 4.4 50 5.0 GHz)

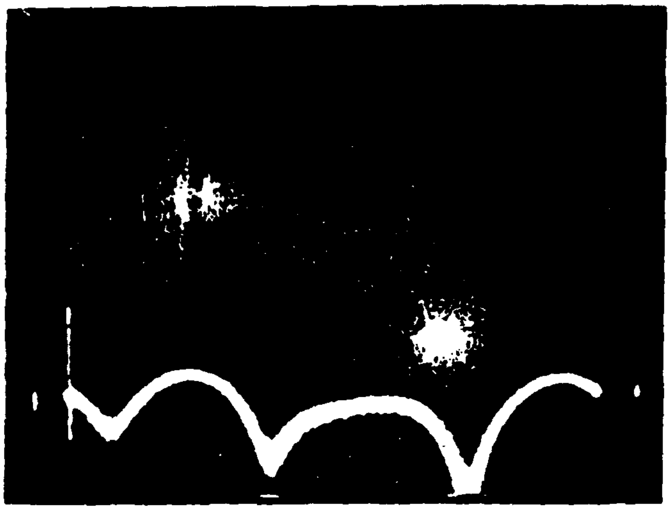

Return Loss of Output

Reference

←10 dB (1.92:1 VSWR)
←20 dB (1.22:1 VSWR)
←30 dB (1.06:1 VSWR)

↑ 4.4 GHz

↑ 5.0 GHz

Figure 8.3.5-2. 4.4 to 5.0 GHz FO Link Output VSWR
(1.0:1 to 1.22:1 over 4.4 - 5.0 GHz Band)

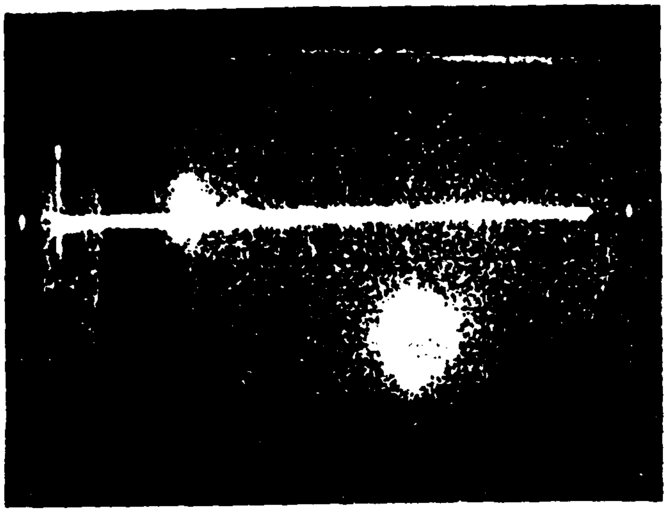

Gain of Single-Stage Amplifier

← 10 dB
← 0 dB gain

↑ 4.4 GHz

↑ 5.0 GHz

Figure 8.3.6-1. Gain Flatness (4.4 to 5.0 GHz) of a Single Stage RF Feedback Amplifier.

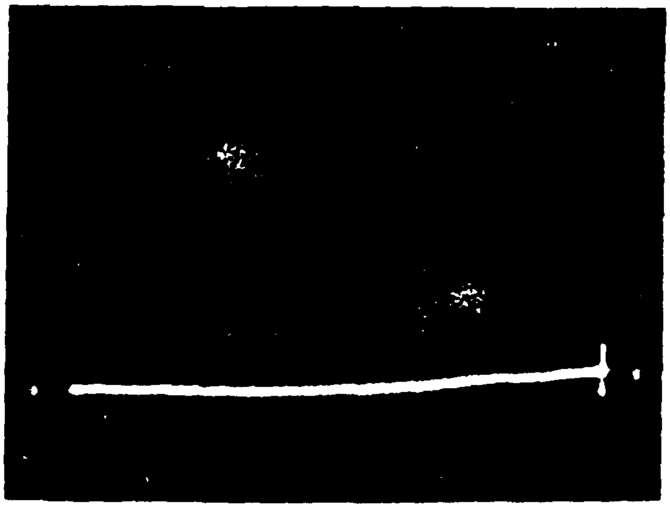

Gain of four-stage amplifier

←34 dB
←30 dB
←20 dB
← 0 dB

↑ 4.4 GHz

↑ 5.0 GHz

Figure 8.3.6-2. Gain Flatness (4.4 to 5.0 GHz) of a four-stage RF Feedback Amplifier

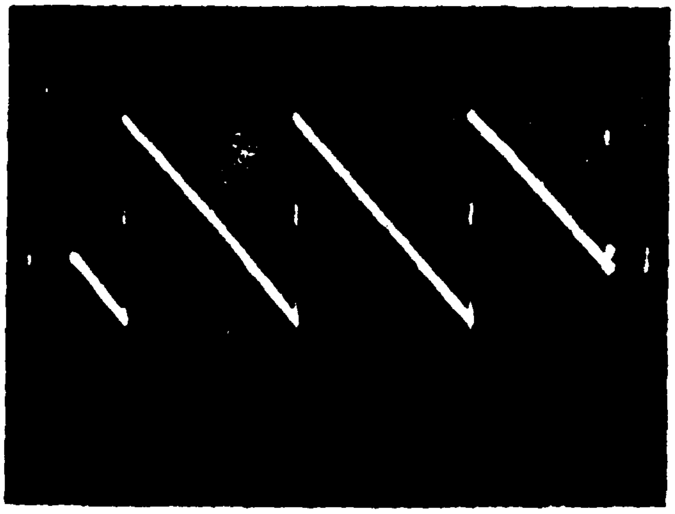

Phase of 4-Stage

Amplifier
90°/Division

4.4 GHz 5.0 GHz

Figure 8.3.6-3. Phase Measurement of a four-stage RF Feedback Amplifier

the optical power output of the laser diode (biased at 60 mA) and a 1 km single-mode fiber with lens

= -17.0 dBm

one km single-mode fiber loss

= 2.4 dB

therefore, the coupling loss was

17 - 2.4 - 1.3 = 13.3 dB

or, the coupling coefficient

4.8 percent

8.4 Comparison Of The Two RF Fiber Optic Links

The previously cited (Paragraphs 8.1, 8.2, and 8.3) measurement results were taken during acceptance tests on July 8 and July 9, 1982. The hardware is depicted in Figure 7.4.6 and referred and Version I. A modified 4.4 - 5.0 GHz RF fiber-optic link was delivered to RADC in April 1983, referred as Version II. The Version II hardware is illustrated in Figure 8.4.

8.4.1 Comparison of Devices Employed in Version I and Version II

The key devices and components used in Version I and Version II of Rf fiber optic link are summarized in Table 8.4.1.

Only 4.8 percent of laser optical power has been coupled into the single mode fiber. However, the coupling efficiency of laser diode fiber has been

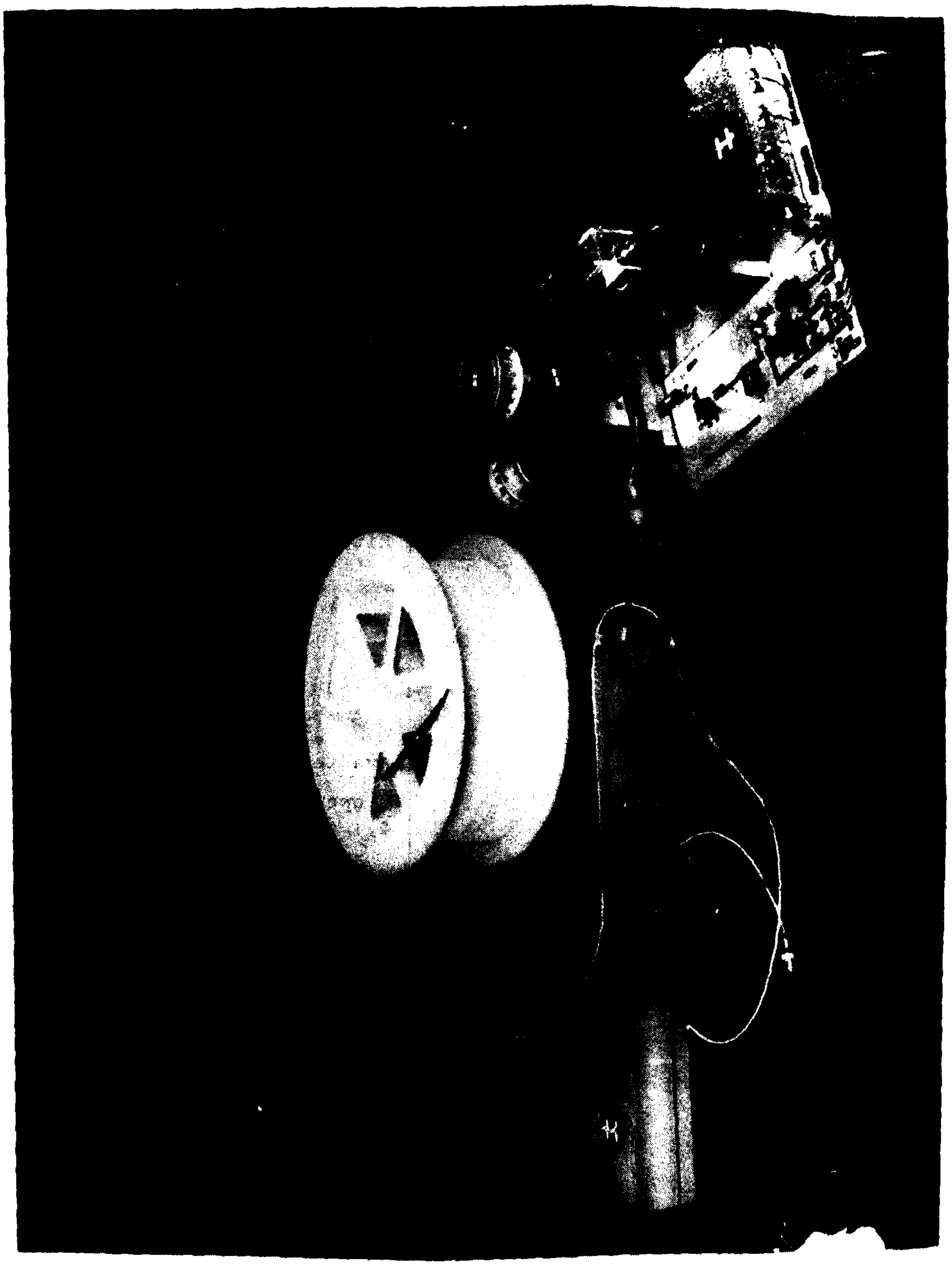

Figure 8.4. Version II 4.4 - 5.0 GHz RF Fiber Optic Link

Table 8.4.1. Comparison of Devices and Components Employed in Version I and Version II of RF Fiber Optic Link

Comparison / Device	VERSION I	VERSION II
o ILD	GOLS-1 (Characteristics: See Figure 4.8 and Paragraph 4.5)	GOLS; biased at 88.5 mA/ 1.9V
o Transistors in ILD Driver	NEC NE 218 NF_{opt} at 4 GHz: 1.0 dB G_a at 4 GHz: 12 dB	NEC NE 720 NF_{opt} at 4 GHz: 1.3 dB G_a at 4 GHz: 10 dB
o APD	AEG - Telefunken S171P Cd: 0.85 pF Gain-bandwidth: 200 GHz Temperature coeff: 0.2%/°C	Hitachi
o Transistors in Receiver	NEC NE 218	Avantek AT8110 NF_{opt}: 1.3 dB G_a: 12 dB
o Connector	Ceramic Capillaries Ferrule/plug	Ceramic Capillaries Ferrule/plug
o Fiber cable	Fujikura single-mode	Fujikura single-mode

achieved at 50 percent[1] to 79 percent[2,3] using a specially fabricated lens at the tip of the fiber. The system's S/N (not quantum noise limited) is directly proportional to the received optical power. This means the previously mentioned S/N of 48 dB can be upgraded if the power coupling between the laser diode and fiber is improved.

The remarkable improvement of high frequency laser diodes and packaging makes the directly modulated 6 to 8 GHz fiber optic system possible. This offers many attractive features for high-quality microwave signal transmissions. Reducing the laser nonlinearity and noise has been instrumental in obtaining the required performance characteristics for microwave analog and digital fiber optic links. Possible applications include secure microwave RF carrier transmissions, ECM, radar signal processing, sensor array, TVRO, and multi-channel CATV.

- Design and fabricate various microwave fiber optic links for radar, WE, ELINT, SATCOM, etc., applications.
- Develop MESFET photodetector pigtailing techniques for practical hardware integration.
- Improve and simplify laser diode to single mode fiber coupling techniques.
- Investigate and develop an external modulator to make microwave fiber optic links above 10 GHz possible.

1. H. Sakaguchi, et al, "Power Coupling From Laser Diode into Single Mode Fibers with Quadrangular Pyramid-Shaped Hemi-Ellipsoidal Ends", Elect. Lett. 11 June 1981, pp 425-426.
2. News, Fiber Optic Technology, February 1982, pp. 103-104.
3. W. Bludan and R. Rossberg, "Characterization of Laser-to-Fiber Coupling Techniques by their Optical Feedback", Allied Optics, January 1982, pp. 1933-1939.

- Continue the investigation of MESFET as a photodetector above 10 GHz.
- Reduce microwave optoelectronic receiver noises to upgrade system S/N.

8.4.2 Integration Comparision of Version I and Version II

The prime differences of system integration between Version I and Version II are listed in Table 8.4.2.

8.4.3 Data Obtained From Both Versions

The test setup and test results of Version I were presented in Paragraphs 8.2 and 8.3, respectively.

- S/N measurements at 4.1 through 5.2 GHz are shown in Figure 8.4.3-1 (a), (b), (c), (d), (e), (f), (g), (h), (i), (j), and (k).
- Gain flatness between 4.375 and 5.025 GHz is shown in Figure 8.4.3-2.
- Second harmonics measurement is shown in Figure 8.4.3-3.
- Two-Tone intermodulation product (IMP) measurements are shown in Figure 8.4.3-4.
- Input and output VSWR's measurement (using return loss measurements) are shown in Figure 8.4.3-5.

8.4.4 Comparison of the Measured Data of Versions I and II

The measured data of Version I and II of RF fiber optic link is tabulated in Table 8.4.3.

Table 8.4.2. Integration Differences of Version I and Version II of 4.4 - 5.0 GHz RF Fiber Optic Link

VERSION I	VERSION II
• ILD was internal mounted and aligned with built-in adjustable positioner.	• ILD was mounted to an external 3-axis adjustable positioner.
• ILD was directly interfaced with amplifier/transformer by microstrip.	• ILD was connected to driver through 1-inch microstrip (on ceramic) and a 50 Ohm semi-rigid coaxial cable.
• Power supplies and regulators were not integrated on motherboards.	• Regulators were integrated on motherboards.

Table 8.4.3. Measurement Results Comparison of Version I and Version II

(GHz) Frequency	Version I	Version II	
	S/N at 300 KHz BW	S/N at 30 KHz BW	Normalized S/N at 300 KHz BW
4.1	38	34	24
4.2	44	38	28
4.3	47	38	28
4.4	47	38	28
4.5	48	35	25
4.6	49	36	26
4.7	49	37	27
4.8	48	38	28
4.9	47	35	27
5.0	45	37	25
5.1	No Measurement	28	18
5.2	38	18	8
3rd IMP	-39 dBc at Input power +10 dBm	-34 dBC at Input power -30 dBm	
2nd Harmonics	No	No	
Throughput Gain	~-38 dB	~ -22 dB	
Input VSWR	1.58:1 to 1.0:1	1.58:1 to 1.1:1	
Output VSWR	1.23:1 to 1.0:1	4.5:1 to 1.23:1	

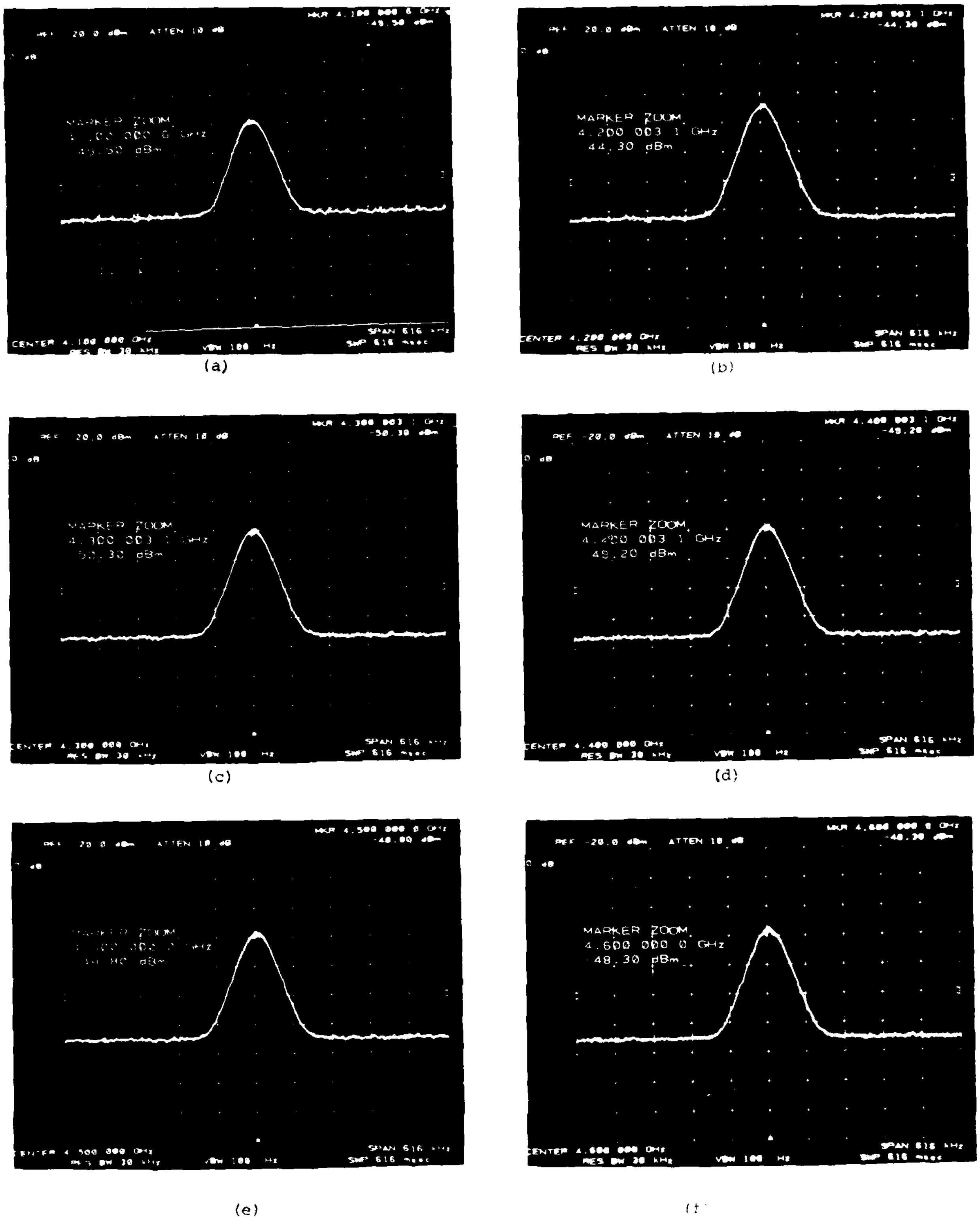

Figure 8.4.3-1 (a). S/N Measurements of Version II RF Fiber Optic Link

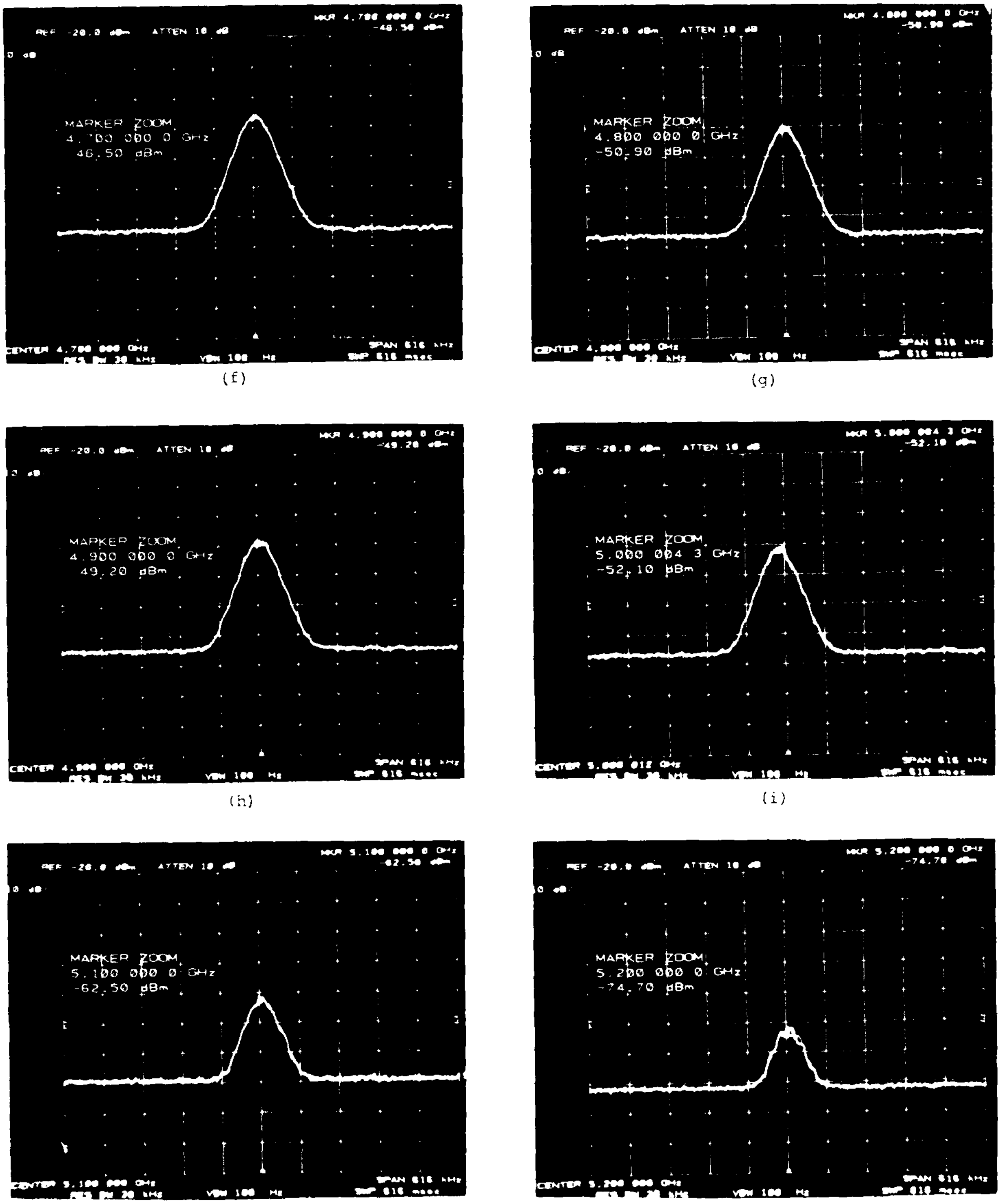

Figure 8.4.3-1 (a). S/N Measurements of Version II RF Fiber Optic Link Between 4.1 and 5.2 GHz (RF input = dBm)

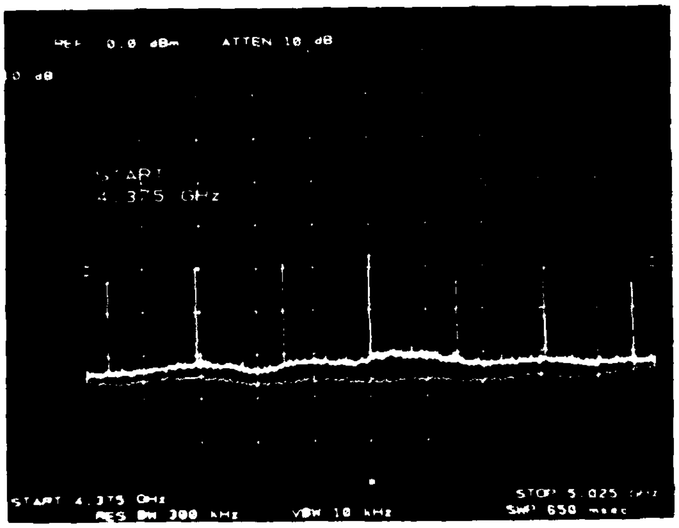

Figure 8.4.3-2. Gain Flatness Measurement of RF Fiber-Optic Link, Version II

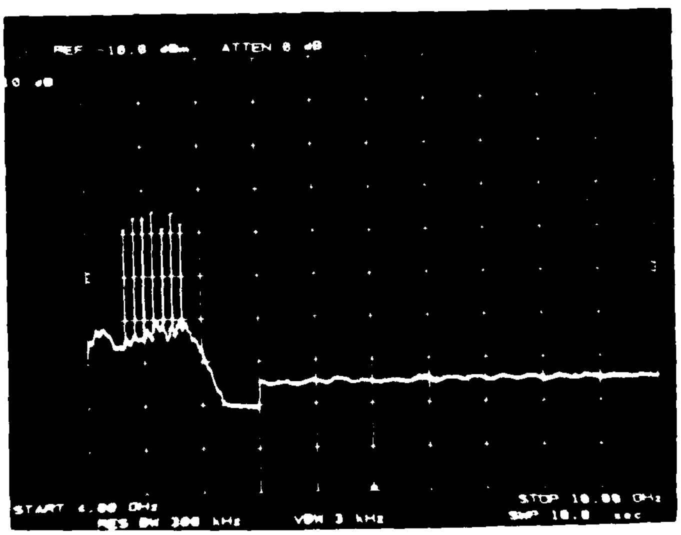

-20 dBm
inputs 4.4. tl
5.0 GHz in
100 MHz steps
no second
harmonics
found

Figure 8.4.3-3. Second Harmonic Measurement of RF Fiber-Optic Link, Version II

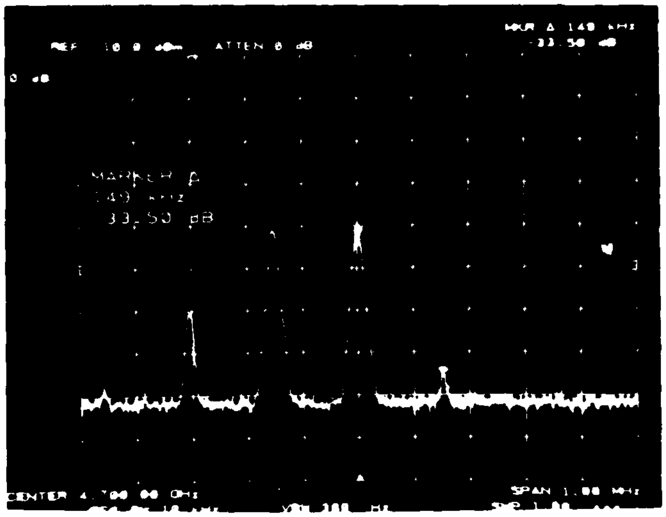

4.700

Δ 1 MHz

4.69990

-30 dBm each tone

$2 f_2 - f_1$ = > 33.5 dBm

f_2 = >50 dBm

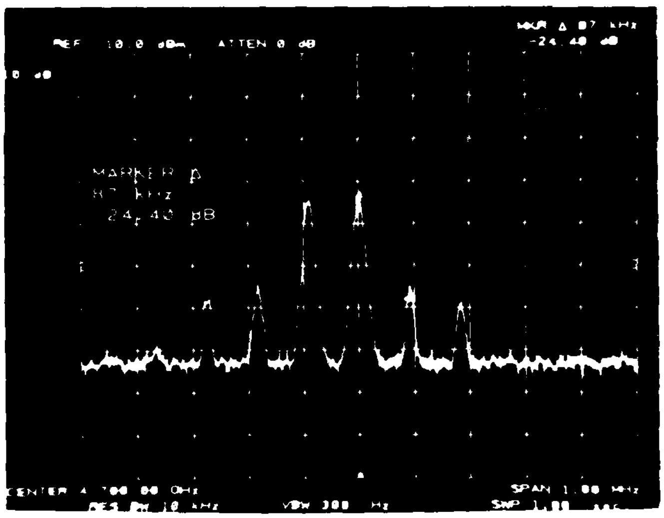

↑5th order

4.7000

Δ 1 MHz

4.6990

-20 dBm each tone

$2 f_2 - f_1$ = > 24.4 dBm

f_1 = > 43 dBm

Also note the 5th project, this shows that σ -20 dBm in IMPs are quite non-linear.

Figure 8.4.3.4. Two-Tone Intermodulation Product (IMP) Measurement of RF Fiber-Optic Link, Version II

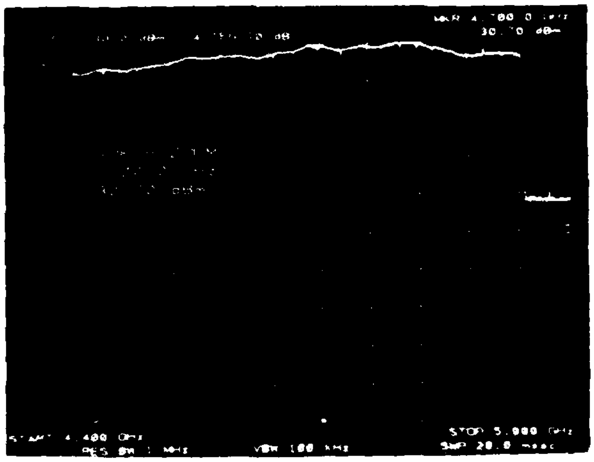

Calibration Curve

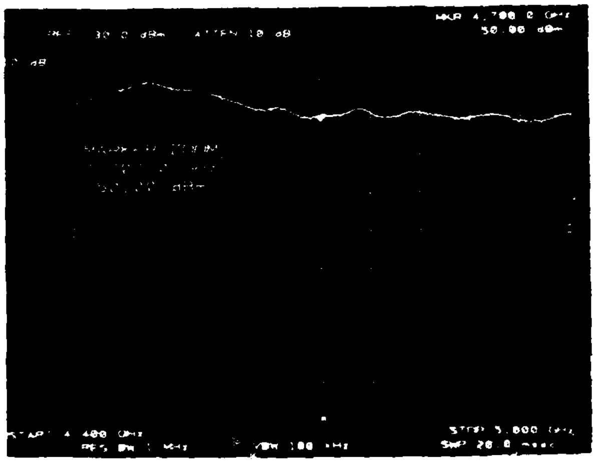

Actual Return Loss
10dB/div.

(a)

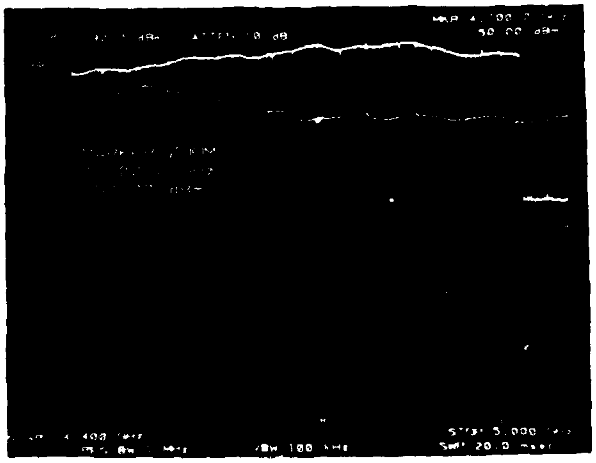

Calibration Curve
-versus-
Return Loss
at 4.7 GHz - 20 dB Return Loss

(b)

Figure 8.4.3-5. Input and Output VSWRs Measurement of RF Fiber Optic Link, Version II

8.4.5 TE Cooler and Control Circuit

As previously mentioned in Paragraph 4.6.2, the ambient temperature varies the threshold current of the laser diode (LD), which affects the optic power output, modulation depth, nonlinearity, and delay distortions.

Since Version II was intended to be the laboratory model, the TE Cooler and its associated circuitry were not incorporated in Version II. Furthermore, in Version II, due to the large heat sink (operating in room ambient temperature) by external ILD mounting, temperature compensation and its associated control circuitry was found not to be necessary to minimize parameter variations and achieve the stated performance.

For ILD fiber optic systems that are either subjected to a hostile environment or require small packages (and hence, small heat sinks) some form of temperature compensation will be required. It may be a simple open loop TE Cooler to reduce the ILD operating temperature or it may be as complex as the optically coupled closed loop system described in section 4.6.2 as utilized in Version I.

8.4.6 Technology Direction

Fiber optic technologies including systems, fiber design and fabrication, laser diode, and photodector are progressing into high data rate and microwave frequencies. Particularly, the microwave fiber optic technology is now budding and will be in full bloom in the near future. Despite the bright future and present progress, there are still many technical hurdles that must be overcome. After evaluating both Version I and Version II of the RF Fiber Optic Link, it is found that the near future technology direction of RF fiber optics will be in the following areas:

- Long-life laser diode operating over wide temperature range without thermal electric cooler. Thermal electric cooler increases laser diode transmitter size/weight and cost, but also requires large currents. Presently, the laser diode has a tested lifetime of more than 7,000 hours at the ambient temperature 70 70^{o}C.

- Laser diode and fiber coupling power improvement. Coupling more optical power from the laser diode to the single mode fiber will improve the system signal-to-noise ratio. A microlens is necessary to be fabricated at the tip of the single mode fiber to increase coupling efficient. Also, the microlens will minimize the sensitivity of fiber laser diode alignment procedure.

- The use of MESFET as a photodetector. MESFET requires lower bias voltage than APD. It also provides advantages of low noise, low cost, and amplification gain.

- The simplicity of single mode fiber connector assembly.

9.0 CONCLUSION AND RECOMMENDATION

Recent advances in microwave fiber optic technology have led to an unprecedented 5.0 GHz FO system using a 1-km single-mode fiber. The laser diode used in the system did not exhibit the resonance-like phenomenon in the frequency reange of 4 to 5 GHz. The laser diode showed the capability of direct modulation up to 6 GHz.

ACKNOWLEDGEMENT

The author would like to express his gratitude to Paul Sierak of RADC for his technical and contractual guidance, to J. B. Wilson for technical assistance, computer design/optimization and test, to M. G. Kunz for link fabrication and evaluation. Thanks also are extended to R. Perry for his project management and support.

MISSION
of
Rome Air Development Center

RADC plans and executes research, development, test and selected acquisition programs in support of Command, Control Communications and Intelligence (C^3I) activities. Technical and engineering support within areas of technical competence is provided to ESD Program Offices (POs) and other ESD elements. The principal technical mission areas are communications, electromagnetic guidance and control, surveillance of ground and aerospace objects, intelligence data collection and handling, information system technology, ionospheric propagation, solid state sciences, microwave physics and electronic reliability, maintainability and compatibility.

END

FILMED

1-85

DTIC